JACOBS UNIVERSITY

On the Isomer Problem of Mixed−Addenda and Heterogroup−Substituted Polyoxometalates

by

Aleksandar Kondinski

a Thesis submitted in partial fulfillment
of the requirements for the degree of

Doctor of Philosophy
in Chemistry

Approved Dissertation Committee

Prof. Dr. Thomas Heine

Prof. Dr. Ulrich Kortz

Prof. Dr. Gerd-Volker Röschenthaler

Prof. Dr. Wolfgang Bensch

Dr. Nina Vankova

Date of Defense: 22.1.2016

Dedicated to Meijie Li

Acknowledgements

Nurturing young scientist and bringing them on the way to adopt the ethical scientific practices is a high responsibility for every doctorate advisor. In this respect I would like to thank my PhD supervisor, **Prof. Dr. Thomas Heine** for providing me with the opportunity to pursue my graduate studies in a professional and inspiring working environment. I also sincerely thank him for aiding my research enthusiasm with financial support, which was very crucial for me to continue my graduate studies.

I am grateful to my immediate supervisor and coworker, **Dr. Nina Vankova**, who continuously provided me with guidance and research insights that helped me to develop skills in organization of the research work, density functional theory calculations and in technical writing. I certainly would like to thank her for the corrections of the submitted manuscripts and this PhD thesis.

I would like to acknowledge **Dr. Lyuben Zhechkov** for his continuous support and guidance on performing the challenging and computationally demanding calculations and for the many fruitful discussions and corrections during the preparation of this thesis.

Prof. Dr. Ulrich Kortz is thanked for sharing his excellent expertise in POM chemistry and for providing opportunities for a collaborative work. From his group, I thank **Dr. Lin Zhengguo** and the former member **Dr. Natalya Izarova** for sharing experimental insights and for collaborating on combined experimental and theoretical projects.

Dr. Kirill Monakhov is kindly thanked for collaborating, guiding the work on the chapter of polyoxovanadates which became a part of this work.

Prof. Dr. Gerd-Volker Röschenthaler and **Prof. Dr. Wolfgang Bensch** are thanked for evaluating my thesis work and for his contributions as a committee member.

Dr. Oliver Hampe, **Dr. Florian Schinle** and **Mr. Patrick Jägger** are kindly thanked for collaborating and for sharing valuable insights from the electrospray mass spectrometry measurements.

I also would like to **Dr. Stan van Gisbergen**, **Dr. Olivier Visser** and **Dr. Erik van Lenthe** and the team at the Scientific Computing and Modeling N.V. in Amsterdam, The Netherlands, who have supported me during my research visit.

I would like to thank, all of my research group members for providing good fellowship throughout the past three years.

Finally, I would like to thank my family for unreserved material and moral support during my graduate studies.

Reviewers

The committee members, **Prof. Dr. Thomas Heine**, **Dr. Vankova**, **Prof. Dr. Ulrich Kortz**, **Prof. Dr. Gerd-Volker Röschenthaler** and **Prof. Dr. Wolfgang Bensch** are kindly thanked for evaluating and for offering corrections of this thesis.

My colleagues, **Dr. Lyuben Zhechkov**, **Ms. Ievgeniia Savchenko**, **Ms. Rosalba Juarez Mosqueda**, **Dr. Lin Zhengguo** and **Mr. Vladimir Bačić** are also thanked for providing many beneficial comments and suggestions for this thesis.

Abstract

Polyoxometalates (POMs) represent nanoscale metal−oxide clusters, conventionally constructed of early transition metals in high oxidation states (mainly V, Mo and W).[1–3] POMs exhibit tunable physicochemical properties, which make them suitable for applications in catalysis, magnetism and preparation of nanostructured materials.[2, 3] The properties of POMs are predominantly tuned by the number, the type and by the arrangement of the involved building blocks in unique structural architectures. The stabilities and the properties rising from the arrangement of the building blocks define the problem of POM isomerism. In this thesis, theoretical techniques are applied to shed light into the isomer problem of mixed−addenda and heterogroup−substituted POMs. Theoretical methods were chosen as they offer advantages to make accurate predictions of the properties of hypothetical POMs or POMs that are difficult or impossible to be studied purely on the grounds of experiment.[4–6]

Chapter 1 introduces the fundamentals of POM chemistry. A brief description is provided on the structural and historic aspects of the well–known POMs. The current state of the art in POM isomerism and the experimental and theoretical approaches used over the past several decades are discussed in detail. This chapter also provides introduction to POMs built of noble metals (Au, Pd and Pt),[7] as this is relevant for the core work summarized in the next chapters. At the end of this chapter, the scope and the general problems of the thesis are outlined.

Chapter 2 provides a brief introduction to the density functional theory (DFT) method. As this thesis benefits from collaboration with experimental partners, section towards understanding the typical means of characterization are introduced.

Chapter 3 provides insights into the effect of the countercations on the calculated UV/Vis spectra of the two reported polyoxoaurates $[Au_4Se_4O_{16}]^{4-}$ and $[Au_4As_4O_{16}]^{8-}$.[8, 9] Understanding of the solution structure of $[Au_4As_4O_{16}]^{8-}$ is of fundamental importance, considering that it shares similar synthetic and structural features with the mixed−addenda species presented in Chapter 4.

Chapter 4 introduces the isomer problem of the mixed gold(III)–palladium(II)–oxo clusters with formula $[NaAu_4Pd_8As_8O_{40}]^{11-}$,[10] and investigates the structure–stability relationship and the spectroscopic properties of these materials.

Chapter 5 addresses the isomerism problem in heteropolyoxovanadates (*hetero*POVs).[11] In the main focus are the isomeric *α*–/*γ*–/*β*–$[V_{14}E_8O_{50}]^{12-}$ and *α*–/*γ*–/*β*–$[V_{14}E_8O_{42}X_8]^{12-}$ (E = Si, Ge and Sn; X = S, Se and Te) *hetero*POVs. The relative stabilities, geometric and electronic properties of different rotational isomers and combinations of E and X atom are studied and discussed.

In Chapter 6, the study of the mixed gold(III)–palladium(II)–oxo clusters is extended to the larger families of $[NaAu_xPd_{12-x}As_8O_{40}]^{(x-15)}$ and $[NaAu_xPd_{12-x}Se_8O_{32}]^{(x-7)}$. Using the approach established in Chapter 4, the most stable isomers for each Au:Pd ratio in $[NaAu_xPd_{12-x}As_8O_{40}]^{(x-15)}$ and $[NaAu_xPd_{12-x}Se_8O_{32}]^{(x-7)}$ were identified. These structures are then used to study the dependence of the gap, protonation and Na^+ encapsulation energies. The sites of substitution are compared to examples of *hetero*POV chemistry and mixed−addenda Keggin type species

Chapter 7 sheds light into two special subjects: (*i*) the comparative study of the $[Na_2Pd_{22}As_{16}O_{76}]^{26-}$ with $[Pd_{13}As_8O_{40}]^{14-}$ and (*ii*) the study of [*anti*–/*syn*–$Pt_2(PW_{11}O_{39})_2]^{10-}$ and their two electron oxidized species [*anti*–/*syn*–$Pt_2(H_2O)_2(PW_{11}O_{39})_2]^{8-}$.

Finally, Chapter 8 outlines the general conclusions of this thesis including directions of future theoretical and experimental efforts.

References

(1) Pope, M. T. *Heteropoly and Isopoly Oxometalates;* Springer-Verlag, Berlin, 1990.
(2) Müller, A.; Peters, F.; Pope, M. T.; Gatteschi, D. *Chem. Rev. (Washington, D. C.)* **1998**, *98*, 239-271.
(3) Long, D.; Tsunashima, R.; Cronin, L. *Angew. Chem. , Int. Ed.* **2010**, *49*, 1736-1758.
(4) Poblet, J. M.; López, X. In *General Physical Chemistry*; 2009, pp 453-466.
(5) Poblet, J. M.; López, X.; Bo, C. *Chem Soc Rev* **2003**, *32*, 297-308.
(6) López, X.; Carbó, J. J.; Bo, C.; Poblet, J. M. *Chem. Soc. Rev.* **2012**, *41*, 7537-7571.
(7) Izarova, N. V.; Pope, M. T.; Kortz, U. *Angew. Chem. Int. Ed.* **2012**, *51*, 9492-9510.
(8) Xiang, Y.; Izarova, N. V.; Schinle, F.; Hampe, O.; Keita, B.; Kortz, U. *Chem. Commun. (Cambridge, U. K.)* **2012**, *48*, 9849-9851.
(9) Izarova, N. V.; Vankova, N.; Heine, T.; Biboum, R. N.; Keita, B.; Nadjo, L.; Kortz, U. *Angew. Chem., Int. Ed.* **2010**, *49*, 1886-1889.
(10) Izarova, N. V.; Kondinski, A.; Vankova, N.; Heine, T.; Jaeger, P.; Schinle, F.; Hampe, O.; Kortz, U. *Chem. - Eur. J.* **2014**, *20*, 8556-8560.
(11) Monakhov, K. Y.; Bensch, W.; Kögerler, P. *Chem. Soc. Rev.* **2015**, *44*, 8443-8483

Table of Contents

List of Figures

List of Tables

List of Abbreviations

BP	Becke–Perdew
COSMO	Conductor Like Screening Model
CV	Circular Voltametry
DFT	Density Functional Theory
EPR	Electron Paramagnetic Resonance
GGA	Generalized Gradient Approximation
HF	Hartree–Fock
HOMO	Highest Occupied Molecular Orbital
IR	Infra–Red
IUPAC	International Union of Pure and Applied Chemistry
KS	Kohn–Sham
LDA	Local Density Approximation
LUMO	Lowest Unoccupied Molecular Orbital
MEP	Molecular Electrostatic Potential
PEP	Pauli Exclusion Principle
POM	Polyoxometalate
POV	Polyoxovanadate
RG	Runge–Gross
SAS	Surface Accessible Surface
SES	Solvent Excluding Surface
SP	Single Point
TD−DFT	Time–Dependent Density Functional Theory
TGA	Thermogravimetric Analysis
TZP	Triple Zeta Polarized
TZ2P	Triple Zeta Double Polarized
UV/Vis	Ultraviolet–visible
vdW	van der Waals
VWN	Vosko–Wilk–Nusair
XRD	X–ray Diffraction

List of Publications

1. Emerging Structures From a Soup of Isomers: DFT Insights from $[NaAu_xPd_{12-x}O_8(AsO_4)_8]^{x-15}$ and $[NaAu_xPd_{12-x}O_8(SeO_3)_8]^{x-7}$
   A. Kondinski, N.Vankova, T. Heine
   (Manuscript in Preparation)

2. *Rotational Isomerism, Electronic Structures and Basicity Properties of "Fully−Reduced" V_{14}−type Heteropolyoxovanadate*
   A. Kondinski, T. Heine, K. Yu. Monakhov
   (Submitted)

3. *Platinum-Containing Polyoxometalates: syn- and anti-$[Pt^{II}_2(\alpha\text{-}PW_{11}O_{39})_2]^{10-}$ and Formation of the Metal-Metal bonded di-Pt^{III} Derivatives*
   Z. Lin, N. V. Izarova, A. Kondinski, X. Xing, A. Haider, L. Fan, N. Vankova, T. Heine, B. Keita, J. Cao, C. Hu, U. Kortz
   (Accepted for publication in Chemistry – A European Journal)

4. *The Polyoxo−22−palladate(II), $[Na_2Pd^{II}_{22}O_{12}(As^VO_4)_{15}(As^VO_3OH)]^{25-}$*
   N. V. Izarova, Z. Lin, P. Yang, A. Kondinski, N. Vankova, T. Heine, U. Kortz
   (Accepted for publication in Dalton Transactions)

5. *How Counterions Affect the Solution Structure of Polyoxoaurates: Insights from UV−Vis Spectral Simulations and Electrospray Mass Spectrometry*
   A. Kondinski, N. Vankova, F. Schinle, P. Jäger, O. Hampe, U. Kortz, T. Heine
   Eur. J. Inorg. Chem. (2014) 3771–3778.

6. The mixed gold−palladium polyoxo−noble−metalate, $[NaAu^{III}_4Pd^{II}_8O_8(AsO_4)_8]^{11-}$
   N. V. Izarova, A. Kondinski, N. Vankova, T. Heine, P. Jäger, F. Schinle, O. Hampe, U. Kortz
   Chemistry Eur. J. 20 (2014) 8556–8560.

Chapter 1. Introduction and Scope of the Work

We are living in an era where large material versatility and in detail understanding of material properties are necessary to ensure advances in many diverse areas such as medicine, communication and information technologies, sustainable energy technologies *etc*. The need to develop cost–efficient manufacturing of novel environmentally friendly materials, sets challenges on the material innovation process. Following this, material development based on our current knowledge and trial and error approach is likely to bring shortcomings in producing materials with desired properties. At the beginning of the 21st century, theoretical methods used for description of material properties (mainly *ab initio* and semi–empirical calculations), have become an indispensable tool in the material development process in academia and industry. In this work, the physicochemical properties of selected novel metal–oxo cluster materials are calculated and predicted using the density functional theory (DFT) method.

Metal oxides are the most abundant materials on Earth[1] and many of them find applications in metallurgy, catalysis, magnetism, electrochromic devices, *etc.* The physicochemical properties of metal oxides are predominantly defined by: (*i*) the type of metal center, and its oxidation state and coordination environment; (*ii*) the periodicity of the material which can be 0D, 1D, 2D or 3D (Figure 1.1); (*iii*) the material dimensions (*e.g.* nanoscale, microscale); (*iv*) the inner structure of material; (*v*) the formal charge of the material. The present work is primarily focused on discrete (zero–dimensional) negatively charged nanoscale metal–oxo clusters, also called *polyoxometalates* (POMs).

Some POM topologies can be also representative for positively charged and neutral metal–oxo clusters (see section 1.4). POMs exhibit large structural versatility, which is partially due to isomerism (section 1.3).

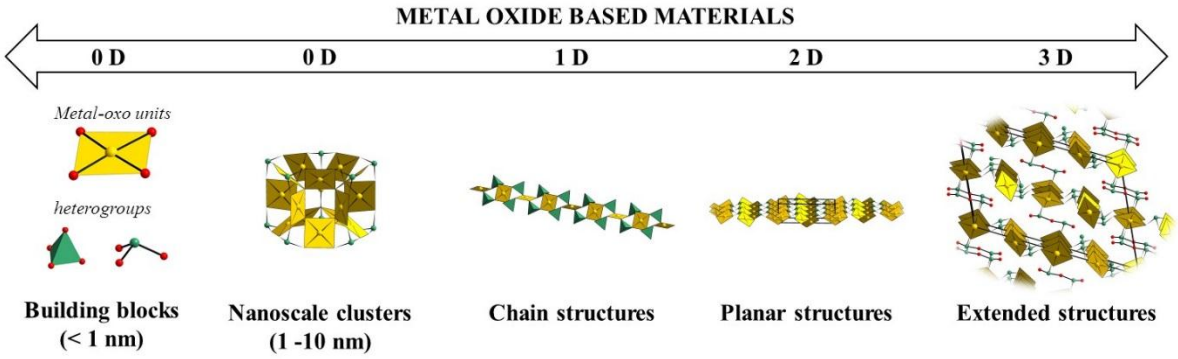

Figure 1.1: Materials from left to right: building units $\{Au^{III}O_4\}$, $\{SO_4\}$ and $\{SeO_3\}$, nanoscale cluster of $[Au_{15}O_8(SeO_3)_{10}]^{5+}$,[2] chain structure of $BaAu_2(SO_4)_4$,[3] planar structure of $Au_2(SeO_3)_2O$ [4] and extended structure of $Au_2(SeO_3)_2(Se_2O_5)$.[5] Color code: $\{Au^{III}O_4\}$ = yellow square planes, $\{SO_4\}$ = green tetrahedra, Se = green balls and O = red balls.

1.1 POM Chemistry

1.1.1 Fundamental Definitions

Conventional POMs are nanoscale metal–oxo clusters built of early transition metal elements in their high oxidation states (mainly Mo, V, W but also Nb and Ta).[1, 6–8] Other than group 5 and 6 metals, iron (Fe),[9] noble metals (Pd, Au and Pt)[10] and actinides (U and Pu)[11, 12] participate in the formation of POMs exhibiting unconventional structures.

The metal atoms involved in building the POMs are commonly referred to as *addenda* atoms. POMs are typically formed through *condensation processes* of building units, triggered by acidification. An example is the formation of $[W_7O_{24}]^{6-}$, which is expressed by the reaction:

$$7\ WO_4^{2-} + 8H^+ \rightleftharpoons [W_7O_{24}]^{6-} + 4H_2O$$

In nature polyoxometalates are forming during slow *weathering* processes. Examples of polyoxometalate based minerals are pascoite ($[V_{10}O_{28}]^{6-}$),[13] hewettite ($[V_6O_{16}]^{2-}$)[13] and sherwoodite ($AlV_{12}^{V}V_2^{IV}O_{40}]^{9-}$).[14]

In POMs, the addenda centers M are connected to terminal and bridging oxo ligands. The connectivity between two octahedral building units $\{MO_6\}$ may occur *via* corner sharing, edge sharing or face sharing (Figure 1.2).

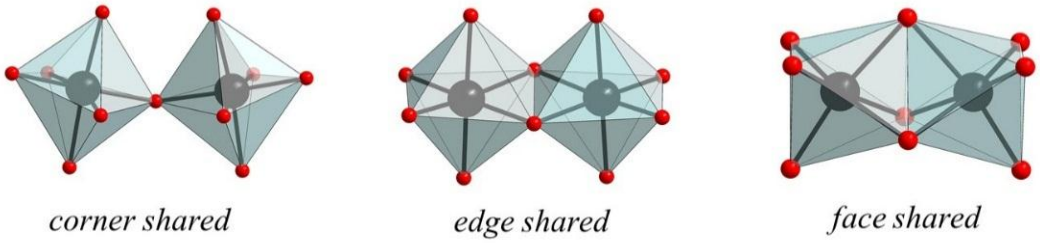

Figure 1.2: Combined ball and stick and polyhedral representation of corner sharing (left), edge sharing (middle) and face sharing (right) connectivity between two {MO_6} octahedra. Color code: {MO_6} = blue octahedra, M = black, O = red.

The formation of POMs is directed by various experimental parameters such as pH, temperature, concentration of the reactants, presence and type of countercations, templating heterogroups and many other (see section 2.9.1).[15] During POM formation, the heterogroups can have the role of molecular templates (*e.g.* as in the Keggin type POMs in Figure 1.3.a), or they can be involved in the stabilization of metal–oxo cores (*e.g.* as in the polyoxopalladate in Figure 1.11.d), leading to formation of the so–called *heteropolymetalates*.[16] POMs formed in the absence of heterogroups, *i.e.* constituted only from oxo/hydroxo ligands and addenda metals, are often referred to as *isopolymetalates*.[16]

POMs which have a "saturated" structure are referred to as *plenary* structures. Plenary POMs (Figure 1.3) are well–known for their thermal, redox and pH stability.[16] Substitution of addenda positions in these plenary POMs by other metal centers leads to formation of *mixed–addenda* species.[16] POMs which are derived from plenary structures by removal of single or multiple addenda atoms with their adjacent terminal oxo/hydroxo ligands are referred to as "unsaturated" structures or *lacunary* POMs.[16] Lacunary POMs exhibit defect sites exposing highly nucleophilic terminal oxygen atoms. These atoms can easily bind to *d*– or *f*–block metal cations. In this sense, lacunary POMs can be considered as all–inorganic polydentate ligands. Depending on the number of formally removed polyhedra, the lacunary POMs are referred to as *monolacunary*, *dilacunary*, *trilacunary*, *etc.*

1.1.2 Well–Known Examples of Plenary POMs

There are numerous examples of polyoxometalate topologies. Herein the structures of the four widely known POM topologies: Keggin, Wells–Dawson, Anderson–Evans and Lindqvist are discussed. The history of structure elucidation of these four POMs is presented in details in Section 1.2. The herein presented Keggin and Wells–Dawson POMs are members of sets of diastereomers. These sets of Keggin and Wells–Dawson isomers are introduced in sections 1.3.1 and 1.3.2 respectively.

***α*–Keggin type $[XM_{12}O_{40}]^{n-}$**: In this structure (Figure 1.3.a), X represents the heteroatom (commonly P^{5+}, Si^{4+}, Ge^{4+} or B^{3+}), M is the addenda atom (commonly Mo or W). The *α*–Keggin type structure is composed of a heterogroup tetrahedron $\{XO_4\}$ which is caged by 12 octahedral $\{MO_6\}$ units. Each of the 12 addenda atoms in the $\{MO_6\}$ units connects to one terminal oxo ligand. The 12 addenda centers are positioned in the vertices of a virtual cuboctahedron and are interconnected by 24 bridging oxygen atoms. The metal centers can be further grouped in four virtual triads $\{M_3O_{13}\}$ interconnected by μ_2–(O) atoms, giving rise to tetrahedral symmetry of the overall structure. The described structure refers to the *α*–Keggin isomer, while four other isomers can be obtained by formal rotation of the $\{M_3O_{13}\}$ triads by 60^o (see section 1.3.1).

***α*–Wells–Dawson type $[X_2M_{18}O_{62}]^{n-}$**: This structure is formally assembled by two trilacunary Keggin type $\{XM_9O_{34}\}$ units (Figure 1.3.b). The lacunary $\{XM_9O_{34}\}$ units are isomeric as they can formally derive from either *α*–Keggin or *β*–Keggin type POMs. The resulting *α*–$\{XM_9O_{34}\}$ or *β*–$\{XM_9O_{34}\}$ can then assemble between each other producing six possible isomer types (see section 1.3).

Anderson–Evans type $[XM_6O_{24}]^{n-}$: In this polyoxoanion (Figure 1.3.c), a central $\{XO_6\}$ heterogroup templates six $\{MO_6\}$ polyhedra in D_{3d} symmetry compounds.

Lindqvist type $[M_6O_{19}]^{n-}$: This polyanion (Figure 1.3.d), is assembled of six $\{MO_6\}$ polyhedra connected between one another *via* edge sharing. The compound exhibits O_h symmetry point group. The structure features a central six coordinated O^{2-} ligand.

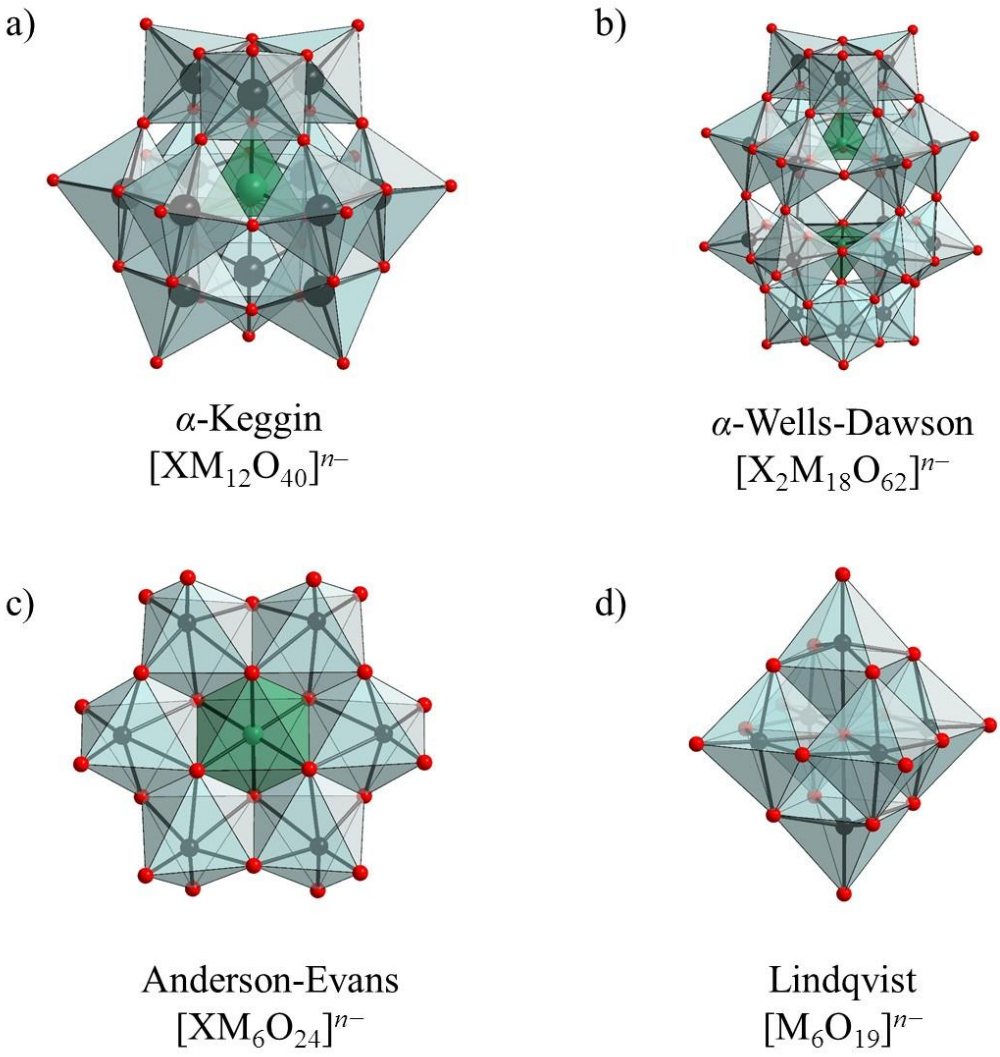

Figure 1.3: Combined polyhedra and ball and stick representation of: a) the Keggin, b) Wells–Dawson, c) Anderson–Evans, and d) Lindqvist strictures. Color scheme: $\{MO_6\}$ = blue octahedra, $\{XO_6\}$ = green octahedra, $\{XO_4\}$ = green tetrahedra, M = black balls, X = green balls and O = red balls.

1.2 Historical Background of POMs

1.2.1 The Beginnings of Structural POM Chemistry

It is believed that the Native Americans were the first to observe POMs, in the form of naturally occurring "blue waters", containing reduced polyoxomolybdates.[17] The first documentation of these "blue waters" in a chemical laboratory was performed by Scheele in the 18th century.[18] On the other hand, the first synthesis and characterization of a POM is contributed to Berzelius who

in 1826 has synthesized $(NH_4)_3[PMo_{12}O_{40}]$.[19] In 1862 the Swiss chemist Jean Charles Galissard de Marignac discovered that there are two isomers of the dodecatungstosilic acid $[H_{4-x}SiW_{12}O_{40}]^{x-}$.[20] Although other synthetic advances have been reported between the end of the 19th and the beginning of the 20th century, until the early 1930's chemists had very limited understanding of the structural complexity of POMs.[21]

The history of chemistry recognizes that the decades between 1930's to early 1950's have brought rapid material characterization by X–ray diffraction (XRD) methods, which led to the foundation of many new concepts in structural inorganic chemistry.[22, 23] Thus, this scientifically prolific period is rightfully referred to as "*renaissance of inorganic chemistry*". The major developments in structural POM chemistry also occurred during this period.

In 1928 professor Linus Pauling, a major forerunner in structural inorganic chemistry (and later a Nobel Laureate), arrived at a proposed the structure of the dodecatungstosilic acid (Figure 1.4).[24] However, at the time using the available X–ray diffraction (XRD) techniques to resolve the structure of the dodecatungstosilic acid was very laborious. As suggested by the available correspondence,[25] Pauling brought this problem to the attention of the X–ray crystallographer and physics Nobel Laureate, Sir Williams Lawrence Bragg, who at the time worked at the University of Manchester. In 1928, Pauling in a personal correspondence to Bragg writes: *"I am pleased with the clarity that the study of crystals has introduced into the very complex tungsten and molybdenum compounds."*, where by complex tungsten and molybdenum compounds he refers to polyoxotungstates and polyoxomolybdates. Interestingly, within four years of this letter in 1933, the doctorate student of Sir Bragg, James Fargher Keggin, reported the structure of the dodecatungstophosphoric acid $[H_3PW_{12}O_{40}]$.[26, 27] Later, Keggin and his coworkers from the Bragg group reported a number of other crystallographic structures baring the same polyanion motifs.[28–30] Following this, the remarkable work of Keggin was communicated within the German[31, 32] Russian[33, 34] and Swedish[35] speaking scientific communities, and with time in his honor the $[XM_{12}O_{40}]^{n-}$ polyoxoanions became referred to as Keggin type structures (1.3.a).

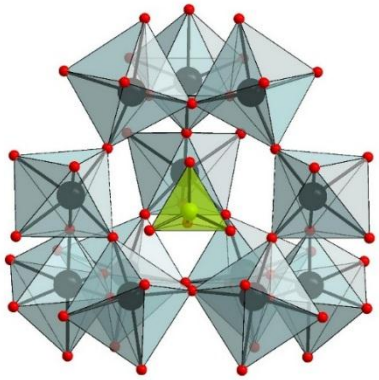

Figure 1.4: Pauling model of the dodecatungstosilic acid, which was incorrectly assigned as $\{(SiO_4)W_{12}O_{54}\}$.[24] Pauling correctly proposed the cuboctahedral topology of the 12 addenda centers, and the central position of the heterogroup $\{SiO_4\}$. However his model did not predict correctly the position of the bridging and terminal oxo ligands. The figure is shown in combined polyhedra and ball–and–stick representation where: $\{WO_6\}$ = blue octahedra, $\{SiO_4\}$ = green octahedra, W = black balls, Si = green balls and O = red balls.

The structure of the Keggin polyanion, inspired the chemist John Stuart Anderson to propose the structure of $[Mo_7O_{24}]^{6-}$ and $[IMo_6O_{24}]^{5-}$.[36] Although, the proposal was correct for $[IMo_6O_{24}]^{5-}$, a decade later the structure of $[Mo_7O_{24}]^{6-}$ was shown to exhibit a different topology.[37] In 1948 the American crystallographer Howard Tasker Evans reported the crystal structure of $[TeMo_6O_{24}]^{6-}$, which was the first experimentally characterized member of the $[XM_6O_{24}]^{n-}$ family.[38] Since the second half of the 20th century, $[XM_6O_{24}]^{n-}$ polyanions are typically referred to as "Anderson–Evans" polyoxoanions (Figure 1.3.c).

Since 1940's, researchers at University of Cambridge showed interest in the structure elucidation of the 18–heteropolytungstic acids. In 1940, the structural chemist Alexander Frank Well proposed the structure of $[P_2W_{18}O_{62}]^{6-}$.[39] Within 10 years, the structure of this polyoxoanion was resolved by the doctorate student Barrie Dawson.[40, 41,42] The proposed and the XRD resolved structures were in a very good agreement and thus with time these type of POMs became commonly referred to as the Wells–Dawson structures (Figure 1.3.b), in honor of the combined effort of both scientists.

During late 1940s, the Swedish doctorate candidate Ingvar Lindqvist at Uppsala University was probably one of the most active synthetic and structural inorganic chemists focusing in polyoxomolybdates.[37, 40, 43–49] Nowadays, Lindqvist is best known for his crystallographic work on

the $[M_6O_{19}]^{n-}$ type polyanions commonly referred to as the Lindqvist structure (Figure 1.3.d). In 1953 he reported $[Nb_6O_{19}]^{8-}$,[49] which is the first member of the Lindqvist type polyoxoanions. However, it has to be stressed that already in 1950 Lindqvist proposed the structure of $[M_6O_{19}]^{n-}$ as part of his thesis work.[40]

1.2.2 Modern POM chemistry

The synthesis of POMs has been majorly developed in the time period between early 1950's to early 1990's.[21] During this period, globally there were numerous research groups, which have been developing the synthetic field. In this period groups with prolific research output include: Souchay (France), Sillén, Lindqvist (Sweden), Baker, Evans, Pope (USA), Spitsyn (USSR) and Ripan (Romania).[21, 50] The interest in POMs during this period was mainly motivated by their applications in catalysis.

In the early 1990's, the emerging nanoscience refreshed the research interest in POMs. This interest probably appeared by the self–evident advantages of the nanoscale POMs versus conventional metal–oxide nanoparticles: POMs are discrete and well defined on atomistic scale, while many metal oxide nanoparticles are often synthetized in ranges of sizes and shapes. However, one remaining challenge is to achieve synthetic control that can lead to large POM architectures exceeding 5 nm diameter One successful example of this is Müller's polyoxoanion $[H_{48-x}Mo_{368}O_{1032}(H_2O)_{240}(SO_4)_{48}]^{x-}$ {Mo_{368}}, which reaches up to 5.5 nm.[51] Beyond the interest in the POM's size, laborious research efforts have been dedicated into the preparation of transition metal or lanthanide containing POMs with desired electronic and magnetic properties.[52–54] Over the past decade there have been reports of POMs constituting of addenda metals outside of 5th and 6th group elements, such as the polyoxo(actinyl)ates by Burns *et al.*[12] and the polyoxopalladates by Kortz *et al.*[55]

Since early 1990's, the fast development of POM chemistry also relied on insights and advances from computational chemistry.[56, 57]

1.3 Defining Isomerism in POMs

Tuning the physicochemical properties of a particular POM formula by controlled changes in geometry and connectivity between atoms, represents the main motivation to study POM isomerism.[58] POM isomerism also follows the general isomer classifications summarized below.

Chemists distinguish between *constitutional isomerism* and *stereoisomerism*, while stereoisomers can be further divided into *diastereoisomers* and *enantiomers* (Figure 1.5). According to the recommendations of the International Union of Pure and Applied Chemistry (IUPAC, http://goldbook.iupac.org/)[59] the above mentioned terms can be defined as follows:

- *Constitutional isomerism* is "isomerism between structures differing in *constitution* and described by different line formulae", where *constitution* is defined as "the description of the identity and connectivity (and corresponding bond multiplicities) of the atoms in a molecular entity (omitting any distinction arising from their spatial arrangement).
- *Stereoisomerism* is "isomerism due to differences in the spatial arrangement of atoms without any differences in connectivity or bond multiplicity between the isomers".
- *Diastereoisomers* (or *diastereomers*) are "stereoisomers not related as mirror images".
- *Enantiomers* are "one of a pair of molecular entities which are mirror images of each other and non–superimposable".

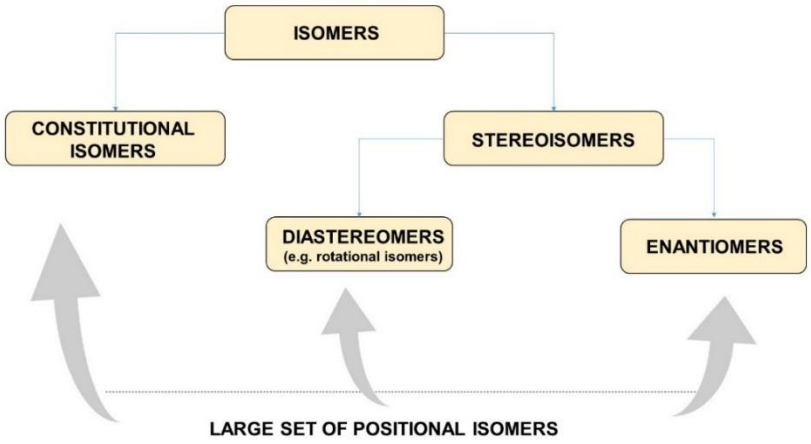

Figure 1.5: A scheme depicting the general types of chemical isomers. Rotational isomers represent an example of diastereomers. In a set of generated positional isomers there can be many isomer types, which can be further grouped according to the general classification.

In POM literature one typically encounters the discussion on *rotational* and *positional isomers*. For instance rotational isomerism refers polyoxoanions connected to one another by a restricted rotation of one or more fragments around a particular bond or an axis. In this respect rotational isomers are type of diastereoisomers. In this respect, rotational isomerism comes closest to the description of an organic *rotamer*, which according to the recommendations of IUPAC is defined as "one of a set of conformers arising from restricted rotation about one single bond". An example of rotational isomerism are the Baker–Figgis derivations of the Keggin and Wells–Dawson species (Figures 1.6 and 1.7).[60]

Formal substitution of addenda centers with heteroelements in polynuclear POMs can lead to isomers that differ in respect to the substitution configuration. These types of isomers are commonly referred to as *positional isomers*. Pairs of positional isomers may be pairs of diastereomers (*e.g.* rotational isomers), enantiomers or constitutional isomers (Figure 1.5). The problem on positional isomerism begins with the synthesis of $[PV_xMo_{12-x}O_{40}]^{(3+x)-}$ (x = 1 – 3) in 1968.[61] In 1975, Pope and Scully have enumerated the possible isomers of the mixed–addenda *α*–Keggin family $[XM_xM'_{12-x}O_{40}]^{n-}$ (section 1.3.4).[62]

1.3.1 Rotational Isomerism in Keggin Type POMs

Keggin type $[XM_{12}O_{40}]^{n-}$ polyanions exhibit five rotational isomers designated by the prefixes *α*, *β*, *γ*, *δ* and *ε*. These isomers are sometimes termed as Baker–Figgis isomers, and depict stepwise rotation of zero, one, two, three and four $\{Mo_3O_{13}\}$ triad units by 60° around the X–O bonds, yielding respectively *α*–, *β*–, *γ*–, *δ*– and *ε*–Keggin isomers (Figure 1.6).[60] The five rotational isomers *α*–/*β*–/*γ*–/*δ*–/*ε*–$[XM_{12}O_{40}]^{n-}$ belong to the T_d, C_{3v}, C_{2v}, C_{3v} and T_d point group symmetries respectively.

The topology of Keggin type isomers is not limited to early transition metal elements (Mo and W) but it has been identified also for Al,[63, 64] Ga,[65] Fe[9] and Sb.[66] Depending on the addenda atom type, the relative stability among the five rotational isomers may vary as demonstrated from the theoretical studies of $[XM_{12}O_{40}]^{n-}$ (M = Mo and W; X = Al^{III}, Ga^{III}, Si^{IV}, Ge^{IV}, P^{V} and As^{V}),[67–69] the reversed–Keggin type $[(MnO_4)(CH_3)_{12}Sb_{12}O_{24}]^{6-}$ [70] and the polyoxoaluminium(III) $[AlO_4(Al(OH)_2(H_2O))_{12}]^{7+}$ cations.[71]

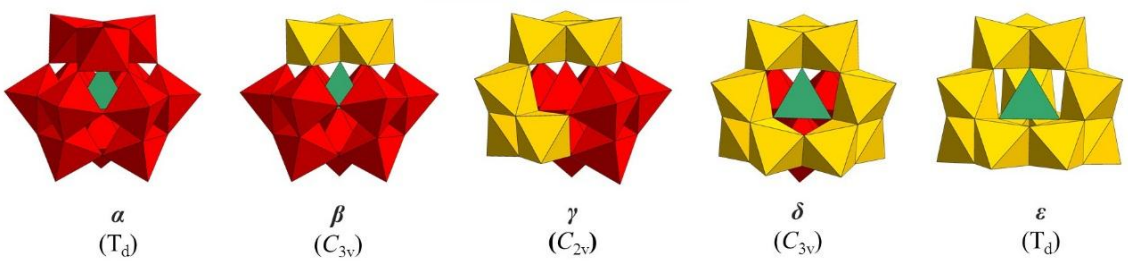

Figure 1.6: Polyhedra representation of the five rotational *α*–, *β*–, *γ*–, *δ*– and *ε*–Keggin isomers shown from left to right. Color code: {XO_4} = green, {MO_6} = both in red and yellow and rotated {M_3O_{13}} = yellow.

1.3.2 Rotational Isomerism in Wells–Dawson POMs

In 1970, Baker and Figgis postulated the existence of six isomer topologies of the Wells–Dawson polyoxoanions $[X_2W_{18}O_{62}]^{n-}$, designated by the prefixes: *α*, *β*, *γ*, *α**, *β** and *γ**. These isomers differ in their relative orientations of the trinuclear {M_3O_{13}} caps or half {XW_9O_{34}} units (Figure 1.7). The six rotational isomers *α*–/*β*–/*γ*–/*α**–/*β**–/*γ**–$[XM_{12}O_{40}]^{n-}$ belong to the D_{3h}, C_{3v}, D_{3h}, D_{3d}, C_{3v} and D_{3d} point group symmetries respectively.

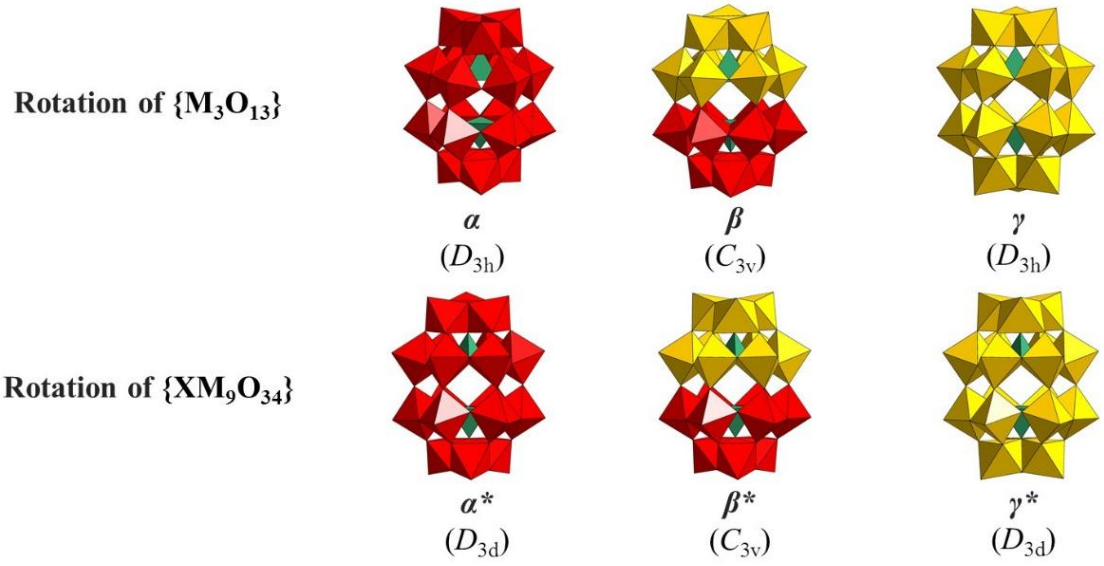

Figure 1.7: Polyhedra representations of *α*–, *β*–, *γ*–, *α**–, *β**–, and *γ**–$[(XO_4)_2W_{18}O_{54}]^{n-}$ isomers. Color code: {XO_4} = green tetrahedra, {MO_6} = red if they represent A–*α*–{XM_9O_{34}} or yellow if they represent A–*β*–{XM_9O_{34}}. Lacunary POM isomerism is clarified in 1.3.5.

Experimentally, up to four rotational isomers *α*–, *β*–, *γ*– and *γ**–$[X_2W_{18}O_{62}]^{6-}$ have been synthesized and characterized for As^V heteroatoms.[15] Theoretical investigations have showed that the six Wells–Dawson isomers exhibit the relative stability order: *α* (most stable) > *β* > *γ* > *γ** > *β** > *α** (least stable).[58, 72] These findings are in agreement with the prediction of Contant and Thouvenot and co–workers who have hypothesized the relative stability considering the isomerization pathway (*γ* → *β* → *α*) and the oxidizing power of (*α* < *β* < *γ*) of $[X_2W_{18}O_{62}]^{6-}$ (X = P and As).[73]

1.3.3 Rotational Isomerism in $[V_{18}O_{42}]^{12-}$ and $[V_{18-x}E'_{2x}O_{42}]^{2x-12}$ (E' = As and Sb)

There are two known isomers of $[V_{18}O_{42}]^{12-}$ polyoxoanions (Figure 1.8).[74, 75] These clusters can be constructed from square planar $\{VO_5\}$ building blocks. The structures can be presented as eight edge sharing $\{VO_5\}$ units forming a virtual $\{V_8O_{16}\}$ ring, while these rings are then connected to two $\{V_5O_{17}\}$ units from both sites. Depending on the configuration between the $\{V_5O_{17}\}$ units in respect to the $\{V_8O_{16}\}$ ring, the $[V_{18}O_{42}]^{12-}$ structure has D_{4h} symmetry point group (*i.e.* rhombicuboctahedral geometry, or herein noted as *α*–isomer) or T_d symmetry point group (*i.e.* pseudo–rhombicuboctahedral geometry, or herein noted as *β*–isomer). $[V_{18}O_{42}]^{12-}$ POMs can be considered as rotational isomers, since they can be related to each other by a virtual rotation of one of the $\{V_5O_{17}\}$ units by 45° around the vertical axis passing through the center of the $\{V_8O_{16}\}$ ring.

A virtual substitution of {VO} with $\{E'_2O\}$ (E' = As and Sb) moieties in the isomeric $[V_{18}O_{42}]^{12-}$ polyoxoanions, leads to isomeric heteropolyoxovanadates (*hetero*POVs) of the type $[V_{18-x}E'_{2x}O_{42}]^{2x-12}$. Examples of such virtual substitutions have been reported by the Bensch group, who synthetized and characterized the isomeric antimonato polyoxovanadates $[V_{16}Sb_4O_{42}]^{8-}$ (Figure 1.8). The herein noted *α*–$[V_{16}Sb_4O_{42}]^{8-}$ exhibits D_{2h} symmetry point group and formally derives from *α*– $[V_{18}O_{42}]^{12-}$. Similarly, the herein noted *β*–$[V_{16}Sb_4O_{42}]^{8-}$ exhibits C_2 symmetry point group symmetry and it formally derives from *β*–$[V_{18}O_{42}]^{12-}$.[76, 77]

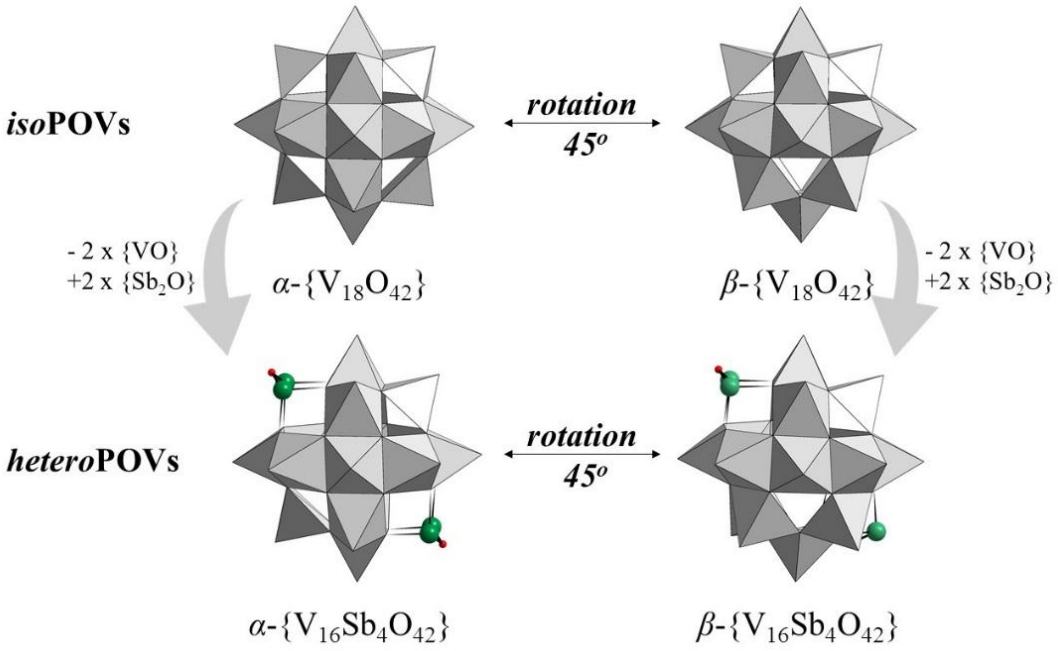

Figure 1.8: Combined polyhedra and ball–and–stick representation of α–$[V_{18}O_{42}]^{12-}$ (top row, left), β–$[V_{18}O_{42}]^{12-}$ (top row, right), α–$[V_{16}Sb_4O_{42}]^{8-}$ (bottom row, left) and β–$[V_{16}Sb_4O_{42}]^{8-}$ (bottom row, right). Color code: $\{VO_5\}$ = gray square pyramids, Sb = green balls and O = red balls.

1.3.4 Positional Isomerism in Keggin Type POMs

Pope and Scully have enumerated the total number of positional isomers for the mixed–addenda α– and β–Keggin type $[XM_xM'_{12-x}O_{40}]^{n-}$ (Table 1.1).[16, 62] As it can be observed from Table 1.1, the number of positional isomers is significantly larger for β–Keggin type $[XM_xM'_{12-x}O_{40}]^{n-}$ due to the lower symmetry.

Table 1.1: Enumeration of the positional isomers derived for mixed–addenda α– and β–Keggin anions $[XM_xM'_{12-x}O_{40}]^{n-}$.[16]

x	α–$[XM_xM'_{12-x}O_{40}]^{n-}$ (T_d)	β–$[XM_xM'_{12-x}O_{40}]^{n-}$ (C_{3v})
1	1	3
2	5	14
3	13	43
4	27	90
5	38	142
6	48	166

The numerical assignment of the addenda centers proposed by Pope and Scully has been revised according to the IUPAC recommendations.[78, 79] An example of application of this scheme to assign the different α–$[XM_2M'_{10}O_{40}]^{n-}$ isomers is shown in Figure 1.9.b.

XRD crystal structure elucidation of salts containing mixed–addenda α–$[XV_xM_{12-x}O_{40}]^{n-}$ (X = P, As, V; M = Mo and W) often provides information that the metal centers are delocalized over all addenda centers.[80–83] This phenomenon indicates that multiple positional isomers have been cocrystallized. Information on the total number of isomers coexisting in solution and their respective abundances can be established on the basis of nuclear magnetic resonance (NMR) spectroscopy. In this light ^{51}V and ^{31}P NMR have been used to establish the number $[PV_xM_{12-x}O_{40}]^{n-}$ (M = Mo and W) isomers[84] and the abundances of α–/β–$[PV_xMo_{12-x}O_{40}]^{(3+x)-}$ (x = 1–3) in solution.[85, 85–87]

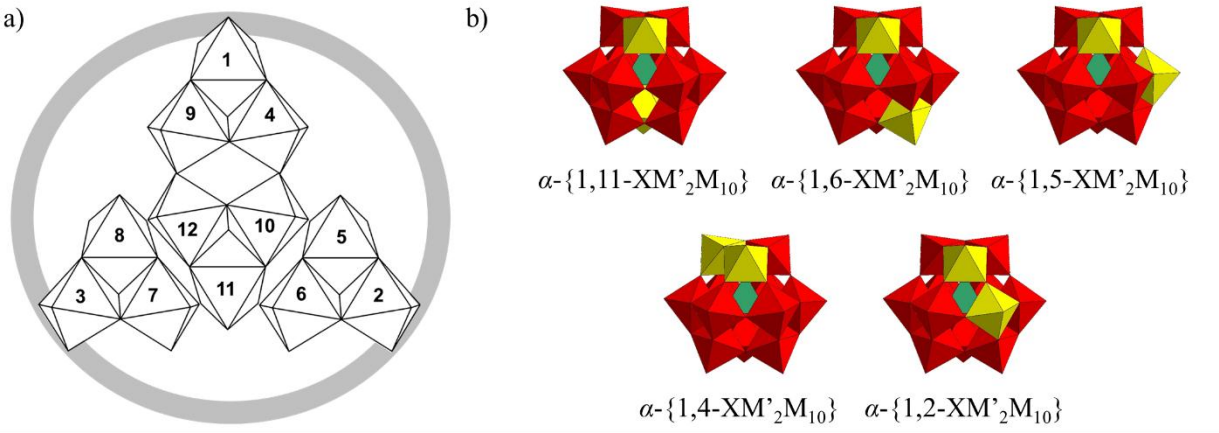

Figure 1.9: a) Unfolded α–Keggin polyoxoanion showing the numerical assignment of the addenda positions, with recommended IUPAC numbering scheme;[62] b) Polyhedra representation of the five α–$[XM_2M'_{10}O_{40}]^{n-}$ isomers. Isomers α–$[1,6–XM_2M'_{10}O_{40}]^{n-}$ and α–$[1,5–XM_2M'_{10}O_{40}]^{n-}$ are enantiomers of α–$[1,7–XM_2M'_{10}O_{40}]^{n-}$ and α–$[1,8–XM_2M'_{10}O_{40}]^{n-}$ respectively (not shown). Color code: $\{XO_4\}$ = green, $\{MO_6\}$ = yellow and $\{M'O_6\}$ = red.

To ensure if a particular partially reduced POM system contains multiple isomers, one may make use of combination of techniques such as electron paramagnetic resonance (EPR) characterization and infrared spectroscopy (IR)[88] In the characterization of $[PV_2M_{10}O_{40}]^{5-}$ (M = Mo and W), EPR has shown that reduction occurs on the V sites, while IR reveals several absorption lines for the stretching modes of the P–O bonds, which origin from the coexistence of several positional isomers .[88]

Theoretical investigations of the electronic, redox, protonation and stability properties have been performed by Guan *et al*. on the five positional isomers of α–$[PTi_2W_{10}O_{40}]^{7-}$.[89] On the basis of the bonding energies, these five isomers follow the stability order given in IUPAC notation: α–$[1,5–PTi_2W_{10}O_{40}]^{7-}$ > α–$[1,6–PTi_2W_{10}O_{40}]^{7-}$ > α–$[1,11–PTi_2W_{10}O_{40}]^{7-}$ > α–$[1,4–PTi_2W_{10}O_{40}]^{7-}$ > α–$[1,2–PTi_2W_{10}O_{40}]^{7-}$.

1.3.5 Isomerism in Lacunary Derivatives of the Keggin Type POMs

Lacunary POMs exhibit nucleophilic terminal oxygen atoms which can facilitate the bonding towards the *d* or *f*–block heterometal. Lacunary anions of the Keggin structure are interesting in the context of POM isomerism since they bring closer concepts of rotational and positional isomerism.

Formal removal of one {MO} moiety from α–$\{XM_{12}O_{40}\}$ and β–$\{XM_{12}O_{40}\}$ leads to formation of α–$\{XM_{11}O_{39}\}$ and three β–$\{XM_{11}O_{39}\}$ isomers respectively (see Figure 1.10).[15] The three β–$\{XM_{11}O_{39}\}$ arise from the three positional isomers exhibited by the plenary β–Keggin framework. Formally, three types of lacunary sites in the monolacunary β–Keggin isomers are distinguished numerically by an additional index next to the β letter (*i.e.* β_1–, β_2– and β_3–$\{XM_{11}O_{39}\}$).

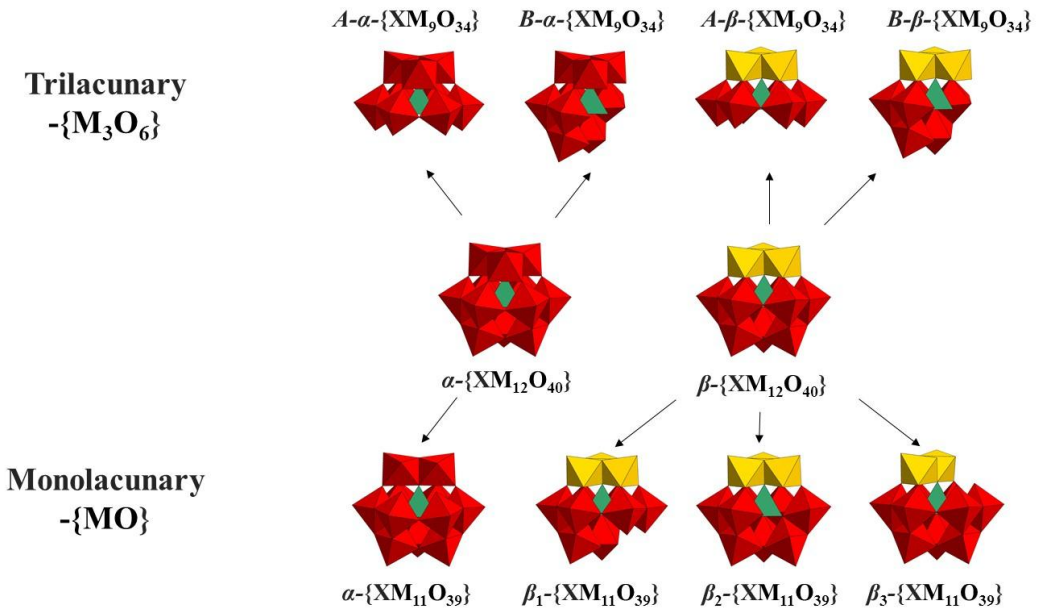

Figure 1.10: Polyhedral representation of the plenary trilacunary (top), plenary (middle) and monolacunary Keggin isomers. One has to note that B–β–$\{XM_9O_{34}\}$ are known only in oligomeric polyoxotungstates.

Experimentally the monolacunary β–$[SiM_{11}O_{39}]^{8-}$ isomers have been proven to have the following stability order: β_1 (least stable) < β_2 < β_3 < α (most stable). On the basis of bonding energies, Chermette *et al.* confirmed the stability orders of the three β–$[SiM_{11}O_{39}]^{8-}$ isomers observed in experiments, but found that the bare β_3 and α showed very similar bonding energies and thus stability.[90] Laurencin *et al*. demonstrated that interactions with the environment (*i.e.* solvent effects and dissolved countercations) are very important and introduce geometric constrains at the lacunary site of the β_3–$[XW_{11}O_{39}]^{m-}$ (X = P and Si), thus making the β_3 isomers sterically less favorable than the α isomers.[91]

Removal of a $\{M_3O_6\}$ moiety from α–$\{XM_{12}O_{40}\}$ and β–$\{XM_{12}O_{40}\}$ leads to the formation of four isomers.[15] Depending on whether the connectivity between the three addenda centers in $\{M_3O_6\}$ occurs *via* corner sharing or edge sharing, one distinguishes A type and B type $\{M_3O_6\}$ removal respectively. Combining the type of the removal of $\{M_3O_6\}$ units (*i.e.* A or B) with the type of rotational Keggin isomers (α–$\{XM_{12}O_{40}\}$ or β–$\{XM_{12}O_{40}\}$) one arrives to the four lacunary POM isomers: A–α–$\{XM_9O_{34}\}$, B–α–$\{XM_9O_{34}\}$, A–β–$\{XM_9O_{34}\}$ and B–β–$\{XM_9O_{34}\}$ (see Figure 1.10). This assignment is not very systematic, as B–α–$\{XM_9O_{34}\}$ can be also formally derived by virtual $\{M_3O_6\}$ removal from β–$\{XM_{12}O_{40}\}$.

1.3.6 Enantiomeric POMs

The research interest in enantiomeric (or also chiral) POMs,[92] is motivated by the applications of these materials in stereoselective catalysis, bio–simulation, sensing, nonlinear optics and medicine.[93, 94]

The self–assembly of POM building blocks can sometimes lead to discrete enantiomeric species.[92] Enantiomeric hybrid–POMs can be also produced by functionalization of lacunary POMs with chiral organic or metalorganic moieties. In this approach, the chirality of the functionalizing moiety is transferred to the formed hybrid–POM.[95]

Stabilization electronic effects in a POM that appears non–chiral may induce structural deformations and thus to reduce the overall symmetry. An example of this is the chiral Wells–Dawson type α–$[P_2Mo_{18}O_{62}]^{6-}$.[96, 97] This feature has been reported by Pope in 1976, who noted that the α–$[P_2Mo_{18}O_{62}]^{6-}$ did not exhibit idealized D_{3h} symmetry, D_3, which renders this POM chiral.[98] Later in 1978 Pope and Garvey have demonstrated that the symmetry break is not induced

by the crystal packing and that it was also present for the solution α–$[P_2Mo_{18}O_{62}]^{6-}$ species, as shown by the observed Pfeiffer effect in the optical rotatory distortion spectrum.[97] The Pfeiffer effect was induced from the ion pairing of the chiral POM and the chiral countercations. Theoretical insights into these problem were reported by Poblet *et al.* in 2008, who studied the family of α–$[X_2Mo_{18}O_{62}]^{q-}$ (X = S^{IV}, Se^{IV}, P^{V}, As^{V}, Si^{IV}, Ge^{IV}).[96] Their study showed that α–$[X_2Mo_{18}O_{62}]^{q-}$ have higher stability with the D_3 symmetry, and the geometric distortions were more pronounced in the POMs with more negative heterogroups. The geometric distortions in α–$[X_2Mo_{18}O_{62}]^{q-}$ stabilize the HOMOs, while the energy stabilization is related to second order Jahn–Teller effect.[96]

1.4 Polyoxonoble–Metal Clusters

Over the past decade there is an increased interest in synthesis, structural characterization and theoretical studies of the electronic and spectroscopic properties of the noble metal (Pd, Au and Pt) based metal–oxo clusters.[10] These materials can adopt positive, neutral or negative formal charges, thus they can be generally referred to as *polyoxonoble–metal clusters*.

Early reports of *polyoxonoble–metal clusters* date back to the late 1980's when Privalov *et al.* reported the crystal structure and the solution NMR spectra of $[(NO_2)_3Pt^{IV}Pt^{II}_3O_3(NO_2)_6]^{5-}$ (Figure 1.11.a)[99, 100] and $[Pt^{IV}(Pt^{II}_3O_3(NO_2)_3)_2]^{8-}$ (Figure 1.11.b)[99, 100] polyoxoanions. However, over the years this work did not receive large research attention. Probably the most impactful works in this family of materials date to 2004 when the Wickleder group has reported the synthesis of $[Pt_{12}O_8(SO_4)_{12}]^{4-}$ (Figure 1.11.c)[101] and in 2009 when the Kortz group has reported the synthesis of the first polyoxopalladate $[Pd_{13}As_8O_{34}(OH)_6]^{8-}$ (Figure 1.11.d).[55] Later in 2010 the Kortz group also reported the first polyoxoaurate $[Au_4As_4O_{20}]^{8-}$ (Figure 1.11.e). [102]

The addenda centers in conventional POMs have formal d^0 or d^1 valence shell, while in polyoxonoble–metal clusters the addenda have partially filled atomic *d* orbitals ($d^6 - d^8$). Addenda centers such as Pd^{II}, Au^{III} and Pt^{II} have d^8 filled valence shell and typically exhibit square planar coordination which contributes towards the formation of unconventional POM architectures. Deviation from this structural feature is possible by incorporating Pt^{IV} (d^6) as addenda centers which exhibit octahedral {MO_6} building units. Pt^{III} (d^7) can involve in the formation of Pt–Pt

bonds and can coordinate up to five oxo bridging ligands as exemplified by $[Pt_{12}O_8(SO_4)_{12}]^{4-}$ (Figure 1.11.c).

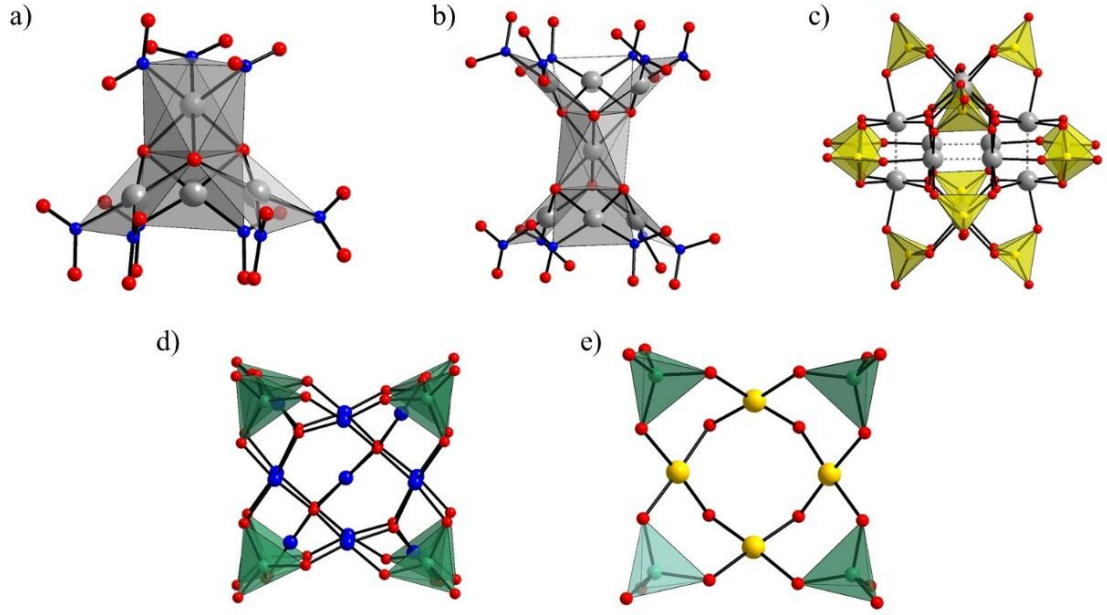

Figure 1.11: Combined polyhedra and ball and stick representation of a) $[(NO_2)_3Pt^{IV}Pt^{II}_3O_3(NO_2)_6]^{5-}$; b) $[Pt^{IV}(Pt^{II}_3O_3(NO_2)_3)_2]^{8-}$; c) $[Pt^{III}_{12}O_8(SO_4)_{12}]^{4-}$; d) $[Pd_{13}As_8O_{34}(OH)_6]^{8-}$; e) $[Au_4O_4\ (AsO_4)_4]^{8-}$.Color code Pt = grey balls, O = red balls, N = blue balls, A u = yellow balls, $\{PtO_4\}$ and $\{PtO_6\}$ = grey polyhedra, $\{SO_4\}$ = yellow tetrahedra and $\{AsO_4\}$ = green tetrahedra.

Similarly to conventional POMs, in a polyoxonoble–structure one can distinguish between compounds built exclusively of one type of a metal–oxo building block (*i.e.* isopolyoxonoble–metal clusters) and structures built of various groups including heterometals and heterogroups (*i.e.* heteropolyoxonoble–metal clusters). From the subclasses, heteropolyoxonoble–metal clusters are far more numerous. All of the up–to–date reported clusters are summarized in Table 1.2. The most relevant topology of these clusters is the cuboidal $\{M'M_{12}O_8(L)_8\}$, where M = Au^{III}, Pd^{II} or mixed Au^{III}/Pd^{II}; L = $\{AsO_4\}$, $\{C_6H_5AsO_3\}$, $\{SeO_3\}$, $\{PO_4\}$ and $\{C_6H_5PO_3\}$ and M' can be various types of cations (see Table 1.2 for details). In these clusters, the twelve noble metal centers arranged in cuboctahedral fashion are interconnected by eight O atoms to form a $\{M_{12}O_8\}$ core. The eight oxygen atoms occupy the vertices of a virtual cube, defining the *inner cavity* of the metal–oxo core (*i.e.* site for incorporation of M'). This core is then stabilized by eight capping groups L, which form the overall cuboidal structure.

Table 1.2: The reported up–to–date noble heteropoly–metal–oxo clusters made of Pd, Au and Pt. Protonation is omitted for clarity.

Addenda nuclearity	Formula	Central metals	Referece
Pd^{II}			
3	$[Pd_3(CH_3COO)_6]$	–	105
7	$[Pd_7V_6O_{24}(OH)_2]^{6-}$	–	106
10	$[Pd_{10}(CH_3COO)_{12}O_4(H_2O)_2]$	–	107
12	$[MPd_{12}O_8(PO_4)_8]^{n-}$	Mn^{II}, Fe^{III}, Co^{II}, Cu^{II}, Zn^{II}	108
	$[MPd_{12}O_8(C_6H_5PO_3)_8]^{n-}$	Cu^{II}, Zn^{II}	108
	$[NaPd_{12}O_8(AsO_4)_8]^{15-}$	Na^{I}	109
	$[MPd_{12}O_8(C_6H_5AsO_3)_8]^{n-}$	Y^{III}, Pr^{III}, Nd^{III}, Sm^{III}, Eu^{III}, Gd^{III}, Tb^{III}, Dy^{III}, Ho, Er^{III}, Tm^{III}, Yb^{III} Lu^{III}, Sc^{III}, Mn^{II}, Fe^{III}, Co^{II}, Ni^{II}, Cu^{II}, Zn^{II} and Ca^{II}	108, 110, 111
	$[MPd_{12}O_8(SeO_3)_8]^{n-}$	In^{III}, Cr^{III}, Co^{II}, Zn^{II}, Ni^{II}, Cu^{II}, Mn^{II}, $Lu^{III,}$ Fe^{III}.	108, 112, 113
	$[SrPd_{12}O_6(OH)_3(PhAsO_3)_6(OAc)_3]^{4-}$	Sr^{II}	111
13	$[Pd_{13}O_8(AsO_4)_8]^{14-}$	Pd^{II}	55
	$[Pd_{13}O_8(SeO_3)_8]^{6-}$	Pd^{II}	114
	$[Pd_{13}O_8(PhAsO_3)_8]^{6-}$	Pd^{II}	114
15	$[Pd_{15}P_{10}O_{50}]^{20-}$	(Na^{I}, K^{I}, and H_2O)	115
	$[Pd_{15}Se_{10}O_{40}]^{10-}$	Na^{I}, H_2O	112, 116
	$[BaPd_{15}O_{10}(C_6H_5AsO_3)_{10}]^{8-}$	Ba^{II}	111
15.4	$[NaPd_{15}P_{10}O_{50}]^{19-}$	Na^{I}	117
	$[Pd_{16}P_{10}O_{50}]^{18-}$	Pd^{II}	
17	$[Pd_{17}P_{10}O_{50}]^{16-}$	Pd^{II}	115
22	$[Cu_2Pd_{22}P_{12}O_{60}(OH)_8]^{20-}$	Cu^{II}	118
22	$[Na_2Pd_{22}As_{16}O_{76}]^{26-}$	Na^{I}	119
84	$[Pd_{84}O_{42}(PO_4)_{42}(CH_3CO)_{28}]^{70-}$	–	120
Au^{III}–Pd^{II}			
12	$[NaAu_3Pd_9O_8(AsO_4)_8]^{12-}$ $[NaAu_4Pd_8O_8(AsO_4)_8]^{11-}$ $[NaAu_5Pd_7O_8(AsO_4)_8]^{10-}$ $[NaAu_6Pd_6O_8(AsO_4)_8]^{9-}$	Na^{I}	109
Au^{III}			
4	$[Au_4Se_4O_{16}]^{4-}$	K^{I}	121
8	$[Na_5Au_8As_8O_{40}]^{11-}$	Na^{I}	102, 122
12	$[Au_{12}O_8(SeO_3)_8]^{4+}$	–	2
15	$[Au_{15}O_{10}(SeO_3)_{10}]^{5+}$	–	2
Pt^{II}, Pt^{III} and Pd^{IV}			
4	$[Pt^{IV}{}_4(\mu_3\text{–}OH)_2(\mu_2\text{–}OH)_4(NO_3)_{10}]$	–	123
4	$[(NO_2)_3Pt^{IV}Pt^{II}{}_3O_3(NO_2)_6]^{5-}$	Pt^{IV}	99, 100
6	$[Pt^{IV}{}_6(\mu_3\text{–}OH)_4(\mu_2\text{–}OH)_6(NO_3)_{12}]^{2+}$	–	123
7	$[Pt^{IV}(Pt^{II}{}_3O_3(NO_2)_3)_2]^{8-}$	Pt^{IV}	99, 100
12	$[Pt^{III}{}_{12}O_8(SO_4)_{12}]^{4-}$	–	101

The condensation of metal–oxo building units of noble metals in aqueous media on their own, is a very slow hydrolysis process. This has been exemplified by the 15 years long aged solutions

which yielded the clusters $[Pd_{10}O_4(OH)_8(H_2O)_{12}]^{4+}$ and $[Pt_{14}O_8(OH)_8(H_2O)_{12}]^{4+}$.[103] To the best of my knowledge, the former two structures and solid state $[Pd_6O_{12}]$ wheel structure,[104] represent the only known reported examples of isopolyoxonoble–metal clusters.

1.5 Application of Density Functional Theory in POM Research

Until date, Density Functional Theory (DFT) is the most commonly used theoretical method in the description of the structural, electronic and spectroscopic properties of POMs. The rationale for this is that DFT offers satisfying accuracy for affordable calculation costs.[56, 57] Some selected achievements of the theoretical POM chemistry in development of the POM research over the past decades, are summarized in the following lines.

In the study of novel POMs, DFT provides information on the energy and distribution of the molecular orbitals.[56] Analysis of the character of the frontier orbitals gives information on the relative stability and on the potential reducibility at particular metal sites. Further on, the electrostatic interactions of POMs with their immediate environment can be investigated, for example through analysis of the molecular electrostatic potential (MEP).[56]

DFT has been commonly applied in the calculation of spectroscopic features of POMs. For instance, calculated IR and Raman spectra of Lindqvist $[M_6O_{19}]^{n-}$ and α/β–$[XM_{12}O_{40}]^{n-}$ (X = Si, P; M = Mo, W) Keggin are shown to be in agreement with experiment and can be used to provide description and prediction of the observed modes.[124–126] A drawback in these calculations is the description of the frequency corresponding to the stretch of the M–O_t (O_t – terminal oxo atoms). These frequencies are inaccurately calculated due to the high partial charges on the O_t and the limitations of the DFT method.

Calculation of excitation spectra (*e.g.* UV/Vis and circular dichroism CD) is another spectroscopy of interest considered in the description of photocatalytic or chiral POMs. In 2011, Bagno *et al.* systematically investigated accuracy of various theoretical levels on the prediction of the UV/Vis spectrum of $[W_6O_{19}]^{2-}$.[127] The application of TD–DFT has been employed by Streb *et al.* to rationalize the improved photocatalytic activity of $[VMo_5O_{19}]^{3-}$ *versus* $[Mo_6O_{19}]^{2-}$.[128] Similar approach has been employed by Casey *et al*. in the study of $[Cr(OH)_4Nb_{10}O_{30}]^{8-}$ polyanions[129] and by groups of Yan and Su to study chiral POMs.[130–132]

Independently, Bagno *et al.* and Vankova *et al.* have shown that the DFT calculation of the NMR chemical shifts of various POMs in solution, can provide indirect insights into the interaction of the POMs with their immediate environment.[133, 134] Examples of good correlation between the experimental and the calculated chemical shifts are protonated species of $[H_2Pt^{IV}V_9O_{28}]^{5-}$ and the models of γ–$[XW_{10}O_{36}]^{8-}$ (X = Si or Ge) with hydrated cations in the lacuna.[134] Similarly such efforts have been prolific in the study of vanadium capped polyoxopalladates[106] and of polyoxomolybdodiphosphonates.[135] These studies imply that the NMR shifts in particular systems may be significantly affected by the environmental effects and thus, the computational chemists has to account them through the POM model.

1.6 Applications of POMs

POMs have wide spectrum of potential applications (Figure 1.12), however only a handful of POMs have obtained commercial application. In industry, POMs have been predominantly applied as homogeneous catalysts in acid catalysis and in selective oxidation catalysis.[136] An example for acid catalysis includes hydration of olefins and the commercial synthesis of ethyl acetate from ethylene and acetic acid.[136] Examples for selective oxidation are the oxidation of methacrolein in methacrylic acid and ethylene to acetic acid. Since early 1970's, such processes have been predominantly carried out and developed by chemical companies in Japan (*e.g.* Ashai Chemical industries, BP Amoco, Nippon Shokubai–Sumitomo, Mitsubishi Rayon and Showa Denko).[136] Nowadays catalytic POMs are mainly used for the preparation of fine organics for research purposes. [137–141]

In the recent years, POMs have attracted interest in the emerging water oxidation technology as their potential role in the preparation of the oxidation catalyst (*e.g.* $[Ru_4(\mu\text{–}O)_4(\mu\text{–}OH)_2(H_2O)_4(\gamma\text{–}SiW_{10}O_{36})_2]^{10-}$)[142–146] and in the preparation of electrolytes for the complete device.[147]

Many POMs show also potential applications as single molecule magnets (SMM)[148] and applications in quantum computing.[149, 150] Spectroscopic properties of POMs have attracted interest for biological imaging[151, 152] and in photocatalysis.[153–156]

In life sciences, POMs aided the XRD refinement of the ribosome crystal structure,[157] which led to the Nobel prize in 2009. Furthermore, POMs have helped crystallization of molybdenum storing proteins.[158] In terms of medicinal applications, particular POMs have even entered clinical trials

due to their antiretroviral activity.[159–162] However, the strong and non–selective interactions of POMs with proteins is a major drawback that needs to be taken into account for future research in these areas.[163]

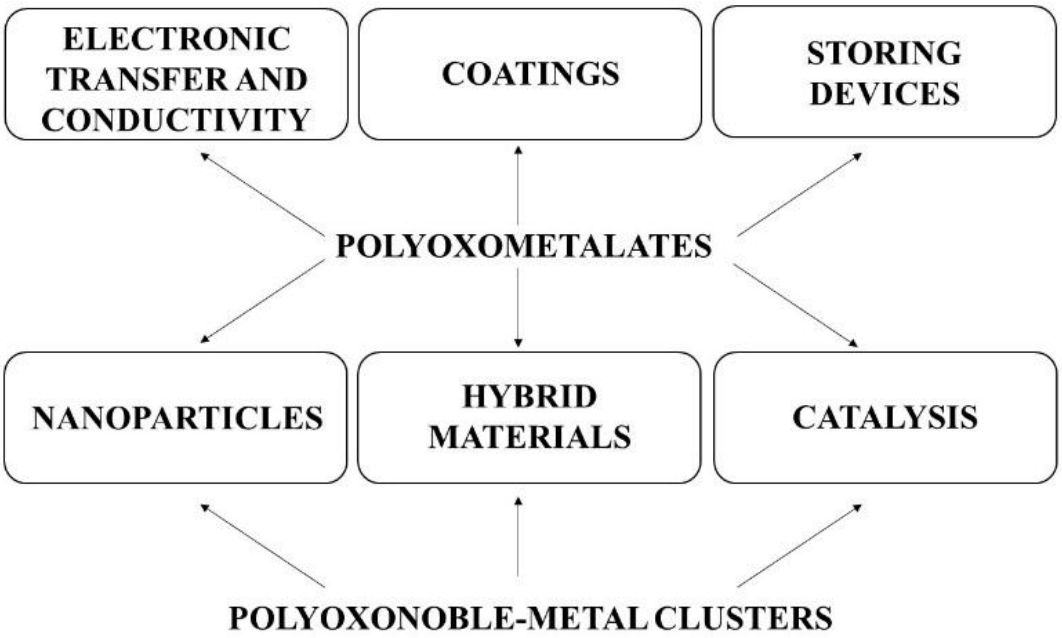

Figure 1.12: Scheme depicting some potential applications of conventional polyoxometalates and polyoxonoble–metal clusters.

The opportunity to link POMs with organic materials, led to a class of hybrid–POMs.[144] These materials are particularly interesting in energy conversion, energy storage and design of nanostructured sensors.[164] POMs are further interesting for the synthesis and functionalization of nanoparticles.[165, 166] It has been recently demonstrated that that POMs can be used as potential non–volatile memory storage devices.[84]

Similarly as many conventional POMs, polyoxonoble–metal clusters exhibit potential application in catalysis,[55, 108, 117] synthesis of hybrid–POMs[108, 110, 111, 114] and in preparation of nanocolloidal materials[107, 167] (Figure 1.12).

1.7 Scope of This Thesis

The aim of this work is to provide a theoretical description to polyoxometalates built of Au^{III}, Pd^{II} and mixed Au^{III}/Pd^{II}, and on the family of heteropoly–(14)–polyoxovanadates. For this purpose, DFT is applied to calculate the geometries and describe the physicochemical properties of number of synthesized and hypothetical metal–oxo clusters: $[NaAu_xPd_{12-x}As_8O_{40}]^{(x-15)}$, $[NaAu_xPd_{12-x}Se_8O_{32}]^{(x-7)}$, $[V_{14}E_8O_{50}]^{12-}$ (E = Si, Ge, Sn) , $[V_{14}E_8O_{42}X_8]^{12-}$ (E = Si, Ge, Sn and X = S, Se, Te) and $[Au_4O_4(L)]^{n-}$ (L = $\{AsO_4\}$ and $\{SeO_3\}$). The theoretical efforts to describe each of these families were motivated by three fundamental problems:

- **Problem 1:** The polyoxoanions $[Au_4O_4(AsO_4)_4]^{8-}$ and $[Au_4O_4(SeO_3)_4]^{4-}$ showed different interactions with the countercations in the solid state. These two polyoxoanions also show different UV/Vis spectra. Can one elucidate their solution structure on the basis of combination of techniques (UV/Vis, TD–DFT and ESI–MS)?
- **Problem 2:** The Au^{III} and Pd^{II} centers in the synthesized $[NaAu_4Pd_8As_8O_{40}]^{11-}$ polyoxoanion could not be determined on the basis of experimental studies. Theoretical investigation aimed to allocate structures with high stability and calculated spectroscopic properties that can explain experimental observations. With development of the work, the original investigation was extended to the larger structural families: $[NaAu_xPd_{12-x}As_8O_{40}]^{(x-15)}$ and $[NaAu_xPd_{12-x}Se_8O_{32}]^{(x-7)}$. How do the Au^{III}:Pd^{II} ratio and positional isomerism affects the intrinsic stabilities, affinities towards protonation and encapsulation of Na^+ cations of these two families?
- **Problem 3:** Heteropolyoxo–(14)–vanadates are subject of rotational isomerism. How do the structural and electronic properties in $[V_{14}O_{38}]^{20-}$, $[V_{14}E_8O_{50}]^{12-}$ and $[V_{14}E_8O_{42}X_8]^{12-}$ (E = Si, Ge, Sn and X = S, Se, Te) are affected by the type rotational isomerism and the combination of E and X atoms?

The capability to bring theoretical insights into the former three problems, opens an opportunity for better understanding of the isomer problem of POMs and for further studied and applications. Thus these opportunities add an additional motivation for working on the above described problems, and they are described in each of the core chapters of this thesis (Chapters 3–7).

This thesis also provided theoretical support in two additional projects:

- **Arsenate capped polyoxopalladates:** The electronic structures of $[Na_2Pd_{22}As_{16}O_{76}]^{26-}$ and $[Pd_{13}O_8(AsO_4)_8]^{14-}$ were described by application of the DFT method. Potential fragmentation pathways were investigated for the novel $[Na_2Pd_{22}As_{16}O_{76}]^{26-}$ and comparison with the reported $[Pd_{13}O_8(AsO_4)_8]^{14-}$
- **Platinum functionalized (11)–tungstophosphates:** The isomers of *anti*–$[Pt^{II}_2(\alpha–PW_{11}O_{39})_2]^{10-}$ and *syn*–$[Pt^{II}_2(\alpha–PW_{11}O_{39})_2]^{10-}$ were described on the basis of DFT. The study also provided description on the two electron oxidized and one electron reduced species, thus providing motivation for additional electrochemistry studies.

1.7.1 Steps Employed During the Development of the Work

The obtained results which address each of the former problems and projects are furnished in five chapters. The individual steps undertaken to obtain clarity in these subjects are summarized in the following lines.

The objectives of Chapter 3 with title "The solution structure of polyoxoaurates: insights from UV/Vis simulations and electrospray mass spectrometry." are:

- Develop and validate a procedure to perform accurate calculations on polyoxoaurates.
- Simulate the UV/Vis spectra of $[Au_4Se_4O_{16}]^{4-}$, $[KAu_4Se_4O_{16}]^{3-}$ and $[Au(OH)_4]^-$ in water.
- Simulate the UV/Vis spectrum of the $[Au_4As_4O_{20}]^{8-}$.
- Model interactions of $[Au_4As_4O_{20}]^{8-}$ with countercations, calculate their UV–Vis spectra, and evaluate how the calculated and observed UV–Vis spectra fit with one another.
- Clarify the contributing effects from the capping groups and the countercations to the excitation spectra of two polyoxoaurates.
- The quality of the predictions is further evaluated on the basis of electrospray mass spectrometry.

The objectives of Chapter 4 with title "*Elucidation of the Structure of the Mixed Gold(III)–Palladium(II) Polyoxo–noble–metalate* $[NaAu_4Pd_8As_8O_{40}]^{11-}$" are:

- Generate the complete isomer set accounting for the different occupancies of Au and Pd in the polyanion $[NaAu_4Pd_8As_8O_{40}]^{11-}$. To increase the efficiency of the calculations, reduce the set of total isomers by allowing only one structure to represent a pair of enantiomers.
- Perform geometry optimization on the set of isomers and rationalize the most stable configurations of respective occupancies of the addenda elements Au *vs.* Pd in the bare polyanion model $[NaAu_4Pd_8As_8O_{40}]^{11-}$. Select structures for further studies.
- Calculate IR and UV/Vis calculations of the selected structures, describe the spectra and compare with the experimental spectra for coherency.

The objectives of Chapter 5 with title "*The Rotational Isomerism Problem in "Fully–Reduced" Heteropolyoxo–(14)–vanadates"* are:

- Design structural models of *α*–/*β*–/*γ*–$[V_{14}O_{38}]^{20-}$ (**I**), *α*–/*β*–/*γ*–$[V_{14}E_8O_{50}]^{12-}$ (**II**) and *α*–/*β*–/*γ*–$[V_{14}E_8O_{42}X_8]^{12-}$ (**III**), where E = Si, Ge, Sn and X = S, Se, Te.
- Optimize the geometries and analyze how the rotational isomerism, E and X atoms affect the structural features of **I**/**II**/**III**.
- Establish relative stabilities of **II**/**III** in terms of HOMO–LUMO gap and bonding energies.
- Investigate how the rotational isomerism, E and X atoms affect the electronic properties of **II**/**III**.
- Study the basicity and the protonation affinities of the different O and X atoms in **II**/**III**.

The objectives of Chapter 6 with title "*The Positional Isomerism Problem in* $[NaAu_xPd_{12-x}O_8(AsO_4)_8]^{x-15}$ *and* $[NaAu_xPd_{12-x}O_8(SeO_3)_8]^{x-7}$*"* are:

- Enumerate and generate the complete isomer set of $[NaAu_xPd_{12-x}O_8(AsO_4)_8]^{x-15}$ and $[NaAu_xPd_{12-x}O_8(SeO_3)_8]^{x-7}$.
- Optimize the geometries and describe the relative stabilities in terms of HOMO–LUMO gap and bonding energies for each stochiometry.
- Select most stable isomers of each Au:Pd radio and compare their electronic properties (HOMO, LUMO and HOMO–LUMO gap energies), protonation at different O atoms and Na^+ encapsulation affinities.

In Chapter 7 with title "*Examples of Interplay of Theory and Experiment in Noble Metal POM Chemistry*" collaborative work between the groups of Thomas Heine and Ulrich Kortz is included. The included work focuses on two projects where the theoretical contributions are:

- Describe the electronic structure of the novel polyoxoanion $[Na_2Pd_{22}As_{16}O_{76}]^{26-}$ and compare it with the reported $[Pd_{13}O_8(AsO_4)_8]^{14-}$.
- Describe the electronic structure of the two polyoxoanion isomers with formula $[Pt_2(PW_{11}O_{39})_2]^{10-}$ and to propose potential protonation sites.
- Provide description on the experimentally observed spectroscopic properties of $[Pt_2(PW_{11}O_{39})_2]^{10-}$ by calculations of the IR and the UV/Vis spectra.
- Provide information of the structural, electronic and spectroscopic properties of the two electron oxidized polyoxoanions derived from $[Pt_2(PW_{11}O_{39})_2]^{10-}$.

Chapter 2. Methodology

This chapter introduces the basics of quantum mechanics and computational chemistry, with a main overview on the density functional theory (DFT) and its time–dependent extension, *i.e.* time–dependent density functional theory (TD–DFT).[168] Description is provided on the Conductor like Screening Model (COSMO)[169] and on the molecular electrostatic potential (MEP)[170] respectively. The software, Amsterdam Density Functional (ADF),[171, 172] the ranges of its capability and advantages are also presented. As large portion of the obtained results in this thesis is relevant to experimental work, a brief introduction in the synthesis and characterization of POMs is provided.

2.1 Quantum Mechanics

The time–independent Schrödinger equation has the simple form $\hat{H}\psi = E\psi$, where $\hat{H}$ is the Hamiltonian operator and ψ is a set of solutions or eigenstates of the Hamiltonian.[173, 174] Each of these solutions ψ_n, has an associated eigenvalue, E_n, which is a real number that satisfies the eigenvalue equation. For some well–know examples such as particle in a box, the Hamiltonian in the Schrödinger equation obtains a simple form and thus it can be solved analytically.[173]

The Hamiltonian for systems considering multiple electron interactions in a nuclear potential obtains a complicated form which includes: (*i*) the kinetic energy of the electrons; (*ii*) the kinetic energy of the nuclei; (*iii*) the potential energy of the nuclear–nuclear interaction; (*iv*) the potential energy of electron–electron interactions; (*v*) the potential energy of the nuclear–electron attraction. Finding analytical solutions to such complex systems is practically impossible and thus it requires use of approximations and numerical approaches.

2.2 Computational Chemistry

Computational chemistry offers sophisticated theories that can calculate molecular orbitals, structural and spectroscopic properties and reactivity of molecules. The full treatment of computational chemistry can be elegantly formulated, however its numerical complexity is often challenging. In 1998, Noble prize in chemistry was awarded to John Pople and Walter Kohn for their contributions to the development of computational techniques for elucidation of molecular

structure and reactivity. This was also the first time the Noble prize in chemistry or physics to be awarded for the development of numerical methods.

The wavefunction and density functional methods that are used for calculation of chemical systems are based on the use of the electronic wave function and the electronic density, respectively. Both methods make use of numerous approximations. The Born–Oppenheimer approximation, which approximates the nuclei in the particular chemical system as "frozen–in–space", is used by both methods. Thus by ignoring the nuclear motion, the system becomes less complicated as one does not need to consider the kinetic energy from the nuclei, while the potential nuclear–nuclear repulsion energy becomes constant that can be calculated using the Coulomb law.

Another approximation that is used in wavefunction and density functional methods is the treatment of the electron–electron repulsive interactions. By ignoring that the electronic motion is correlated, and by replacing the instantaneous electrostatic field with an average one (Figure 2.1), it is possible to recover even over 95 % of the electron interaction energy. The potential in this approximation is called the Hartree potential, and it has the following form:

$$V_H(r) = e^2 \int \frac{n(r')}{|r - r'|} d^3r' \tag{2.1}$$

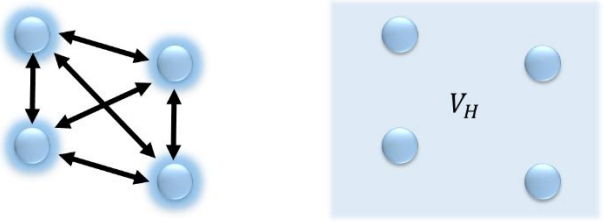

Figure 2.1: A scheme depicting the replacement of individual electron–electron interactions (left) with the uniform Hartree potential field (right).

2.2.1 Hartree−Fock (HF) Theory

The HF theory is representative for the wavefunction methods. This theory merges the Hartree theory (which ignores the electron correlation) and the Fock theory (which takes into account the electron exchange exactly). The former is important as the exchange energy, which arises from the antisymmetry of the quantum mechanical wavefunction, must be included for accurate description. The Fock theory takes care of the electron exchange by constructing antisymmetric wavefunctions.

This begins by approximating that the many–electron wavefunction is a product of one–electron wavefunctions:

$$\psi(x_1, \ldots\ldots, x_N) = \chi_{j_1}(x_1)\chi_{j_2}(x_2) \ldots \chi_{j_N}(x_N) \tag{2.2}$$

The wavefunction must satisfy the Pauli Exclusion Principle (PEP) and change sign under permutation of pairs of electrons. Thus the wavefunction can be written as a sum of all possible permutations with the appropriate sign, which are them expressed as Slater determinants:

$$\psi(x_1, \ldots\ldots, x_N) = \frac{1}{\sqrt{N!}}\, det\, \left|\chi_{j_1}(x_1)\chi_{j_2}(x_2) \ldots \chi_{j_N}(x_N)\right| \tag{2.3}$$

In equation 2.3, the coefficient $(1/N!)^{1/2}$ ensures that the wavefunction is normalized if the component spin orbitals are normalized. By combining the detrimental wavefunction and the variational principle one can obtain an optimal wavefunction that gives the lowest total energy.

As indicated earlier, the HF theory ignores the correlation energy which may contribute *ca.* 5% to the total energy. This can be a source of an error when calculating bond distances and bond energies of molecules which have areas of high electron density (*e.g.* multiple bonds). To correct for this, there are wavefunction methods that go beyond the HF. Separate to these, DFT overcomes some of these errors by approximating both the exchange and the correlation energies (*vide infra*).

2.2.2 Density Functional Theory (DFT)

The electron density, *n*(r), which represents a probability to find an electron at position r can be expressed in terms of individual wave functions:

$$n(r) = 2\sum_i \psi_i^*(r)\psi_i(r) \tag{2.4}$$

When calculating the properties of a particular system, the product of the many one–electron wavefunctions and the electron density can provide equivalent chemical information. However, the number of scape variables necessary to describe the many one–electron wavefunctions and the electron density of a particular system are not same. The electron density is dependent on three space variables (x,y,z), while the many one–electron wavefunctions 3N variables, where N is the

number of electrons. Therefore, the use of electronic density instead of many one–electron wavefunctions can provide computational advantages.

DFT is founded over two fundamental mathematical theorems proved by Hohenberg and Kohn (HK).[175] The first HK theorem addresses the ground state energy of a particular collection of atoms: *The ground–state energy from Schrödinger's equation is a unique functional of the electron density.* This theorem implies that there is one–to–one mapping between the ground state wave function and the ground state electron density. The HK theorem shows that the ground–state electron density uniquely determines all properties rising from the energy and the wave function of the ground state.

The electron density in a system, which makes use of the Born–Oppenheimer approximation, affects the following energy terms: (*i*) the kinetic energy of the electrons; (*ii*) the potential energy of electron–electron interactions; (*iii*) the potential energy of the nuclear–electron attraction. The potential energy of electron–electron includes energy terms that come from the repulsive forces and an unknown exchange–correlation energy term. Although the first HK theorem guarantees that there is a functional that can do correct mapping of the electron density to the ground state energy of the system, it does not describe the nature of this functional. This phenomenon is described by the second HK theorem: *The electron density that minimizes the energy of the overall functional is the true electron density corresponding to the full solution of the Schrödinger equation*. Thus, hypothetically if "true" functional form is known, by using the variational procedures one can optimize the electron density and the energy of the system.

However, finding an electron density that can be correct for a particular system is not trivial as one encounters the many–body problem. This problem in HK DFT is can be resolved by using sets of Kohn–Sham (KS) equations.[176, 177] The KS equations postulate a hypothetical system where the many–body problem of interacting electrons in a static external potential is reduced to a problem of non–interacting electrons in an effective potential. The KS equations have the following term:

$$\left[-\frac{\hbar^2}{2m_e}\nabla_1^2 + V(r) + V_H(r) + V_{XC}(r)\right]\psi_i(r) = \varepsilon_i\psi_i(r) \qquad (2.5)$$

The terms in the Hamiltonian are: the electron kinetic energies, the external potential (V), the Hartree potential (V_H), and the exchange–correlation potential (V_{XC}). The form of the Hartree

potential is already presented in equation 2.1. The Hartree potential includes an error of self–interaction, which is unphysical and its correction is contained into the exchange–correlation term.

The exchange–correlation potential is given by the functional derivative of the exchange–correlation energy:

$$V_{XC}(r) = \frac{\delta E_{XC}(n)}{\delta n(r)} \tag{2.6}$$

Although in principle an exact and universal functional exists, its mathematical expression is not known yet. However, there are many approximate functionals (see section 2.4) which differ in the way they describe the exchange–correlation potential.

To solve the KS equations, one first needs to define the electron density and the Hartree potential. The electron density might origin from experimental data or it may be a single–electron wave function which has been obtained by solving the KS equations. To solve the problem, the calculation is treated in an iterative way.

2.4 Exchange–Correlation Functionals

The universal form of the exchange–correlation functional is not known, but nowadays there are many approximate functionals available. Examples are the Local Density Approximation (LDA), Generalized Gradients Approximation (GGA) and the hybrid functionals, which are briefly presented in the next subsections. These exchange–correlation functionals can be ordered by hierarchy considering the quantity of physical information that they include, in the so called "Jacob's ladder" (Figure 2.2).[178] Nevertheless, it is incorrect to conclude that higher ranked functionals are more accurate for all applications.

The need to have ever better accuracy in the prediction of the physicochemical properties of various types of materials, motivates development of new exchange–correlation functionals. In order to obtain practical application, the new functionals need to show significantly better accuracy in their predictions of particular type of chemical system than other that are already available and that their implementation in computer codes is reasonably fast.

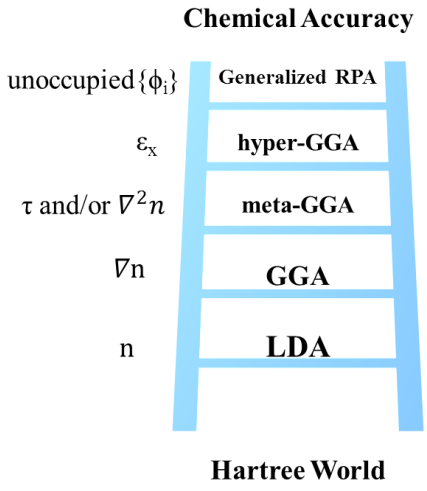

Figure 2.2: Jacob's ladder of density functional approximations to the exchange–correlation energy.[178]

2.3.1 Local Density Approximation (LDA)

One example where the exchange–correlation functional can be completely derived is the uniform electron gas model. However, the uniform electron gas model provides a practical way to apply the KS equations. To do this, one has to set the exchange–correlation potential at each position to be the known exchange–correlation potential from the uniform electron gas at the electron density observed for that position.

$$V_{XC}(r) = V_{XC}^{electron\ gas}[n(r)] \tag{2.7}$$

This approximation uses only the local density to define the approximate exchange–correlation functional and therefore it is called local density approximation (LDA). Over the years there have been a variety of LDA functionals, and one of the most widely used is the Vosko–Wilk–Nusair (VWN).[179] Typically LDA functionals are not used for the calculation and the description of the electronic properties of POMs, but it has been suggested that they can provide a very good prediction of the IR and Raman spectra for affordable calculation cost.[124–126, 180]

2.3.2 Generalized Gradient Approximation (GGA)

The Generalized Gradients Approximation (GGA) functionals were developed during the 1980's. These functionals use information about the local electron density (n) and the local gradient in the electron density (∇n). This approach defines a generalized gradient in the electron density. On the

basis of how the information from the gradient of the electron density is included, one can derive different types of GGA functionals. One of the most widely used functional in calculations of structures and electronic properties of POMs is the Becke exchange and the Perdew correlation (BP86) functional.[181, 182] It has an empirical parameter which is added to reproduce the known exchange energies of the noble gases and to reproduce the correlation energy of the Ne atom respectively. Other widely used functionals are: Perdew–Wang (PW91),[183, 184] Perdew– Burke–Ernzerhof (PBE),[185–187]Becke–Lee–Yang–Parr (BLYP).[181, 188, 189]

2.3.3 Hybrid Functionals

LDA and GGA functionals do not describe well the exchange contributions towards the total energy, although the exchange contributions are typically more significant than the corresponding correlation effects. This problem is minimized in the hybrid functionals, which partially incorporate HF exact exchange energy. One of the most widely used hybrid functionals is B3LYP, which is constructed from 80% of Becke 3–parameters exchange functional and 20% Hartree–Fock exact exchange.[190] There are many other hybrid functionals and they differ in the percentage of exact exchange: O3LYP (12%),[191] X3LYP (21.8%),[192] KMLYP (55.7%),[193] *etc.*

Hybrid functionals are rarely used in the optimization of POM geometries, as they are computationally very demanding. However, hybrids are superior to GGA functionals when it comes to calculation of spectroscopic properties and reactivity. Further on, considering that hybrid functionals "localize" the electron density at around the metal centers, they have been shown to be useful in description of spin configuration as in $[PMo_8V_4O_{40}(VO)_4]^{5-}$.[194]

2.4 Advantages and Limitations of DFT Application

The application of the DFT method has the following advantages:

1. In principle HK DFT approach deals only with the electron density which depends on three space variables (x,y,z), irrespectively of the size of the system. In contrast, the HF methods, the calculation of the wavefunction is based on 3N variables. For a small CO_2 molecule with 22 electrons this yields 66 dimensional wave function, while for the bare Keggin $[PW_{12}O_{40}]^{3-}$ model with 1226 electrons, the wave function has 3678 dimensions.

2. For the same chemical model, DFT can show similar or even better accuracy than HF (*e.g.* the shape, symmetry and energetic sequence of the KS orbitals can coincide with those obtained at the HF level).
3. DFT approximates the all the electronic correlation energy, whereas HF cannot.

However, the application of the DFT method can also come to some limitations:[174]

1. Despite that DFT can be computationally less demanding than HF, it still experiences practical limitations in terms of computational resources when it comes to treatment of large molecules with many heavy elements.
2. DFT fails to provide accurate description of dispersion forces, alkane isomerism, strongly correlated systems, degenerated states, band gaps in semiconductors and *etc.*

2.5 Time–Dependent Density Functional Theory (TD–DFT)

Time–dependent density functional theory (TD–DFT) is a modification of DFT for accurate calculation of excited state systems.[195] TD–DFT is routinely employed in chemistry to calculate the electronic transitions, based on the response of the ground–state electron density to the oscillating optical field. In this context, TD–DFT can provide information on the magnitude and the features of the excitation energies, frequency–dependent response properties, and photo–absorption spectra. In principle, TD–DFT can be applied to calculate excited states regardless of the spin and symmetry of the system of interest. In the case of closed–shell molecules TD–DFT can be used to calculate singlet and triplet excited states having transition energies smaller than the vertical ionization potential.

The foundation of TD–DFT is based on the Runge–Gross (RG) theorem which is an analogue of the HK theorem.[196] RG theorem shows that the time–dependent wave function is equivalent to the time–dependent electronic density. In this respect, the derivation of the effective potential of a particular hypothetical non–interacting system should provide the same density as the particular physically interacting system. The problem with constructing TD–DFT systems is that the time–dependent effective potential at any given instant depends on the value of the density at all previous times. Following this, the memory requirements for TD–DFT calculations are significantly larger in comparison to DFT, which in a way limits its routine application to large systems.

In TD–DFT, the electron density $n(r,t)$ is time–dependent and obtains the following form:

$$n(r,t) = 2\sum_{i} \psi_i^*(r,t)\psi_i(r,t) \tag{2.8}$$

Similarly, the ground state energy in TD–DFT calculations uses the linear response approximation, whereby changes of the electron density are assumed to be proportional to the changes of the external field. Behavior of a molecule in a time–dependent field is described by a set of time–dependent KS equations:

$$\left[-\frac{\hbar^2}{2m_e}\nabla_1^2 + V(r) + V_H(r,t) + V_{XC}(r,t) + V_{ext}(t)\right]\psi_i(r) = \varepsilon_i\phi_i(r,t) \tag{2.9}$$

In the above formula, $V_{ext}(t)$ represents the time–dependent external perturbation, *i.e.* the electromagnetic field of the incident light, which oscillates with a frequency v. Practical computations use the adiabatic approximation, whereby the exchange–correlation potential $V_{XC}(r_1, t)$ is assumed to be time–independent (*i.e.* identical to that used in stationary ground–state DFT). Solution of time–dependent KS equations yields the time dependent electron density. Using the time dependent electron density one can calculate the frequency–dependent dynamic polarizability $\alpha(\nu)$ which has the following form:

$$\alpha(v) = \frac{\hbar^2 e^2}{m_e}\sum_{n}\frac{f_n}{(E_n - E_0)^2 - E^2} \tag{2.10}$$

Where, the index n is the number of the electronic transitions and f_n corresponds to the oscillator strength of each particular transition. This summation is carried over all electronic excited states. E_0 and E_n are the energies of the ground and n–th electronic excited state, respectively, while v_0 and v_n are the corresponding frequencies of the oscillating optical field ($E = hv$). The magnitude of the transition energies ($E_n - E_0$) is calculated for the points where frequency–dependent dynamic polarizability function discontinuities, *i.e.* when the incident light energy equals the excitation energy: $E = (E_n - E_0)$ or when the incident light frequency v equals the transition frequency $v_n - v_0$. Finally, the oscillator strengths are calculated as:

$$f_n = \left(\frac{4\pi m_e}{3e^2\hbar}\right)\nu_n|\mu_n|^2 = \left(\frac{2m_e}{3e^2\hbar^2}\right)E_n|\mu_n|^2 \quad (2.11)$$

In equation 2.11, μ_n is the transition dipole moment. The oscillator strength determines the absorption band intensity that is its integrated area A: $f_n = 6.257\times10^{-19}$A (for A in $m^2\cdot mol^{-1}\cdot s^{-1}$).

2.6 Interactions with the Environment: Modeling and Analysis

POMs as negatively charged clusters exhibit electrostatic interactions with their environment. POMs are typically studied in solution, where they can exist as non–protonated and polyprotonated species and can pair with the dissolved countercations and the solvent molecules. First step towards improvement of the studied POM models is to include solvation effects. For this purpose, the Conductor like screening Model (COSMO) which is fully implemented in the Amsterdam Density Functional (ADF) program suite,[172] is introduced in this section. The molecular electrostatic potential (MEP), which is relevant for determining nucleophilic sites of various POMs, is introduced as well. In chapters 5 and 7, MEP was used to allocate sites in the POMs which are likely to bind strongly to protons and countercations.

2.6.1 Conductor–like Screening Model (COSMO)

COSMO is an approximation when modeling electrostatic interaction of a molecule with a solvent.[169, 197, 198] In COSMO the solvent is treated as a dielectric medium where the dielectric permittivity (ε) induces charge polarization on the surface around the model, while the solute molecule represents a "cavity" within this dielectric continuum. The uniform description of the solvent with the dielectric permittivity constant classifies COSMO as one of the "continuum solvation" models.

The polarization charges in COSMO are derived from a scaled conductor approximation and are affected by the polarity of the solute. Thus for ideal conductor solvents, the electric potential on the cavity surface must disappear. In order to determine the solvent charges q, one needs to have the charge distribution on a particular molecule. From a quantum mechanical calculations one can calculate the charge (q^*) localized at particular surface segments. The solvent charges are then calculated as a function of the dielectric constant and solute charges at surface segments:

$$q = f(\varepsilon)q^* \tag{2.12}$$

In equation 2.12, the function $f(\varepsilon)$ is approximated as:

$$f(\varepsilon) = \frac{\varepsilon - 1}{\varepsilon + x} \tag{2.13}$$

Once the information on the solvent charges is obtained, the energy of the interaction between the solvent and solute molecule can be calculated.

The charge q^* is defined by the molecular cavity and therefore its value can be affected by the method of cavity surface construction. The initial solute's surface is constructed from atom–centered spheres where the radii can be a van der Waals radii or other type of atomic or elemental specific radii. However, the surfaces van der Waals (vdW) surface constructed may exhibit sharp crevices, which can potentially cause calculation problems for the continuum model (*e.g.* by creating dielectric cusps). For this purpose, algorithms are used to create smoother surfaces.

In the COSMO approach, a "ball shaped" solvent molecule with defined radius R_{solv}, rolls over the vdW surface and depending on this physical encounter, two types of surfaces are created: (*i*) smooth solvent–excluding surface (SES) is generated by the center of the spherical solvent molecule; (*ii*) solvent–accessible surface (SAS) is generated as an envelope surface extended to the solvent sphere. Both surfaces "encapsulate" the interior of the molecule as envisioned in Figure 2.3.

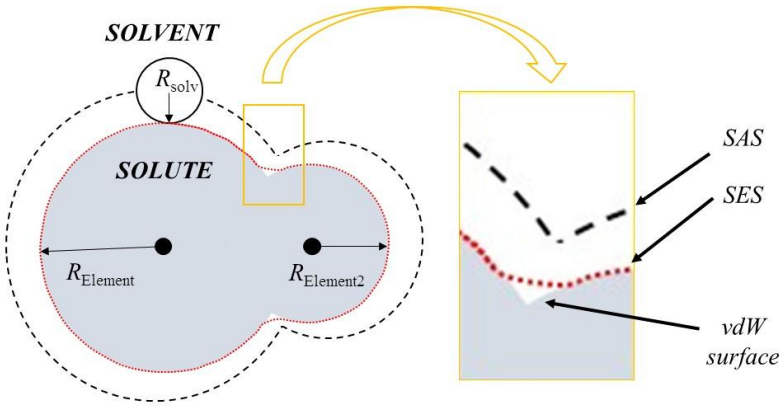

Figure 2.3: Scheme of the cavity construction method (left). The three different type of molecular surfaces: van der Waals surface (vdW) solvent–accessible surface (SAS) and solvent–excluding surface (SES) are shown in the detail window (right).

During a calculation, the program first obtains the electron density of the solute in vacuum ($\varepsilon = 0$) and then the COSMO model is activated which includes the solvent effects variationally. The model generates a molecular cavity and then it positions the point charges on the surface of this cavity. The point charges then generate an interaction potential. This potential is then added to the calculation in vacuum and to the energy of the systems, and then the molecular orbitals are recalculated. This process is repeated until self–consistency is reached.

2.6.2 Molecular Electrostatic Potential (MEP)

The molecular electrostatic potential (MEP) is a physical quantity that can be calculated or obtained experimentally by diffraction methods.[170] Molecular electrostatic potential, provides information of the nucleophilicity and can be certainly used to predict acid–base properties of POMs.[199] The MEP is defined as the force acting on a positive test charge located at position *r* through the electrical charge cloud generated through the molecule's electrons and nuclei. The electrostatic potential V_{ME} at a particular point *r* is defined as:

$$V_{ME}(r) = \sum_{A=1}^{N} \frac{Z_A}{|r - R_A|} - \int \frac{n(r')}{|r - r'|} d^3r \qquad (2.14)$$

In equation 2.14, the first term of the sum corresponds to the nuclear contributions (positive charges, Z_A) and the second term corresponds to the integral of the negative electronic distribution over all space since the electron density $n(r')$ is formally a continuous function.

Provided that the MEP can be calculated at any point in space, it can be visualized through mapping its values onto the electron density isosurface of a given molecule, thus reflecting the molecule boundaries and regions which are electrophilic and nucleophilic.

2.7 Amsterdam Density Functional (ADF) Program Suite

The ADF program suite is a commercial software that offers KS DFT calculations and modeling of discrete and periodic materials. ADF was first developed in the early 1970's by research groups working at Vrije Universiteit (Amsterdam, The Netherlands) and at University of Calgary (Alberta, Canada).[171, 172] ADF can be operated through a user friendly interface (Figure 2.4).

ADF is used both in academia and in industry. In particular, ADF has been widely used in research domains of pharmacochemistry, homogeneous and heterogeneous catalysis, inorganic chemistry, biochemistry and spectroscopy. In the context of POM chemistry, ADF provides opportunities for accurate treatment of closed and open—shell electronic systems, with multiple heavy elements by making use of relativistic effects and Slater basis functions.

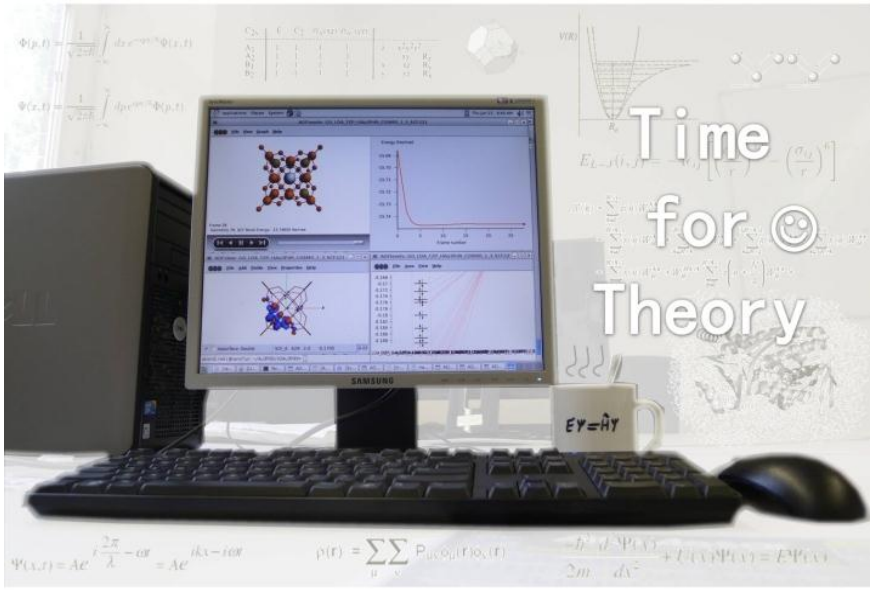

Figure 2.4: Desktop machine showing features of the ADF suite program. Photograph of the author, submitted for "The Chemist's View" – Picture Competition in 2013.

2.8 General Calculation Strategies Used Throughout This Work

The calculation of the geometries, IR and UV/Vis spectroscopic properties of all structures, was carried with ADF code (official releases 2012, 2013 and 2014).[172] All calculations were performed using the resources of the Computational Laboratory for Analysis, Modeling, and Visualization (CLAMV) at Jacobs University.[200] For computational details in each particular work, the reader will find the coils of each particular work in the respective manuscripts.

Geometry Optimization: Typically all structures are optimized with standard gradient–corrected Becke–Perdew (BP86) functional and all–electron triple–zeta polarized (TZP) basis sets.[201] Exceptions to this are:

- The optimized structures, which were used in the simulation of the UV/Vis spectra, were optimized using the BP86 functional[181, 182] and all–electron triple–zeta double–polarized (TZ2P) basis sets (Chapter 3). The preoptimized structures using TZ2P have blue shifted first excitation energies in comparison to those calculated using TZP.
- All bare models in Chapter 6 and Chapter 7 (The Heteropolyoxo–22–palladate), were optimized using BP86 and triple–zeta polarized basis sets with large frozen electron cores. The large frozen cores were found to help the converging of the self–consistent field during the calculation of optimization of highly negative bare POM models.

Spin unrestricted formalism was used only for the open–shell electronic systems in Chapter 4. In all calculations, scalar relativistic corrections were considered within the Zero–Order Regular Approximation (ZORA).[202–204] Spin–orbit coupling relativistic corrections were performed and reported for only in three test calculations in Chapter 5. Solvent effects were modeled with COSMO using default parameters for water (ε = 78.9; solvent radius = 1.93 Å).[197, 205]

Single Point Calculations and UV/Vis Spectra Calculation

Single point calculation, represents a calculation of the energy of the molecule at specific arrangement of the nuclei. Single point calculations using the hybrid B3LYP[190] and PBE0[206, 207] functionals were performed in order to obtain a better estimate of the HOMO–LUMO gap energy and description of the frontier orbitals for the POMs in Chapter 5 and Chapter 7 (The *anti*–/*syn*–$[Pt_2(PW_{11}O_{39})_2]^{10-}$) respectively.

The UV/Vis spectra of the polyoxoanions in Chapter 3 is calculated using the meta–hybrid functional M06.[208] The POMs in Chapter 4 and 7 contain many multiple heavy metals and exhibit low symmetries, which renders the calculation of the UV/Vis spectra of these POMs using hybrid or meta–hybrid functionals computationally very demanding and technically unaffordable with the available computing resources. The UV/Vis spectra for these POMs is calculated on the same level as their geometries.

Calculation of IR Spectra

The studies by Bridgeman *et al.*,[124–126] demonstrated that the use of the Vosko–Wilk–Nusair (VWN)[179] functional provides optimal computational costs and accuracy for the calculation of IR

and Raman spectra of POMs. Following this, all IR calculations were performed using this functional with triple zeta polarized basis sets (see for details in Chapter 4 and 7).

2.9 Experimental Methods

In the next subsections, some major experimental techniques typically applied in the POM synthesis and characterization process are highlighted. The electrospray mass spectrometry (ESI–MS) techniques and its application in the study of POMs is reviewed separately, as this technique had important contribution in the development of the work furnished in chapters 3, 4 and 7.

2.9.1 Synthesis and characterization

On a laboratory scale, synthesis of POMs is often performed in aqueous media, although synthesis in organic media is not unusual.[209–211] The formation of POMs is typically carried in a one–pot synthesis, where experimental parameters such as temperature, pH, countercations, presence of redox agents *etc*., can influence the direction of product formation and isolation (Figure 2.5).[15]

Nowadays it is still an open discussion whether POM synthesis follows a rational design or it is heavily dependent on serendipity.[212, 213] Nevertheless, preparation of novel POMs can be motivated by theoretical or experimental predictions and hypotheses. In this context, the synthetic chemist often prepares POMs under wet chemical conditions, in which the building blocks can interact and self–assemble into larger species. A desired product of the synthesis is a pure crystalline and homogeneous material that contains single type of POM species. Single crystals can be then studied by diffraction methods (*e.g.* Single crystal XRD).[214]

Once the crystal structure has been elucidated, additional methods can be used as a complementary characterization. For a new POM, a particular feature to be determined is the number of cocrystallized water molecules, ligands coordinated to the metal centers (*e.g.* aqua and hydroxo), oxidation states of the various centers and number of countercations. In “fully oxidized” or “fully reduced” POMs these features can be determined by combination of complementary techniques (*e.g.* bond–valence sum calculations,[215] thermogravimetric analysis and elemental analysis). On the other hand, in mixed valence POMs where the charge can be delocalized over several metal centers, obtaining unambiguous characterization may be very challenging and may require additional studies of the properties related to the electronic and spin properties (*e.g.* X–ray

photoelectron spectroscopy, magnetic susceptibility, electron spin resonance *etc.*). Ideally, the results of the complementary characterization techniques should be consistent and in agreement with each other, thus an accurate working POM formula can be deduced.

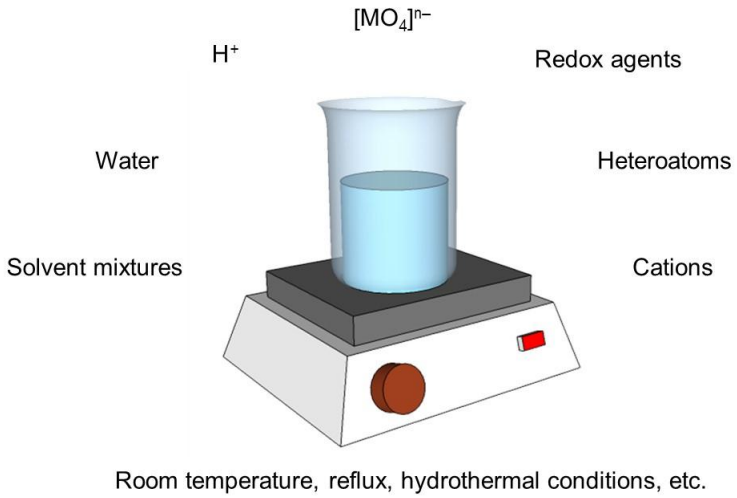

Figure 2.5: Representation of most of the experimental parameters involved in the "one–pot" synthesis approach for formation and isolation of novel POMs.

After POM synthesis, the obtained product can be characterized by vibrational spectroscopy (IR and Raman). [214, 216] Characterization by IR spectroscopy provides a rapid and inexpensive check of the purity of the synthesized product. IR can be also used to compare spectral fingerprints (*i.e.* the region 400 – 1000cm^{-1}), in order to obtain initial indication if a novel POM has been isolated.

Information on the solution stability of a particular POM is of a practical value prior considering potential application in homogeneous catalysis. Study of the solution stability of fully oxidized POMs can be made on the basis of study of NMR active nuclei (*e.g.* ^{29}Si, ^{31}P, ^{51}V, ^{183}W *etc.*).[214, 217–219] Once the stability of a particular POMs is proven on the basis of NMR, UV/Vis spectroscopy as a fast and affordable technique can be further used to investigate solution stability ranges of the POM as a function of time, temperature, pH, concentration *etc.* UV/Vis is also practical technique to confirm if a particular product can undergo reversible electron transfer processes in circular voltammetry (CV), where typically low concentrations of POMs are utilized.[220]

In scenarios where the POM salt forms in small quantities or the classical solution technique are not applicable, one may consider to utilize mass spectrometry (MS) techniques.[213] However, one drawback of this technique is that one has to carefully choose the type of ionization technique, as

some of observed the mass–to–charge ratio (*m*/*z*) signals may correspond to POMs generated during the ionization process.[213]

Theoretical description of the particular POM in question, usually begins once there is sufficiently good guess of the POM structure. Therefore the initial structure can be proposed based on chemical intuition (*i.e.* it holds chemical rationale) or it can have an experimental foundation (*e.g.* XRD). The modeling and calculations are then usually carried until, a "good" POM models is reached, which exhibits set of physicochemical properties that can be experimentally verified (*e.g.* structural parameters, spectroscopy, protonation chemistry, solution stability, magnetism, *etc.*). [214]

2.9.2 Electrospray Ionization Mass Spectrometry (ESI–MS)

The ESI–MS represents a "soft" technique for generation of vapor phase ions that can be analyzed for mass–to–charge ratio (*m*/z) within a mass spectrometer. During the electrospray ionization, a diluted analyte in solution is slowly (0.1 – 10 ml/min) injected through a capillary in the ionization chamber. The capillary is surrounded by high voltage (2 – 5 kV) which can be positive or negative and creates electric field gradient required to produce the charge separation at the surface of the liquid. The solution at the tip of the capillary is shaped in the form called "Taylor cone", which is defined by the Rayleigh limit,[221, 222] *i.e.* the degree at which Coulombic surface repulsion equals the solution surface charge tension. In this way, depending on the voltage, droplets that contain an excess of positive or negative charges detach from the "Taylor cone" and propagate through a drying atmosphere towards the entrance to the mass spectrometer. During this flight, the droplets separate into charged analyte ions following different mechanisms.[221, 222]

The choice of the solvent for the ESI–MS analysis can vary depending on the application. Moderately polar solvents can be used for the study of charged analytes such as POMs. The primary role of the solvent is to allow the formation of diluted solution of the analyte. The solvent is preferred to be reasonably volatile, in order to facilitate its evaporation from charged droplets in the drying atmosphere. For study of POMs, acetonitrile and water are among the most widely used solvents because of their moderate boiling points (<100 ºC) and polarities.

In recent years, ESI–MS became an indispensable method for characterization of POM species in solutions.[213] In 1997 Howarth *et al.* first used the ESI–MS technique to investigate the aqueous solutions of isopolytungstates, peroxotungstates and heteropolymolybdates.[223] His study showed

the presence of $[W_6O_{19}]^{2-}$ and $[W_2O_7]^{2-}$ species. In 2012 it was reviewed that the ESI–MS technique has been already successfully applied in the characterization of many conventional POM families such as: vanadates, niobates, tantalates, chromates, molybdates, tungstates and rhenates.[213]

Photographs of the nanoESI source and the capillaries used in the ESI–MS studies by our experimental partners at Karlsruhe Institute of Technology are shown in Figure 2.6.

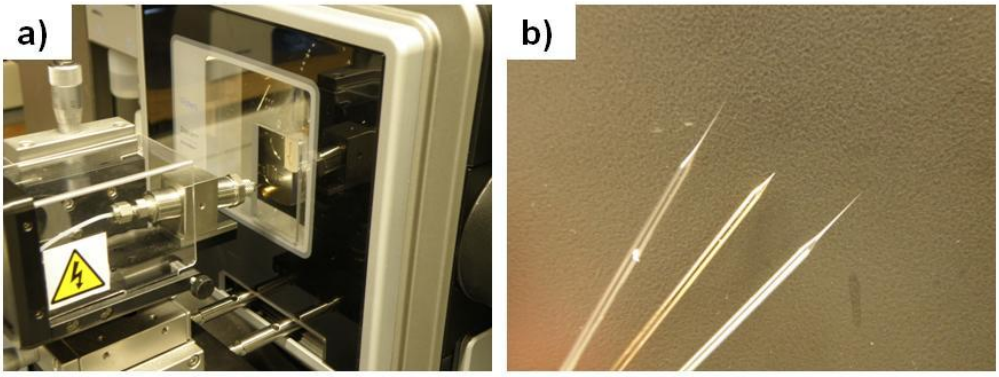

Figure 2.6: a) The nanoESI source of the mass spectrometer b) Capillaries used for spraying process in nanoESI mode. The photographs are used with permission of Mr. Patrick Jäger, Karlsruhe Institute of Technology.

Chapter 3. The Solution Structure of Polyoxoaurates: Insights from UV/Vis Simulations and Electrospray Mass Spectrometry

In 2010, Kortz group reported the arsenate capped polyoxoaurate $[Au_4As_4O_{20}]^{8-}$ (Au_4As_4) (Figure 3.1.a)[102] and two year later the selenite capped polyoxoaurate $[Au_4Se_4O_{20}]^{4-}$ (Au_4Se_4) (Figure 3.1.b).[121] The structure of these polyoxoanions can be described as $\{Au_4O_4\}$ ring structures stabilized by four $\{AsO_4\}$ or $\{SeO_3\}$ heterogroups. The four μ_2–(O) atoms in the ring moiety of Au_4As_4 and Au_4Se_4 have high basicities, thus they can chelate to alkaline cations. In the solid state, Au_4As_4 is found as dimeric species $[Na_5Au_8As_8O_{40}]^{11-}$ ($Na_5Au_8As_8$) (see Figure 3.3), where two Au_4As_4 units sandwich a virtual plane of five sodium cations. The sandwiching of sodium cations is facilitated by one of the two terminal oxygen atoms of each $\{AsO_4\}$ group. Such structural features are not present in Au_4Se_4, thus Au_4Se_4 is found as monomeric species in the solid state and in solution, as demonstrated by combination of XRD, ESI–MS and ^{71}Se NMR techniques.[121]

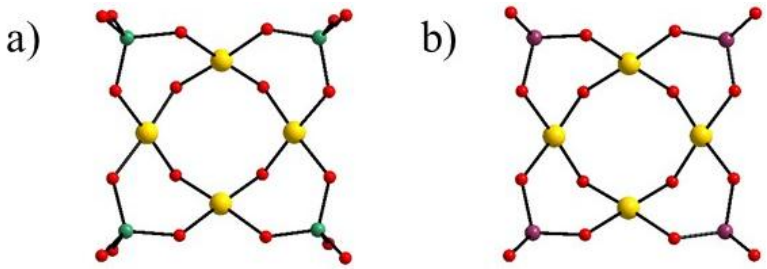

Figure 3.1: Ball–and–stick representation of a) $[Au_4As_4O_{20}]^{8-}$; b) $[Au_4Se_4O_{20}]^{4-}$. Au = yellow, As = green, Se = purple and O = red.

The potential application of Au_4As_4 as a precursor in the formation of hypothetical sandwich type species $[NaM_4Au_8As_8O_{40}]^{q-}$ (M = Pd^{II}, Cu^{II}, Pt^{II} *etc.*), motivated interest in elucidating its solution structure.

The report of Au_4Se_4 allowed comparison of its UV/Vis spectroscopic properties with that of Au_4As_4. The positions of the experimentally measured UV/Vis absorption bands of Au_4As_4 $\lambda_1(Au_4As_4)$ = 403 nm and $\lambda_2(Au_4As_4)$ = 285 nm are very different than those of Au_4Se_4 $\lambda_1(Au_4Se_4)$ = 429 nm and $\lambda_2(Au_4Se_4)$ = 228 nm. Considering the earlier reports on the influence of the

counteractions on the NMR shifts of POMs,[106, 134, 135] we hypothesized that the differences in ion pairing chemistry of Au_4As_4 and Au_4Se_4 with dissolved countercations may be the origin of the differences in the observed UV/Vis spectra.

In order to solve this problem we used the time–dependent density functional theory (TD–DFT) method. Prior addressing the above hypothesis, it was crucial to allocate a theoretical level and spectroscopic range at which we could reliably calculate the wavelengths of the two main absorption bands for Au_4As_4 and Au_4Se_4 (Figure 3.2). The molecular models were designed considering the synthesized salts (Figure 3.3). *i.e.* bare polyanions Au_4As_4 and Au_4Se_4 and ion pairs of countercations and polyoxoanions: $[KAu_4Se_4O_{16}]^{3-}$ (KAu_4Se_4), $[NaAu_4As_4O_{20}]^{7-}$ ($NaAu_4As_4$), $[Na_5Au_4As_4O_{20}]^{3-}$ ($Na_5Au_4As_4$), $[Na_5Au_8As_8O_{40}]^{11-}$ ($Na_5Au_8As_8$).

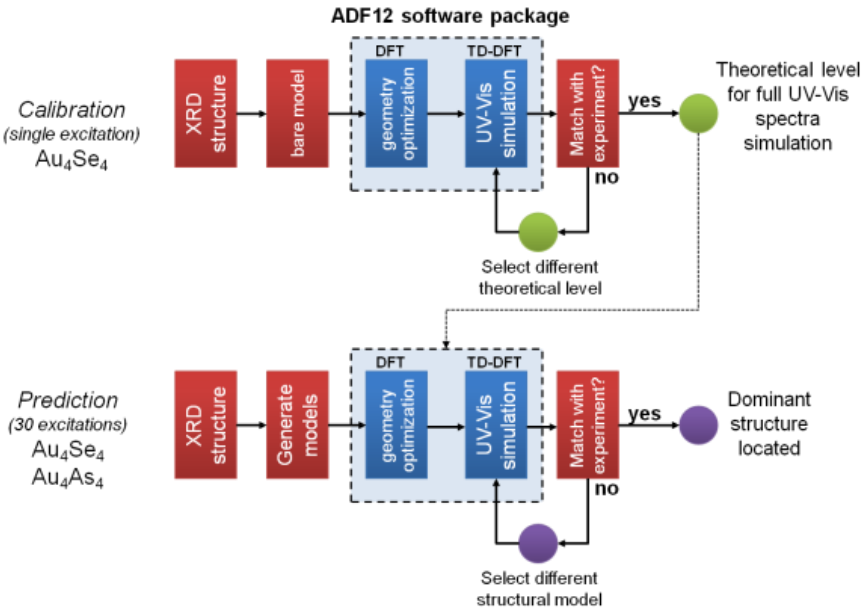

Figure 3.2: Flowchart depicting the approach applied in this work.

Following the approach of Bagno *et al.* on the study of $[W_6O_{19}]^{2-}$,[127] we calculated the first excitation of preoptimized bare Au_4S_4 using GGA, meta–GGA, hybrid and meta–hybrid, long range corrected functionals and on HF level. Best estimation is achieved by the M06 meta–hybrid functional, using triple zeta polarized (TZP) and triple zeta doubly–polarized (TZ2P) basis sets. Due to the higher computational cost of TZ2P, spectra calculations are performed with TZP basis set.

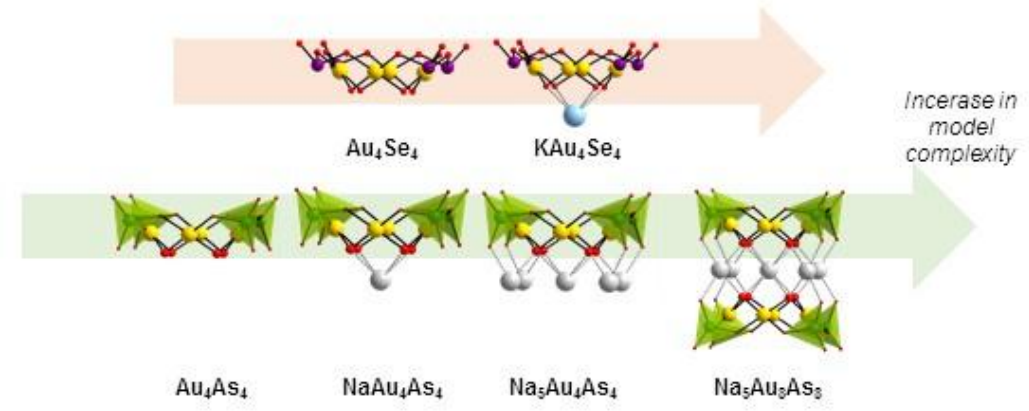

Figure 3.3: Combined polyhedra and ball–and–stick representation of Au_4Se_4 and KAu_4Se_4 (top), Au_4As_4, $NaAu_4As_4$, $Na_5Au_4As_4$ and $Na_5Au_8As_8$ (bottom). {AsO_4} = green tetrahedra, Au = yellow, As = green, Se = purple and O = red.

The calculated spectra of Au_4Se_4 and KAu_4Se_4 models predict well the positions of the first UV/Vis absorption (maxima at 432 nm and 423 nm respectively) and shoulder at about 300 nm. In both models, the calculated second UV/Vis absorption is with lower accuracy (maximum at 249 nm). This can be related to the limitations of the TD–DFT approach to provide reliable predictions of excitations which approach the ionization threshold of the polyanion

The calculated spectrum of Au_4As_4 (maxima at 425 nm and 257 nm) exhibits similar features as the one of Au_4Se_4, and therefore cannot account for the observed spectrum. $NaAu_4As_4$ model improves the position of the first absorption in comparison to experiment, however it does not affect significantly the position of the second absorption (maxima at 405 nm and 262 nm). The second absorption is better estimated in $Na_5Au_4As_4$, but this also affects the position of the first excitation which appears in the UV region (maxima at 384 nm and 285 nm). Best agreement is achieved by the "sandwich" model $Na_5Au_8As_8$ (maxima at 403 nm and 277 nm) (See Figure 3.4).

In collaboration with Dr. Hampe and coworkers, electrospray mass spectrum (ESI–MS) was recorded, revealing a main m/z peak at 979.32 corresponding to $H_8[Na_5Au_8As_8O_{40}]^{3-}$.

As TD–DFT is computationally more demanding than ground–state DFT, its current application is limited to small and symmetric POMs (see Chapter 1.5). Computation of the first 30 excitations of $Na_5Au_4As_4$ requires 7–10 days on the current CLAMV supercomputer resources,[200] using 6 nodes with 12 processors and memory up to 128 GB. With the development of faster computer

technology and more efficient quantum mechanical codes it is expected that accurate calculation of the UV/Vis POM spectra will be accessible in near future.

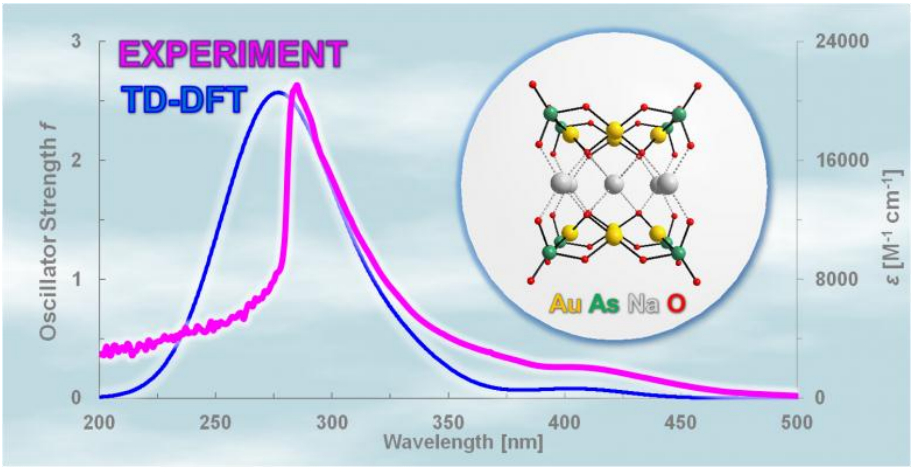

Figure 3.4: Experimental (purple line) of the dissolved sodium salt of $[Au_4As_4O_{20}]^{8-}$ in water, and TD–DFT calculated (blue line) of the $[Na_5Au_8As_8O_{40}]^{11-}$ model in aqueous medium.

This work has been published as:

How Counterions Affect the Solution Structure of Polyoxoaurates: Insights from UV/Vis Spectral Simulations and Electrospray Mass Spectrometry
A. Kondinski, N. Vankova, F. Schinle, P. Jäger, O. Hampe, U. Kortz, T. Heine Eur. J. Inorg. Chem. (2014) 3771–3778. (DOI: 10.1002/ejic.201402494)
Online link: http://onlinelibrary.wiley.com/doi/10.1002/ejic.201402494/abstract

Towards this work, I have contributed with performing the DFT and TD–DFT calculations, the documentation of the calculations and in the preparation of the first draft of the manuscript. The work presented in this section has inspired further investigations of the binding of countercations towards polyoxoaurates.[224]

Chapter 4: Elucidation of the Structure of the Mixed Gold(III)–Palladium(II) Polyoxo–noble–metalate $[NaAu_4Pd_8As_8O_{40}]^{11-}$

Mixed–addenda POMs are of a fundamental research interest as their electronic and spectroscopic properties are tuned by the ratio of the incorporated metal centers and the positional isomerism. In this chapter the focus in on the first mixed gold(III)–palladium(II)–oxo cluster with formula $[NaAu_4Pd_8As_8O_{40}]^{11-}$ ($NaAu_4Pd_8As_8$) and on its positional isomerism problem.

By simple modification of the synthetic conditions developed by Kortz *et al.* for formation and isolation of $[Au_4As_4O_{20}]^{8-}$, it was found that a new polyoxoanion with formula $[NaAu_4Pd_8As_8O_{40}]^{11-}$ can be formed and isolated. [102, 109] Elemental analysis and XRD studies provided the information that the respective Au^{III}:Pd^{II} atom ratio in $[NaAu_4Pd_8As_8O_{40}]^{11-}$ is 4:8. However these techniques could not allocate the respective positions of Au^{III} and Pd^{II} within the metal–oxo cluster. This motivated application of theoretical techniques in elucidating the structural and the electronic properties of $[NaAu_4Pd_8As_8O_{40}]^{11-}$. After the most stable configurations of Au^{III} and Pd^{II} in $[NaAu_4Pd_8As_8O_{40}]^{11-}$ are allocated, isomers with these noble metal configurations are used to predict their spectroscopic properties.

Prior performing any calculation, it was necessary to define the complete set of positional isomers that describe $[NaAu_4Pd_8As_8O_{40}]^{11-}$. In this respect, by ignoring the overall symmetry of the system, one can generate a total number of *C* structures using the combinatorial formula:

$$C = \frac{n!}{r!\,(n-r)!} \tag{4.1}$$

In the above equation, *n* is the total number of addenda centers and *r* is the number of Au^{III} substituting centers. This formula yields 495 structural combinations for four Au^{III} and eight Pd^{II} atoms. Considering that the structural framework describing the mixed–addenda POM $[NaM_{12}As_8O_{40}]^{q-}$ is highly symmetrical (O_h), one can conclude that within these 495 structural combinations there are many degeneracies. In order to effectively reduce the number of degenerate structures, without excluding particular isomers, one can consider a point of reference, *i.e.* a single

occupied position with Au^{III}. In this case *n* and *r* are reduced to 11 and 3 respectively, which yields 165 structural combinations.

The 165 combinations can be easily generated by an online software or a spreadsheet program (*e.g.* Microsoft Excel). The numerical combinations can be translated into a 2D graph as shown in Figure 4.1. The grouping of these 165 structural combinations into original isomers was performed manually. The process yields 18 positional isomers (including only one isomer from a pair of enantiomers), which is in agreement with the Pólya enumeration theory for a cuboctahedral network with 4:8 occupancies.[225]

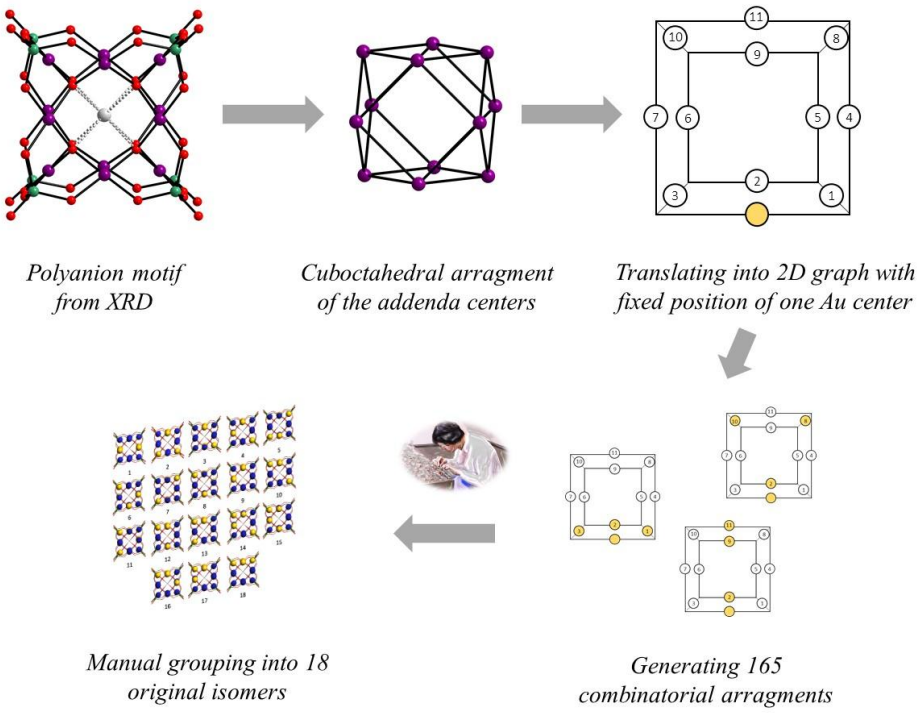

Figure 4.1: The steps involved in the generation of the 18 positional isomers of $[NaAu_4Pd_8As_8O_{40}]^{11-}$ beginning with the polyanion motif obtained from XRD where Au and Pd atoms are indistinguishable (Au/Pd = purple, O = red, As = green and Na = grey), representation of the isomer problem of the cuboctahedral noble core with 2D graph, inscription of the 165 combinations and their grouping in 18 original isomers.

The reader may recall that in chapter 1.3.4 it was noted that the Keggin type α–$[XM'_4M_8O_{40}]^{q-}$ has 27 positional isomers (see Table 1.1.).[62] The reason why $[NaAu_4Pd_8As_8O_{40}]^{11-}$ exhibits less isomers is due to the symmetry of (12)–polyoxonoble–metalate motif $[NaM_{12}As_8O_{40}]^{q-}$ (O_h), which is higher than that of α–$[XM_{12}O_{40}]^{q-}$ (T_d).

The geometries of the eighteen isomers were then submerged to DFT optimizations. TD–DFT calculations of the most stable $NaAu_4Pd_8As_8$_1 and $NaAu_4Pd_8As_8$_2 and the least stable isomer $NaAu_4Pd_8As_8$_18 were performed on the same level as the geometry optimization. The IR spectra of the former three isomers was also calculated.

On the basis of the bonding and the HOMO–LUMO gap energies, it was found that the isomer $NaAu_4Pd_8As_8$_1 (D_{4h}) (Figure 4.2.a) and $NaAu_4Pd_8As_8$_1 (D_{2d}) (Figure 4.2.b) have highest stabilities. In $NaAu_4Pd_8As_8$_1 the four gold atoms and the central sodium cation are in one plane that is sandwiched between two virtual $\{Pd^{II}_4O_4(AsO_4)_4\}$ moieties. In $NaAu_4Pd_8As_8$_2, the four Au^{III} centers are arranged in a tetrahedral fashion around the central sodium cation. Only in these two configurations, each Au^{III} center coordinates to a μ_4–oxo ligand which links to two other Pd^{II} centers and the central sodium cation. Isomers $NaAu_4Pd_8As_8$_1 and $NaAu_4Pd_8As_8$_2 have calculated HOMO–LUMO gap energies of about 1.1 eV and have relative difference in the bonding energies of about 0.7 $kJ \cdot mol^{-1}$. In addition, of a particular interest was isomer $NaAu_4Pd_8As_8$_18 which exhibits C_{4v} point group symmetry (Figure 4.2.c). In this isomer, the four Au^{III} centers are connected by four μ_4–oxo in a circular $\{Au_4O_4\}$ moiety which is capped by four $\{AsO_4\}$ heterogroups. The resulting fragment $\{Au^{III}_4O_4(AsO_4)_4\}$ is reminiscent of the $[Au_4As_4O_{20}]^{8-}$ polyoxoanion. Isomer $NaAu_4Pd_8As_8$_18 is about 80 $kJ \cdot mol^{-1}$ higher in bonding energy than isomers $NaAu_4Pd_8As_8$_1 and $NaAu_4Pd_8As_8$_2 and has calculated HOMO–LUMO gap energy of only 0.18 eV.

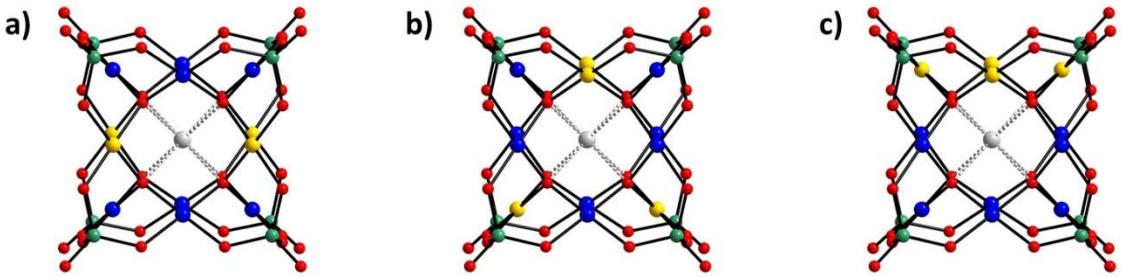

Figure 4.2: Ball–and–stick representation of three $[NaAu_4Pd_8As_8O_{40}]^{11-}$ isomers: a) Isomer 1 (D_{4h}); b) Isomer (D_{2d}); c) isomer 18 (C_{4v}). Au = yellow, Pd = blue, O = red, Na = grey, As = green balls.

Calculation of IR spectra predicts a singlet absorption for the stretching mode of the terminal As–O_t bond in isomers $NaAu_4Pd_8As_8$_1 and $NaAu_4Pd_8As_8$_2, however it predicted a doublet absorption for isomer $NaAu_4Pd_8As_8$_18. The experimental spectrum shows only one absorption

corresponding to this stretching mode, indicating that isomers $NaAu_4Pd_8As_8$_1 and $NaAu_4Pd_8As_8$_2 are in a good agreement with experiment.

Electrospray mass spectrometry studies revealed that the redissolved salts of the isolated $[NaAu_4Pd_8As_8O_{40}]^{11-}$ indeed contain the former polyoxoanion, but they showed that polyoxoanions of the type $[NaAu_xPd_{12-x}As_8O_{40}]^{(x-15)}$ (x = 3, 5 and 6) are also present. The complete study on the remaining structures is discussed in Chapter 6.

This work is published as:

The mixed gold–palladium polyoxo–noble–metalate $[NaAu^{III}{}_4Pd^{II}{}_8O_8(AsO_4)_8]^{11-}$

N. V. Izarova, A. Kondinski, N. Vankova, T. Heine, P. Jäger, F. Schinle, O. Hampe, U. Kortz Chemistry Eur. J. 20 (2014) 8556–8560. (DOI: 10.1002/chem.201403032)

Online link: http://onlinelibrary.wiley.com/doi/10.1002/chem.201403032/abstract

To this work I have contributed by performing all calculations, documentation of the data and providing the first draft of the theoretical contribution.

Chapter 5: The Rotational Isomerism Problem in "Fully–Reduced" Heteropolyoxo–(14)–vanadates

Polyoxovanadates (POVs) represent a subclass of POMs. Depending on the oxidation state of the vanadium addenda, POVs can be characterized as "fully oxidized" (*i.e.* all V^{V}), mixed–valence (mostly V^{IV} and V^{V}, but V^{III} as well) and "fully reduced" clusters (V^{IV}).[75, 226] The building units of POVs also can differ in geometry and stochiometry, thus they can be $\{VO_4\}$ tetrahedra, $\{VO_5\}$ trigonal pyramids and $\{VO_6\}$ octahedra.[226]

The cage type polyanions α–$[V_{18}O_{42}]^{12-}$ and β–$[V_{18}O_{42}]^{12-}$ can undergo formal substitution of {VO} square pyramids with hetero moieties L, where L = $\{As_2O\}$, $\{Sb_2O\}$, $\{Si_2O_3\}$, $\{Ge_2O_3\}$ or $\{Ge_2OS_2\}$ (Figure 5.1.a).[75] Substitution of four {VO} with L in α–$[V_{18}O_{42}]^{12-}$ leads to two $\{V_{14}O_{38}L_4\}$ rotational isomers with D_{2d} (α – isomer) and D_{4h} (β – isomer) symmetry. The former two isomers are related to each other by rotation of one $\{V_3O_7L_2\}$ unit to 90°. A survey of the up–to–date known α–/β–$\{V_{14}O_{38}L_4\}$ polyoxoanions is presented in Table 5.1.

Table 5.1: Chronology of synthesis and crystal structure elucidation for semimetal–functionalized *hetero*POVs with general formulas $[V^{IV}{}_{14}E_8O_{50}]^{12-}$ and $[V^{IV}{}_{14}E_8O_{42}X_8]^{12-}$(E = Si^{IV} and Ge^{IV}; X = S) and $[V^{IV}{}_{14}E_8O_{42}]^{4-}$ (E = As^{III} and Sb^{III}).

Isomer type	Group 14 heteroelement	*hetero*POV	Corresponding author (year)
α	Si	$[V_{14}Si_8O_{50}]^{12-}$	Clearfield *et al.* (**2003**)[227]
α	Ge	$[V_{14}Ge_8O_{50}]^{12-}$	Clearfield *et al.* (**2003**)[227]
α	Ge	$[V_{14}Ge_8O_{42}S_8]^{12-}$	Bensch *et al.* (**2006**)[228]
Isomer type	Group 15 heteroelement	*hetero*POV	Corresponding author (year)
α	As	$[V_{14}As_8O_{42}]^{4-}$	Huan *et al.* (**1991**)[229]
β	As	$[V_{14}As_8O_{42}]^{4-}$	Yang *et al.* (**2005**)[230]
α	Sb	$[V_{14}Sb_8O_{42}]^{4-}$	Xu *et al.* (**2004**)[231]
β	Sb	$[V_{14}Sb_8O_{42}]^{4-}$	Xu *et al.* (**2002**)[232]

In this work the novel topology of γ–$\{V_{14}O_{38}L_4\}$ isomer is reported for the first time. This topology can be derived from β–$[V_{18}O_{42}]^{12-}$ by formal substitution of four {VO} moieties with four L The hypothetic γ–$\{V_{14}O_{38}L_4\}$ is related to α–/β–$\{V_{14}O_{38}L_4\}$ by rotation of one $\{V_3O_7L_2\}$ unit for 45°.

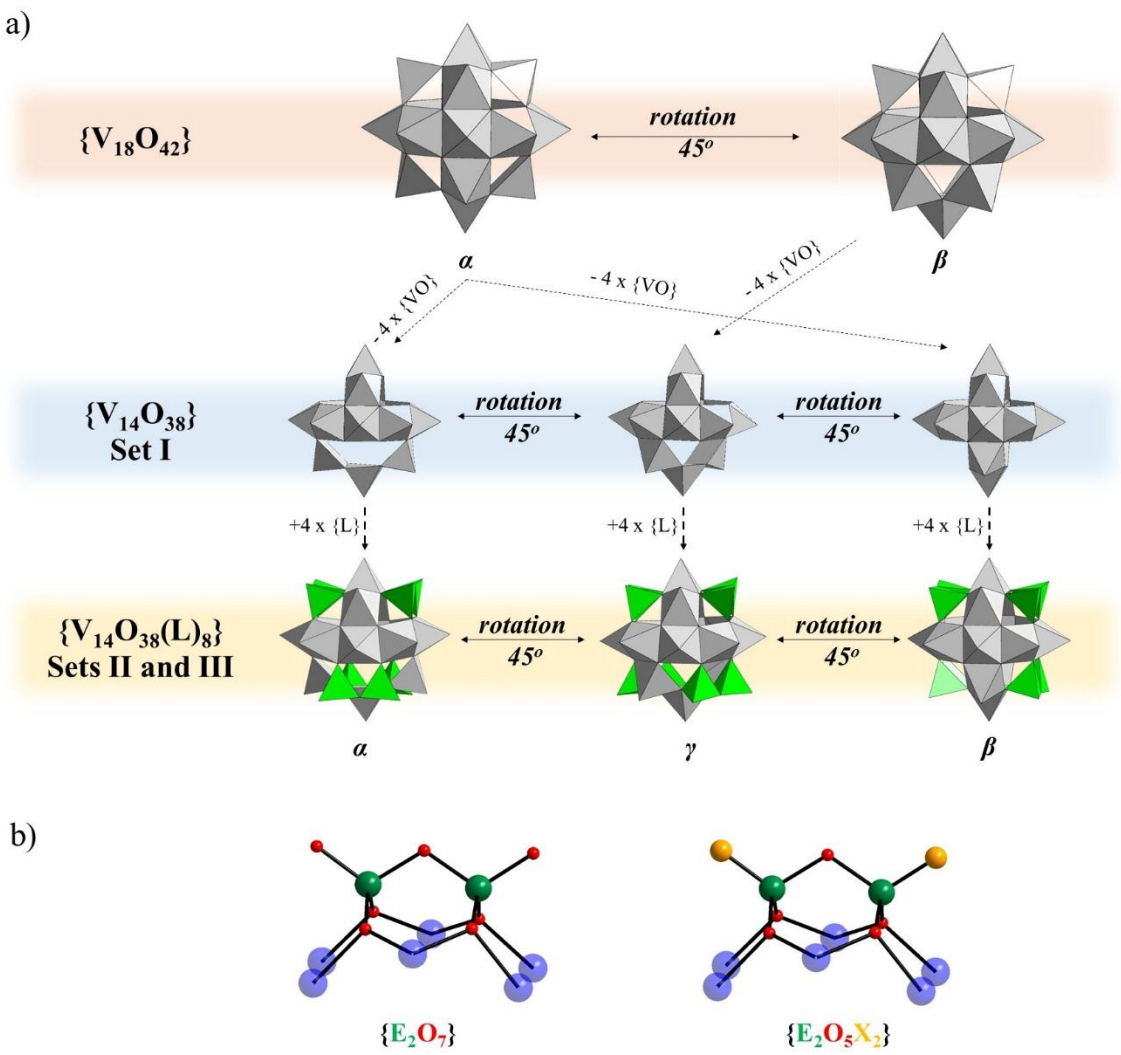

Figure 5.1: Polyhedral and ball and stick representation of: a) *α–/β–*{$V_{18}O_{42}$} (top row) and the derived *α–/β–/γ–*{$V_{14}O_{38}$} (middle row) and *α–/β–/γ–*{$V_{14}O_{38}L_4$} isomers (bottom row); b) The structure of the handle–like moieties {E_2O_7} or {$E_2O_5X_2$}. Color code: {VO_5} = grey square pyramids, {EO_4} or {EO_3X} tetrahedra, V = blue balls, O = red balls, E = green balls and X = yellow balls.

In this work we focus on the investigation of the rotational isomerism, relative stability, electronic and protonation properties of *α–/β–/γ–*$[V_{14}O_{38}]^{20-}$ (**I**), *α–/β–/γ–*$[V_{14}E_8O_{50}]^{12-}$ (**II**) and *α–/β–/γ–*$[V_{14}E_8O_{42}X_8]^{12-}$ **(III)**, where E = Si, Ge and Sn and X = S, Se and Te (Figure 5.1.a). The E atoms construct handle–like moieties {E_2O_7} or {$E_2O_5X_2$} (Figure 5.1.b). In these moieties, the E atoms are connected between each other by one μ_2–(O) ligand and they connect with four μ_3–(O) ligands to the (14)–vanadium(IV)–oxo core. Each {E_2O_7} or {$E_2O_5X_2$} exhibits a pair of terminal O or X atoms.

There are three main motivations to address this system: (*i*) Fully reduced mixed–valence POVs present technical challenges for theoretical studies due to the combination of high negative charge, complicated charge distribution and spin configuration. (*ii*) The outcome of the theoretical results can guide future synthetic efforts. In this respect, practical chemists can benefit from being aware of the intrinsic stabilities and the effect the presence of E and X atoms. (*iii*) Description of the electronic properties and intrinsic stabilities of **II** and **III**, is the first step towards further studies of their magnetisms, possibilities for functionalization with organic moieties and application in functionalization of conducting surfaces.

In order to understand how E and X atoms induce changes in the geometry, we have modeled hypothetical $[V_{14}O_{38}]^{20-}$ (**I**) skeletons (Figure 5.1.a). The effect of the rotational isomerism, E and X atoms on the protonation chemistry was inspected by analysis of the atomic charges, molecular electrostatic potential and by modeling monoprotonated species of *α*–**II** and *α*–**III** at different oxygen sites.

The geometries of **I**, **II** and **III** including the monoprotonated models *α*–**II** and *α*–**III** were submerged to DFT optimization. As all addenda centers in **I**, **II** and **III** are V^{IV} and exhibit single unpaired electron, the current work is limited to ferromagnetically coupled systems, *i.e.* 14 spin up electrons scenario. The calculation of the bonding and electronic properties of the optimized **II** and **III** was performed using the hybrid B3LYP functional.

The study revealed that the geometric parameters defining skeletons **I** are influenced by the E atoms only. On the basis of the relative energies and the HOMO–LUMO energy gaps it was established that the stability of the bare polyoxoanions **II** and **III** decreases in the order $\alpha > \gamma > \beta$. The bonding energy between the *α*– and the *γ*–isomeric **II** and **III** vary from 8 $kJ \cdot mol^{-1}$ to 40 $kJ \cdot mol^{-1}$, while between the *α* and the *β* isomers from 15 $kJ \cdot mol^{-1}$ to 82 $kJ \cdot mol^{-1}$. **II** and **III** exhibit HOMO–LUMO gap energies in the range of 2.9–4.2 eV.

The LUMOs in Si^{IV}– and Ge^{IV}–substituted **II** and **III** are predominantly located on the V^{IV} centers, which suggests that upon reduction vanadium ions can be further reduced. In Sn^{IV}–substituted **II**

and **III** the LUMOs are mainly distributed over the Sn^{IV} centers, which suggests that possibility of two–electron redox reactions involving tin ions (Sn^{IV}–Sn^{II}).

Energetically most favorable sites for monoprotonation of *α*–**II** are the terminal oxygen atoms of the $\{E_2O_7\}$ heterogroups. Most of *α*–**III** exhibit highest proton affinities at the terminal X_t sites of $\{E_2O_5X_2\}$, except for the three *hetero*POVs *α*–$[V_{14}Ge_8O_{42}Te_8]^{12-}$, *α*–$[V_{14}Sn_8O_{42}Se_8]^{12-}$ and *α*–$[V_{14}Sn_8O_{42}Te_8]^{12-}$ which were predicted to show different behavior.

This work has resulted in a prepared manuscript:

Rotational Isomerism, Electronic Structures and Basicity Properties of "Fully–Reduced" V14–type Heteropolyoxovanadates
A. Kondinski, T. Heine, K. Yu Monakhov

The manuscript has been submitted and revised for publication in the American Chemical Society journal Inorganic Chemistry.

Chapter 6: The Positional Isomerism Problem in $[NaAu_xPd_{12-x}O_8(AsO_4)_8]^{x-15}$ and $[NaAu_xPd_{12-x}O_8(SeO_3)_8]^{x-7}$

In this chapter the isomer problem in mixed–addenda $[NaAu_xPd_{12-x}O_8(AsO_4)_8]^{x-15}$ ($NaAu_xPd_{12-x}As_8$) and $[NaAu_xPd_{12-x}O_8(SeO_3)_8]^{x-7}$ ($NaAu_xPd_{12-x}Se_8$) clusters is addressed by using DFT. The work focuses on the electronic properties of the most stable $NaAu_xPd_{12-x}As_8$ and $NaAu_xPd_{12-x}Se_8$ species, their predicted protonation affinities and Na^+ encapsulation energies. The work was motivated by the unknown structural and electronic properties of $NaAu_xPd_{12-x}As_8$ compounds with x = 3, 4 and 6, which are reported in Chapter 4. [109]

The hypothetical families $NaAu_xPd_{12-x}As_8$ (Figure 6.1.a) and $NaAu_xPd_{12-x}Se_8$ (Figure 6.1.b) exhibit cuboctahedral noble metal networks cores. The cuboctahedral addenda cores are also present in *α*–Keggin $[XM_{12}O_{40}]^{n-}$ (Figure 6.1.c) and *α*–$[V_{18}O_{42}]^{12-}$ *i.e.* $[(V_{12}O_{36})(VO)_6]^{n-}$ (Figure 6.1.d). The *α*–Keggin structure is known to form mixed–addenda species of the type $[XM'_xM_{12-x}O_{40}]^{n-}$ (see section 1.3.4), while *α*–$[V_{18}O_{42}]^{12-}$ to form heterogroup–substituted species of the type *α*–$[(V_{12-x}O_{36-5x})(E_2O_7)_x(VO)_6]^{n-}$and *α*–$[(V_{12-x}O_{36-5x})(E'_2O_5)_x(VO)_6]^{n-}$(see Chapter 5).

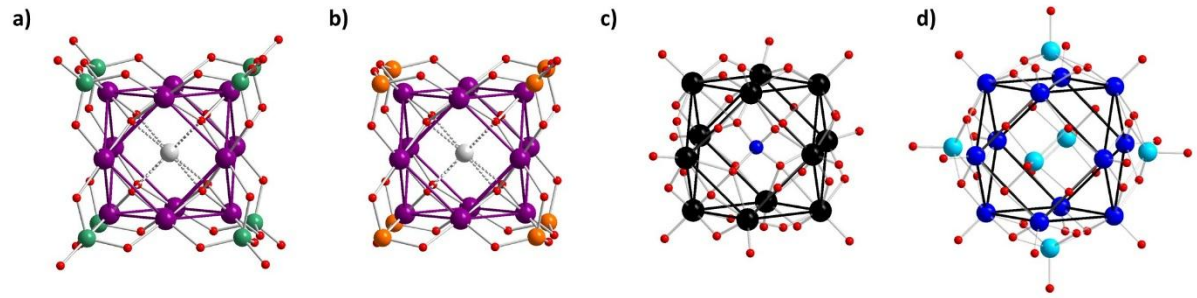

Figure 6.1: Ball–and–stick representation of the cuboctahedra cores in a) $[NaAu_xPd_{12-x}O_8(AsO_4)_8]^{x-15}$ b) $[NaAu_xPd_{12-x}O_8(SeO_3)_8]^{x-7}$ c) $[XM_{12}O_{40}]^{n-}$ d) $[(V_{12-x}O_{36-5x})(E_2O_7)_x(VO)_6]^{n-}$and $[(V_{12-x}O_{36-5x})(E'_2O_5)_x(VO)_6]^{n-}$. Color code: Au/Pd = purple, O = red, Na) grey, As = green, Se = Brown, M = black, V = blue/cyan.

All $NaAu_xPd_{12-x}As_8$ isomers in this study were generated manually using the approach described in chapter 4. Application of Pólya enumeration theory[225] renders the total positional isomer set of each of these families up to 144 structures (Figure 6.1.a). All of these structures were then submerged to DFT optimization.

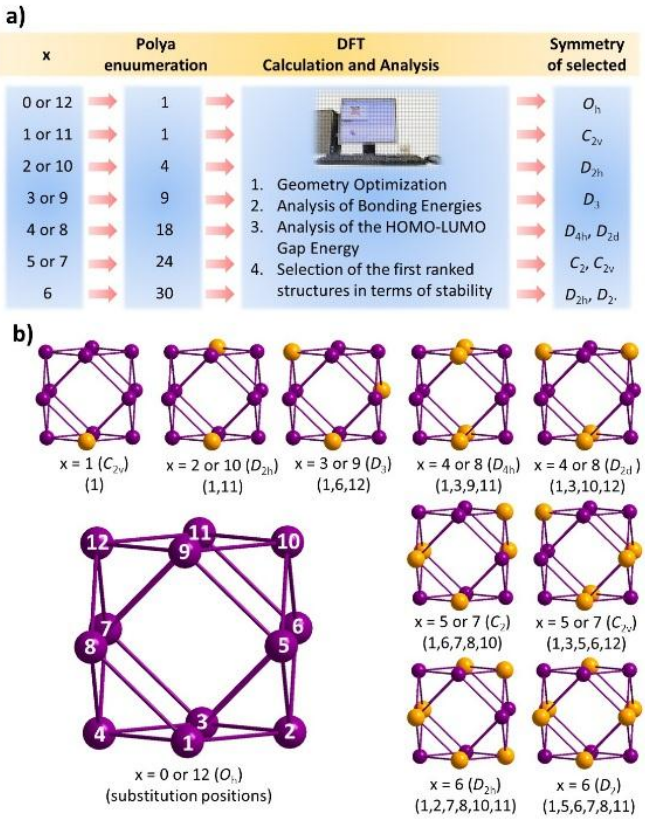

Figure 6.2: a) A scheme of the strategy employed to screen and to narrow the most stable structural configurations of $NaAu_xPd_{12-x}As_8$: b) Large cuboctahedral network enumerating the twelve positions of the noble metal centers and the positions of the most stable isomers of each $NaAu_xPd_{12-x}As$ compositions showing relative occupancies and their notation.

The twelve noble centers of the cuboctahedral network are enumerated from 1–12 (Figure 6.2.b). The isomers with highest stabilities of each Au:Pd ratio typically exhibit high point group symmetries. The substitution positions are shown in Figure 6.1.b and summarized below:

1. For x = 0 and 12 cluster exhibits overall O_h symmetry point group.
2. For x = 1 or 11 the clusters exhibit to C_{2v} point group. This substitution may be considered equivalent to the numerous monosubstituted Keggin type POMs.
3. For x = 2 or 10, we have found that substitution in positions 1 and 11 is most favorable, yielding D_{2h} symmetry. The substitution (1,11) is also presented for the synthesized $[V_{16}As_6O_{42}]^{6-}$ and $[V_{16}Sb_6O_{42}]^{6-}$ (D_{2h}) clusters.[77]

4. For x = 3 or 9, most favorable substitution occurs for positions 1,6 and 12, which leads to overall D_3 symmetry point group. This substitution configuration is similar to that in $[V_{15}As_6O_{42}]^{6-}$ (D_3) cluster. [149, 233]
5. For x = 4 and 8, most stable configurations are (1,3,9,11) and (1,3,10,12). These configurations yield clusters belonging to the D_{4h} and D_{2d} symmetry point groups, respectively. These substitution configurations are reminiscent to the $[V_{14}As_8O_{42}]^{4-}$ (D_{2d}) and β–$[V_{14}As_8O_{42}]^{4-}$ (D_{4h}) structures,[75, 233] while some Mn–substituted Keggin type structural orientation such as $\{H_4Mn_8W_4O_{40}\}$ are present in the center of the $[W_{36}Si_4O_{136}Mn_{10}OH_4]^{14-}$ polyoxoanion.[234]
6. For x = 5 or 7 the first two most stable configurations are (1,6,7,8,10) and (1,3,5,6,12), which belong to the C_2 and C_{2v} symmetry point groups, respectively.
7. For x = 6, the most stable configurations are (1,2,7,8,10,11) and (1,5,6,7,8,11) which belong to D_{2h} and D_2 symmetry point groups.

The differences in the stability are mainly related to the different electronic properties. Pd and Au atoms have similar covalent radii, which does not induce significant geometric differences. This is indicated by the interatomic As···As and Se···Se distances differ only in the pm range. Consequently, within $NaAu_xPd_{12-x}As_8$ and $NaAu_xPd_{12-x}Se_8$ there are many isomers which differ between each other for less than 1 kJ·mol^{-1}. The structural configurations in $NaAu_4Pd_8As_8$ (1,3,9,11) and (1,3,10,12) differ with only 1 kJ·mol^{-1}. For instance, in α–$[V_{14}As_8O_{42}]^{4-}$ and β–$[V_{14}As_8O_{42}]^{4-}$(see Chapter 5) where the substituting heterogroups exert geometric constraints on the $\{V_{14}O_{38}\}$ skeletons, the relative difference in the bonding energy is 37.6 kJ·mol^{-1}. These differences in relative energies can also provide insights why in *hetero*POVs such isomers can be formed and separately isolated, while in mixed noble POMs this is more challenging task.

HOMO–LUMO gap energies of the most stable $NaAu_xPd_{12-x}As_8$ and $NaAu_xPd_{12-x}Se_8$ show maxima for x = 0, 4, 8 and 12 and minima for x = 1 and 11 (Figure 6.3). The HOMO–LUMO gap energies in $NaAu_xPd_{12-x}Se_8$ are *ca.* 0.2 eV higher than those in $NaAu_xPd_{12-x}As_8$. $NaPd_{12}As_8$ and $NaPd_{12}Se_8$ exhibit HOMO–LUMO gap energies of about 1 eV, which is similar to that of $Pd_{13}As_8$ and $Pd_{13}Se_8$.

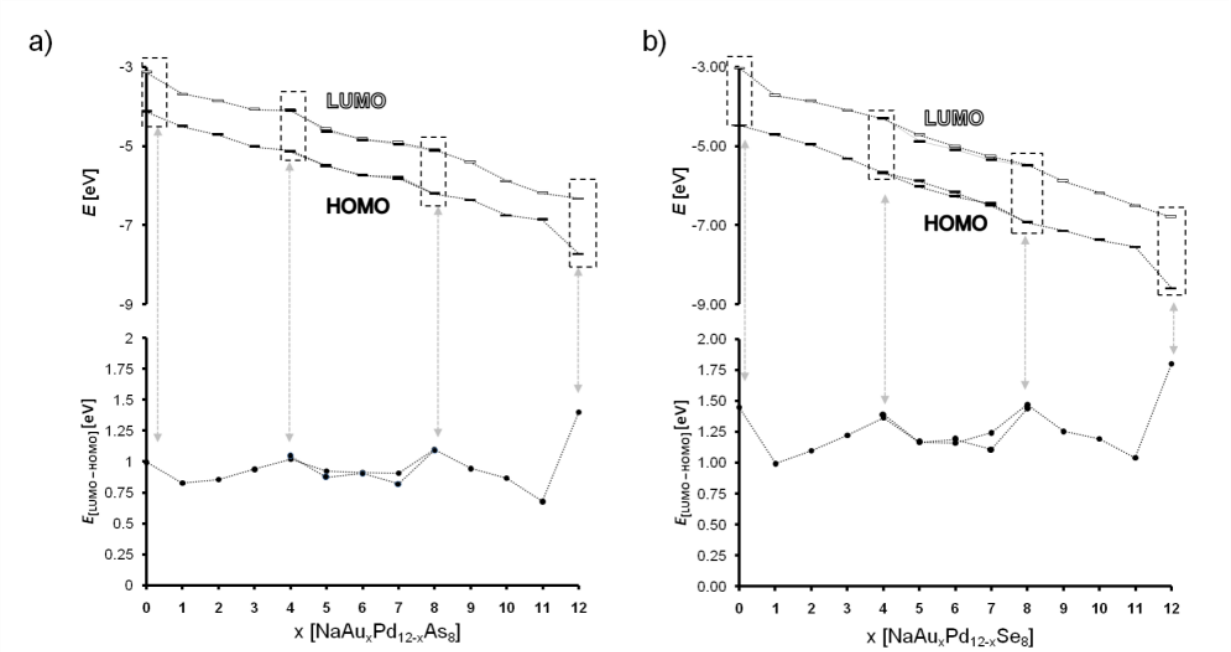

Figure 6.3: HOMO–LUMO gap energy trends of the most stable: a) $NaAu_xPd_{12-x}As_8$; b) $NaAu_xPd_{12-x}Se_8$. For $NaAu_xPd_{12-x}As_8$ and $NaAu_xPd_{12-x}Se_8$ where x = 4 – 8 the two most stable polyoxoanions are depicted.

The protonation affinities of $NaAu_xPd_{12-x}As_8$ and $NaAu_xPd_{12-x}Se_8$ were assessed by probing single proton at different oxygen atoms and then by calculating the enthalpy of the following model reactions:

$$[NaAu_xPd_{12-x}O_8(AsO_4)_8]^{x-15} + H_3O^+ \rightarrow [HNaAu_xPd_{12-x}O_8(AsO_4)_8]^{x-14} + H_2O$$

$$[NaAu_xPd_{12-x}O_8(SeO_3)_8]^{x-7} + H_3O^+ \rightarrow [HNaAu_xPd_{12-x}O_8(SeO_3)_8]^{x-7} + H_2O.$$

The protonation of the bare $[Pd_{13}O_8(AsO_4)_8]^{14-}$ ($Pd_{13}As_8$) and $[Pd_{13}O_8(SeO_3)_8]^{6-}$ ($Pd_{13}Se_8$) structures was also considered in order to evaluate the predicting power of the model equation in respect to experimental observations:

$$[Pd_{13}O_8(AsO_4)_8]^{14-} + H_3O^+ \rightarrow [HPd_{13}O_8(AsO_4)_8]^{13-} + H_2O$$

$$[Pd_{13}O_8(SeO_3)_8]^{6-} + H_3O^+ \rightarrow [HPd_{13}O_8(SeO_3)_8]^{5-} + H_2O$$

$$[Au_{12}O_8(SeO_3)_8]^{4+} + H_3O^+ \rightarrow [HAu_{12}O_8(SeO_3)_8]^{3+} + H_2O.$$

Similarly, the encapsulation energies of single Na^+ cation within virtual host structures were investigated following the model reactions:

(c) $[Au_xPd_{12-x}O_8(AsO_4)_8]^{x-16} + Na^+ \rightarrow [NaAu_xPd_{12-x}O_8(AsO_4)_8]^{x-15}$

(d) $[Au_xPd_{12-x}O_8(SeO_3)_8]^{x-8} + Na^+ \rightarrow [NaAu_xPd_{12-x}O_8(SeO_3)_8]^{x-7}$

Assessment of the protonation and encapsulation enthalpies showed the following observations:

1. The protonation enthalpy for $Pd_{13}As_8$ is –191.1 kJ·mol^{-1}, which suggests strong affinity towards protonation. This polyoanion has been isolated as polyprotonated species.[55]
2. $Pd_{13}Se_8$ and $Au_{12}Se_8$ show protonation enthalpies of 859.2 kJ·mol^{-1} and 71 kJ·mol^{-1} respectively, which suggest no affinity towards protonation. These structures have not been shown to exhibit protonation in the solid state. [2, 114]
3. In the family of $NaAu_xPd_{12-x}As_8$, protonation at all oxygen sites yields positive enthalpies for $NaPd_{12}As_8$ (O_h), $NaAu_4Pd_8As_8$ (D_{4h}) and $NaAu_4Pd_8As_8$ (D_{2d}). The synthesis of the former polyoxoanion occurs at pH 7–8 and these polyoxoanions are isolated are isolated as sodium salts.[109]
4. Protonation of $NaAu_8Pd_4As_8$ (D_{4h}) at the terminal oxygen atoms yields enthalpy of –98.6 kJ·mol^{-1}, which is lowest among $NaAu_xPd_{12-x}As_8$ (x = 7–12). This implies that among $NaAu_xPd_{12-x}As_8$ (x = 7–12), the formation and isolation of $NaAu_8Pd_4As_8$ (D_{4h}) can be facilitated in proton rich environment.
5. $NaAu_xPd_{12-x}Se_8$ (x = 1 and 2) exhibit positive protonation enthalpies, which suggests that they can be potentially isolated in proton poor environments.
6. Encapsulation of Na^+ in $Au_xPd_{12-x}Se_8$ shows has enthalpy of 59.3 kJ·mol^{-1}. In the solid state the reported $Au_{12}Se_8$ does not encapsulate cationic guests.
7. Positive Na^+ encapsulation enthalpies of 50.0 kJ·mol^{-1} are observed also for $Au_{11}PdSe_8$. This suggests that based on the absence of Na^+ and presence of Pd^{II}, one may direct the synthesis towards isolation of the hypothetical $Au_{11}PdSe_8$.
8. Anomalous encapsulation enthalpies in the region $Au_xPd_{12-x}As$ (x = 0 – 6) are observed for $Pd_{12}As_8$ (O_h) and Au_4Pd_8As (D_{4h}) and (D_{2d}), which is an indication that Na^+ can be strongly templating the formation of these clusters in respect to other.

The combination of H^+ and Na^+ directing effects is summarized on Figure 6.4.

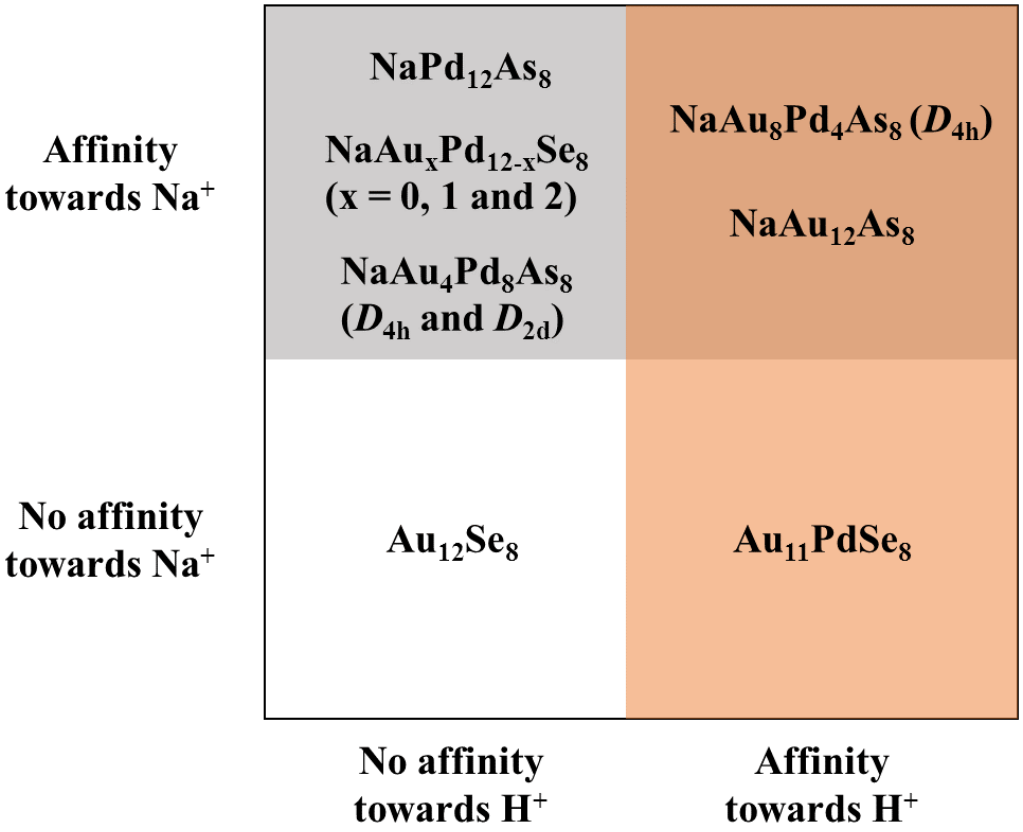

Figure 6.4: A scheme of $NaAu_xPd_{12-x}As_8$ and $NaAu_xPd_{12-x}Se_8$ polyoxoanions which show or do not show affinities towards protonation, encapsulation of sodium cations or combination of affinities.

This work has resulted in a first draft of a manuscript titled:

Emerging structures from a soup of isomers: DFT insights from $[NaAu_xPd_{12-x}O_8(AsO_4)_8]^{x-15}$ *and* $[NaAu_xPd_{12-x}O_8(SeO_3)_8]^{x-7}$

A. Kondinski, N. Vankova, T. Heine.

The manuscript is currently in a preparation phase. My contribution in this work are: performing all calculations, documentation of data and preparation of the current draft of the manuscript.

Chapter 7: Theoretical Description of Dimeric Species Built of M_{11}–Oxo Clusters (M = Pd and W)

This chapter covers theoretical description of polyoxoanions that belong to the domain of noble metal POM chemistry.[10] The polyoxoanions were synthetized and experimentally characterized by the Kortz group. The first project focuses on the study of the novel $[Na_2Pd_{22}As_{16}O_{76}]^{26-}$ polyoxoanion. The second project concerns the diplatinum cores and their interaction with monolacunary α–$[PW_{11}O_{39}]^{7-}$ polyoxoanions.

7.1 The Heteropolyoxo–(22)–palladate

The polyoxoanion $[Na_2Pd_{22}As_{16}O_{76}]^{26-}$ is constructed by square planar $\{PdO_4\}$ and tetrahedral $\{AsO_4\}$ building units. Depending on the reaction conditions (*i.e.* pH and concentration of the precursors of the building units and Na^+ cations), one can direct the synthesis towards formation and isolation of $[Pd_{13}As_8O_{40}]^{14-}$, $[NaPd_{12}As_8O_{40}]^{15-}$ and $[Na_2Pd_{22}As_{16}O_{76}]^{26-}$ (Figure 7.1).

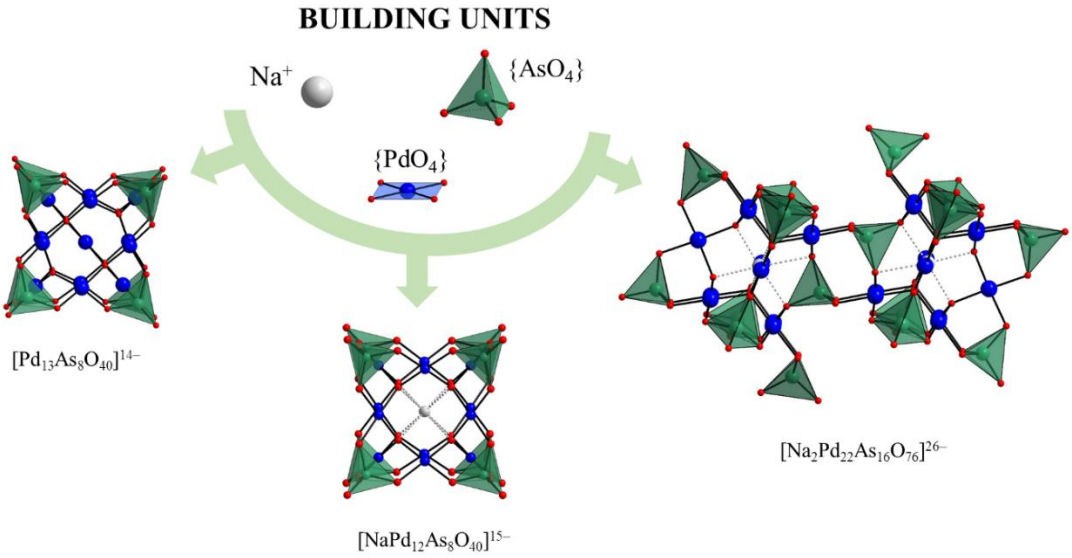

Figure 7.1: Schematic representation of the building blocks involved in the synthesis of $Pd_{13}As_8$, $NaPd_{12}As_8$ and $Na_2Pd_{22}As_{16}$. The compounds are shown in combined polyhedra and ball–and stick representation with $\{AsO_4\}$ = green tetrahedra, As = green, Pd = blue, Na = grey and O = red balls.

The motivation for theoretical study of $[Na_2Pd_{22}As_{16}O_{76}]^{26-}$ in comparison to $Pd_{13}As_8$ was to obtain insights on their relative stabilities. Further on, theoretical study of $Na_2Pd_{22}As_{16}$ can also provide information on the electronic, spectroscopic and electrostatic properties, which can be used to rationalize experimental observations.

$[Na_2Pd_{22}As_{16}O_{76}]^{26-}$ can be viewed as a dimer of two $\{NaPd_{11}As_8O_{38}\}$ fragments. The monomeric $\{NaPd_{11}As_8O_{38}\}$ fragment can be formally derived from $[NaPd_{12}As_8O_{40}]^{15-}$ (Figure 7.2), where one square planar $\{PdO_4\}$ unit is formally substituted by one tetrahedral $\{AsO_4\}$ moiety. The link between the two separate half units is facilitated by substituting μ_4–$\{AsO_4\}$. In this respect the current system represents the first type of a heterogroup–substituted polyoxopalladate. In this respect this system is comparative to *hetero*POVs, where heterogroups substitute {VO} moieties (see Chapter 5).[75]

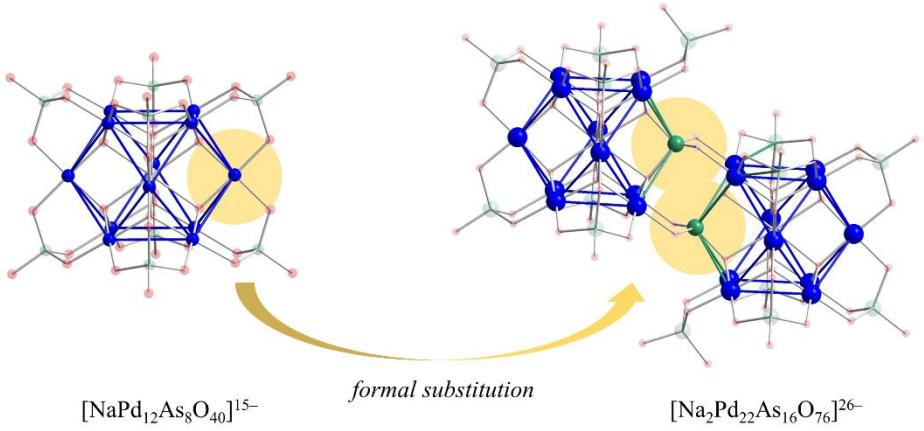

Figure 7.2: Illustration of the formal substitution of an addenda center in $NaPd_{12}As_8$ (left) with a heteroatom As as in and $Na_2Pd_{22}As_{16}$ (right). Color code: As = green, Pd = blue, Na = grey and O = red balls.

First the geometries of $[Na_2Pd_{22}As_{16}O_{76}]^{26-}$ and $[Pd_{13}As_8O_{40}]^{14-}$ were optimized. In order to understand the potential fragmentation of $[Na_2Pd_{22}As_{16}O_{76}]^{26-}$ in solution, the fragments $[Na_2Pd_{22}As_{14}O_{68}]^{20-}$, $[AsO_4]^{3-}$ and $[NaPd_{11}As_8O_{38}]^{13-}$ were also modeled and optimized.

The calculated HOMO–LUMO gap of $[Na_2Pd_{22}As_{16}O_{76}]^{26-}$ is 0.8 eV whereas that of $[Pd_{13}As_8O_{40}]^{14-}$ is 1.0 eV. In both $[Na_2Pd_{22}As_{16}O_{76}]^{26-}$ and $[Pd_{13}As_8O_{40}]^{14-}$ the HOMOs and LUMOs are composed mainly of Pd^{II}–centered *d* atomic, but they differ in respect to their distribution, *i.e.* in $[Na_2Pd_{22}As_{16}O_{76}]^{26-}$ these orbitals are localized over some Pd centers, while in

$[Pd_{13}As_8O_{40}]^{14-}$ they are distributed over all Pd centers. The smaller gap energies and the localized nature of the HOMO and LUMO of $[Na_2Pd_{22}As_{16}O_{76}]^{26-}$, suggests lower solution and electrochemical stability in respect to $Pd_{13}As_8$.

It has been shown that the most negative molecular electrostatic potentials are on the oxygen centers of μ_4–{AsO_4}, which suggests that these sites are strongly prone to protonation. On the other hand, it was found that the fragmentation of $[Na_2Pd_{22}As_{16}O_{76}]^{26-}$ to two units of $[NaPd_{11}As_8O_{38}]^{13-}$ is more favorable, and can explain the instability of the dimeric assembly in solution

This work has resulted in a written manuscript:

The Polyoxo–22–palladate(II), $[Na_2Pd^{II}_{22}O_{12}(As^{V}O_4)_{15}(As^{V}O_3OH)]^{25-}$

N. V. Izarova, Z. Lin, P. Yang, A. Kondinski, N. Vankova, T. Heine, U. Kortz

The article has been accepted for publication by Dalton Transactions (DOI: 10.1039/C5DT04526F)

Online link: http://pubs.rsc.org/en/Content/ArticleLanding/2016/DT/C5DT04526F#!divAbstract

My contribution to this manuscript are the theoretical calculations, documentation of data and preparation of the draft of the theoretical contribution in the final manuscript.

7.2 The *anti*–/*syn*–$[Pt_2(PW_{11}O_{39})_2]^{10-}$ polyoxoanions

Transition metals in low oxidation state (*e.g.* Cr^{I}, Mo^{II}, Re^{III}, Pt^{III}, Rh^{II} *etc.*) are typically involved in the formation of dinuclear complexes.[235] In the formation of a dimetalic molecule M_2, the five *d* atomic orbitals of the metal atoms interact thus forming five bonding (one σ, two π and two δ) and five antibonding orbitals (one σ^*, two π^* and two δ^*). Due to the strength of interactions, the relative energy of these orbitals increases in the order $\sigma < \pi < \delta < \delta^* < \pi^* < \sigma^*$. The molecular orbital diagrams of dinuclear coordination complexes often are complicated and for detail description one may need to apply theoretical techniques.

Monolacunary POMs, can be applied in the stabilization of dinuclear metal cores. The stabilization of the dinuclear transition metal cores with two monolacunary α–$[PW_{11}O_{39}]^{7-}$ can lead to formation of complexes having one of the following reported topologies:

- **L–M–M–L,** where **L =** lacunary POM: In these types of structures, single transition metal center M is accommodated in the lacuna of the monolacunary POM, while the bridging occurs *via* metal–metal bonds. Depending on the type of metal centers, the orientation of the lacunary sites in respect to one another can be eclipsed or staggered. An example of an eclipsed configuration is reported by in 2009 Sokolov *et al.* who have synthetized $[Re^{III}_2(\alpha$–$PW_{11}O_{39})_2]^{10-}$ (Figure 7.1.a).[236] DFT calculations by Liu in 2011 showed the presence of quadruple bond between the two Re^{III} centers.[237] A staggered configuration has been reported in 1998 by Pope *et al.* who synthesized $[Rh^{II}_2(\alpha$–$PW_{11}O_{39})_2]^{10-}$ (Figure 7.1.b).[238] Between the two Rh^{II} centers there is a single bond as the system exhibits $\sigma^2\pi^4\delta_n{}^4\pi^{*4}$ configuration (where δ_n in a non–bonding molecular orbital).[239]

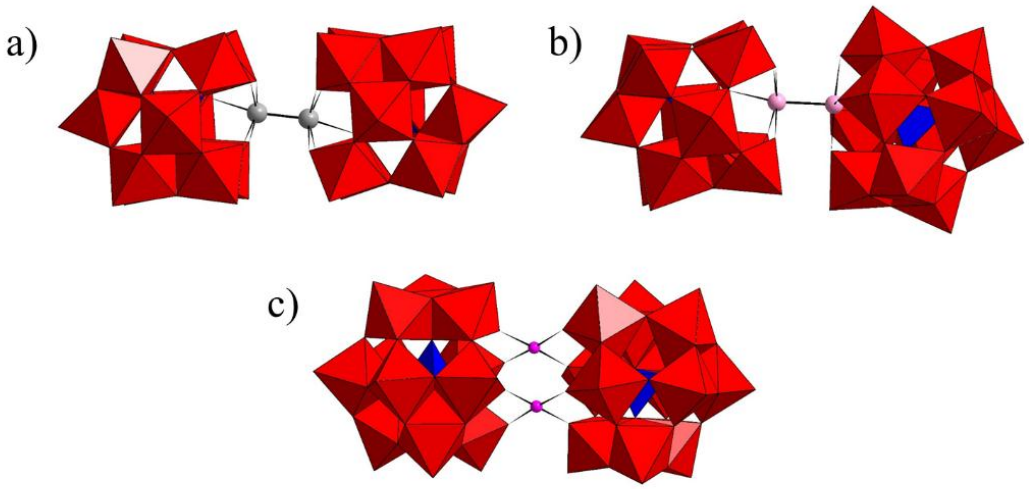

Figure 7.3: Combined polyhedra and ball–and–stick representation of the three types of M_2 connectivity between two α–$[PW_{11}O_{39}]^{7-}$ polyanions: a) Eclipsed metal–metal bonded $\{MO_4L\}$ units where M = Re and L = μ_4(O). b) Staggered metal–metal bonded $\{MO_4L\}$ units where M = Rh and L = μ_4(O). c) Eclipsed metal–metal contacts between $\{MO_4\}$ units where M = Pd^{II} and Pt^{II}. Color code: $\{WO_6\}$ = red octahedra, $\{PO_4\}$ = blue tetrahedra, Re = grey, Rh = pink and Pd/Pt = purple.

- **L–μ_2(M_2)–L** (**L =** lacunary POM): The pair of metal centers is outside the lacuna, while metal center binds to two terminal oxygen atoms from each lacunary POM (Figure 7.1.c).

In these structures, the two M centers may or may not be linked by M–M bond. In 2011 Izarova *et al.* reported the synthesis the stabilization of two Pd^{II} centers by α–$[PW_{11}O_{39}]^{7-}$ units.[240] As both Pd^{II} in square planar coordination have filled atomic d_{z^2} atomic orbitals, interaction between them will not result in M–M bond formation.

In this work the isomeric L–μ_2(M_2)–L type structure with M = Pt^{II} and L = α–$[PW_{11}O_{39}]^{7-}$ was investigated. The motivation for experimental and theoretical efforts in the area of diplatinum(III) complexes comes from their applications in luminescence.[241,242] In this work two $[Pt_2(PW_{11}O_{39})_2]^{10-}$ isomers depicting cisoidal (*syn*) and transoidal (*anti*) configurations, have been synthesized and characterized by number of experimental techniques. The initial theoretical efforts in studying this system provided insights into the electronic and spectroscopic properties and protonation affinities of *anti*–/*syn*–$[Pt_2(PW_{11}O_{39})_2]^{10-}$. By combination of DFT and electrochemical studies, it is shown that *anti*–/*syn*–$[Pt_2(PW_{11}O_{39})_2]^{10-}$ can undergo two electron oxidation to form hypothetical species with formula *anti*–/*syn*–$[Pt_2(H_2O)(PW_{11}O_{39})_2]^{8-}$ (Figure 7.4). Our DFT results of *anti*–/*syn*–$[Pt_2(H_2O)_2(PW_{11}O_{39})_2]^{8-}$, combining molecular orbital structure and Pt···Pt distances, imply that between the two Pt^{III} centers there is a single Pt–Pt bond.

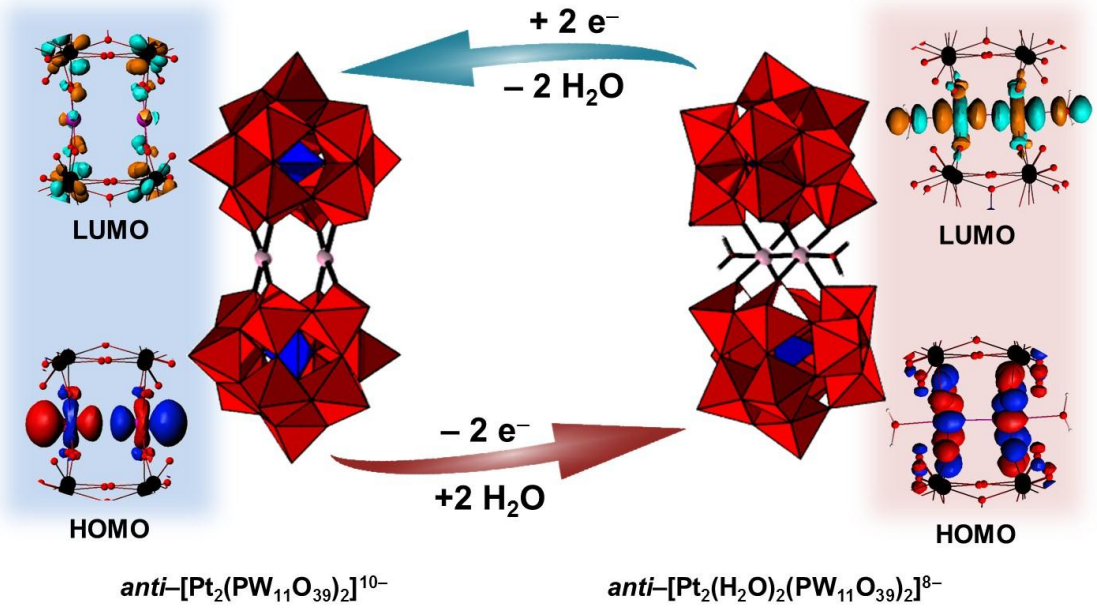

Figure 7.4: Schematic representation of the reversible redox process between the [*anti*–$Pt_2(PW_{11}O_{39})_2]^{10-}$ (left) and *anti*–$[Pt_2(H_2O)_2(PW_{11}O_{39})_2]^{8-}$ (right) polyoxoanions. The HOMOs and LUMOs of the former two polyoxoanions are shown respectively. Color code: {WO_6} = red octahedra, {PO_4} = blue tetrahedra, Pt = purple.

Platinum-Containing Polyoxometalates: syn- and anti-$[Pt^{II}_2(\alpha\text{-}PW_{11}O_{39})_2]^{10-}$ and Formation of the Metal-Metal bonded di-Pt^{III} Derivatives

Z. Lin, N. V. Izarova, A. Kondinski, X. Xing, A. Haider, L. Fan, N. Vankova, T. Heine, B. Keita, J. Cao, C. Hu, U. Kortz

The manuscript has been accepted for publication in Chemistry – A European Journal. To this work I have contributed by performing all calculations, documentation of the results and preparation of the draft of the theoretical section in current manuscript.

Chapter 8: Summary and Outlook

The general conclusions from the work furnished in chapters 3 – 7 are discussed in section 8.1 of this chapter. The emerging applications and follow–up work of this thesis is summarized in section 8.2.

8.1 Summary of the Overall Work

This thesis provided theoretical description on gold(III), palladium(II) and mixed gold(III)/palladium(II) based polyoxonoble–metal clusters. The thesis also addressed conventional POMs such as the isomeric $\{V_{14}\}$–*hetero*POVs and the isomeric platinum functionalized POMs. Considering the similar cuboctahedral network of the addenda centers, mixed–addenda polyoxonoble–metal clusters and heteroPOVs were shown to have similar virtual substitution patterns resulting in clusters with highest intrinsic stabilities.

Chapter 3: *The Solution Structure of Polyoxoaurates: Insights from UV/Vis Simulations and Electrospray Mass Spectrometry*

The interaction of the polyoxoaurates with their environment was investigated using a combination of UV/Vis spectroscopy, TD–DFT and ESI–MS. By probing different models of $[Au_4As_4O_{20}]^{8-}$ and calculating their UV/Vis spectra, it was found that the dimer model $[Na_5Au_8As_8O_{40}]^{11-}$ (D_{4h}) can best account for the observed UV/Vis spectral features. During the ESI–MS experiment, an intense *m*/*z* signal corresponding to the dimeric species was recorded.

Chapter 4: *Elucidation of the Structure of the Mixed Gold(III)–Palladium(II) Polyoxo–noble–metalate* $[NaAu_4Pd_8As_8O_{40}]^{11-}$

Largest HOMO–LUMO gap energies and lowest bonding energies among the eighteen isomers of $[NaAu_4Pd_8As_8O_{40}]^{11-}$ ($NaAu_4Pd_8As_8$) were exhibited by the highly mixed isomers $NaAu_4Pd_8As_8$_1 (D_{4h}) and $NaAu_4Pd_8As_8$_2 (D_{2d}), which indicated that these are structures with highest intrinsic stabilities. The calculated IR and UV/Vis spectra of $NaAu_4Pd_8As_8$_1 and $NaAu_4Pd_8As_8$_2 were shown to provide good description of the experimentally observed spectrum.

Chapter 5: *The Rotational Isomerism Problem in "Fully–Reduced" Heteropolyoxo–(14)–vanadates*

On the basis of bonding and HOMO–LUMO gap energies it was shown that the stability of the isomeric $[V_{14}O_{38}]^{20-}$ (**I**), $[V_{14}E_8O_{50}]^{12-}$ (**II**) and $[V_{14}E_8O_{42}X_8]^{12-}$ (**III**) (E = Si, Ge and Sn; X = S, Se and Te) increased in the order β (least stable) < γ < α (most stable). The nature of the E atoms were found to have major impact on the geometric features and on the relative energy difference between α, γ and β isomers of a fixed composition. X atoms were shown to have major role in defining the nature of the HOMOs and LUMOs (and thus the HOMO–LUMO gap energies) and in determining the electrostatic and protonation chemistry of the different clusters.

Chapter 6: *Positional Isomerism in* $[NaAu_xPd_{12-x}O_8(AsO_4)_8]^{x-15}$ *and* $[NaAu_xPd_{12-x}O_8(SeO_3)_8]^{x-7}$

On the basis of the bonding and HOMO–LUMO gap energies of $[NaAu_xPd_{12-x}As_8O_{40}]^{(x-15)}$ it was shown that for a fixed value of x (where x = 2 – 10), stability gradually increases as the distribution of Au^{III} and Pd^{II} within the cluster becomes homogeneous and obtains high symmetries. The most stable isomers with x = 2 – 10 exhibit the following symmetry point groups: (*i*) x = 2 or 10 yields D_{2h}; (*ii*) x = 3 or 9 yields D_3; (*iii*) x = 4 or 8 yields D_{4h} or D_{2d}; (*iv*) x = 5 or 7 yields C_2 or C_{2v}; (*v*) x = 6 yields D_2 or C_{2h}. For x = 0 or 12 and of x = 1 or 11 only single type species is present belonging to O_h and C_{2v} point group respectively. From the most stable configurations of $[NaAu_xPd_{12-x}As_8O_{40}]^{(x-15)}$ and $[NaAu_xPd_{12-x}Se_8O_{32}]^{(x-7)}$, highest HOMO–LUMO gap energies are obtained for x = 0, 4, 8 and 12 clusters and lowest for x = 1 and 11.

Chapter 7: *Examples of Interplay of Theory and Experiment in Noble Metal POM Chemistry*

The Heteropolyoxo–(22)–palladate: The comparative theoretical description of $[Na_2Pd_{22}As_{16}O_{76}]^{26-}$ and $[Pd_{13}As_8O_{40}]^{14-}$ shed light into their electronic and electrostatic properties and on the origin of their different solution and electrochemical stabilities. The proposed solution fragmentation pathway of $[Na_2Pd_{22}As_{16}O_{76}]^{26-}$ narrows the m/z window for future ESI–MS studies.

The *anti–/syn–*$[Pt_2(PW_{11}O_{39})_2]^{10-}$: The study the electronic and spectroscopic properties of the isomeric *anti–/syn–*$[Pt_2(PW_{11}O_{39})_2]^{10-}$ showed that both isomers have very similar intrinsic stabilities which explain their simultaneous formation in solution. The study revealed a potential

two electron oxidation of *anti*–/*syn*–$[Pt_2(PW_{11}O_{39})_2]^{10-}$ to the proposed *anti*–/*syn*–$[Pt_2(H_2O)_2(PW_{11}O_{39})_2]^{8-}$ species.

8.2 Outlook

8.2.1 UV/Vis Spectra Prediction in the Engineering of Novel and Functional POM Materials

The reported studies by Bagno *et al.* and us, demonstrate the strength of TD–DFT in accurate prediction of the UV/Vis spectra of polyoxoaurates and polyoxotungstates.[122, 127] Considering this, we currently apply the obtained experience to follow the properties of novel $[Au_nO_n(SeO_3)_n]^{n-}$ (n = 3, 4, 5 and 6) polyoxoanions and various types platinum functionalized monolacunary POMs such as $[Pt^{II}_2(L)_2]^{q-}$ and $[Pt_2(H_2O)_2(L)_2]^{(q-2)-}$ (where L = $\{M_5O_{18}\}$, $\{XM_{11}O_{39}\}$ and $\{X_2M_{17}O_{61}\}$; M = Mo, W and X = P^V, As^V, Si^{IV} and Ge^{IV}).

8.2.2 Systematic Study of Mixed–Addenda and Heterogroup–substituted POM Materials

Following the studies in Chapters 4 – 6 the relative stabilities in the Müller's *hetero*POV family *α*–$[V_{18-x}(As_2O)_xO_{42-x}]^{(2x-12)}$ can be further investigated.[233] Further on, theoretical investigations will be focused on the mixed–addenda type species *α*–$[V_{18-x}M_xO_{42}]^{q-}$ and *α*–$[M'_xM_{12-x}O_{40}]^{q-}$.

The current study addressed POMs with inner cuboctahedral arrangement of the addenda centers. In near future, one can further examine POMs with addenda networks other than cuboctahedra such as the mixed–addenda *β*–Keggin type $[M'_xM_{12-x}O_{40}]^{q-}$ and the heterogroup–substituted *β*–$[V_{18-x}(E'_2O)_xO_{42-x}]^{(2x-12)}$ (E' = As and Sb) species.

References

(1) Pope, M. T. In *Polyoxometalate Molecular Science*; Borrás–Almenar, J. J., Coronado, E., Müller, A. Pope, M. T., Eds.; Springer Netherlands: 2003; Vol. 98, pp 3–31.

(2) Büchner, O. Münzmetalle mit und in komplexen Anionen: Synthese, Struktur und Eigenschaften. Ph.D., Thesis, Carl von Ossietzky Universität Oldenburg, Oldenburg, 2005.

(3) Logemann, C.; Wickleder, M. S. *Z. Anorg. Allg. Chem.* **2014**, *640 (11)*, 2346–2346.

(4) Jones, P. G.; Sheldrick, G. M.; Schwarzmann, E.; Vielmäder, A. *Z. Naturforsch. B Chem. Sci.* **1983**, *38(1)*, 10–11.

(5) Jones, P. G.; Schwarzmann, E.; Sheldrick, G. M.; Timpe, H. *Z. Naturforsch. B Chem. Sci.* **1981**, *36(8)*, 1050–1052.

(6) Müller, A.; Peters, F.; Pope, M. T.; Gatteschi, D. *Chem. Rev.* **1998**, *98*, 239–271.

(7) Miras, H. N.; Yan, J.; Long, D.; Cronin, L. *Chem. Soc. Rev.* **2012**, *41*, 7403–7430.

(8) Long, D.; Tsunashima, R.; Cronin, L. *Angew. Chem. Int. Ed.* **2010**, *49*, 1736–1758.

(9) Michel, F. M.; Ehm, L.; Antao, S. M.; Lee, P. L.; Chupas, P. J.; Liu, G.; Strongin, D. R.; Schoonen, M. A. A.; Phillips, B. L.; Parise, J. B. *Science* **2007**, *316*, 1726–1729.

(10) Izarova, N. V.; Pope, M. T.; Kortz, U. *Angew. Chem. Int. Ed.* **2012**, *51*, 9492–9510.

(11) Nyman, M.; Burns, P. C. *Chem. Soc. Rev.* **2012**, *41*, 7354–7367.

(12) Soderholm, L.; Almond, P. M.; Skanthakumar, S.; Wilson, R. E.; Burns, P. C. *Angew. Chem. Int. Ed.* **2008**, *47*, 298–302.

(13) Hillebrand, W. F.; Merwin, H. E.; Wright, F. E. *Proc. Am. Phil. Soc.* **1914**, *53*, 31–54.

(14) Evans, H. T., Jr.; Konnert, J. A. *Am. Mineral.* **1978**, *63*, 863–868.

(15) Hervé, A. G.; Tézé, A.; Contant, R. In *Polyoxometalate Molecular Science*; Borrás–Almenar, J. J., Coronado, E., Müller, A. Pope, M. T., Eds.; Springer Netherlands: **2003**; *98*, pp 33–54.

(16) Pope, M. T. In *Heteropoly and Isopoly Oxometalates;* Jorgensen, C. K., Lappert, M. F., Lippard, S. J., Margrave, J. L., Niedenzu, K., Nöth, H., Parry, R. W., Yamatera, H., Eds.; Inorganic Chemistry Concepts; Springer–Verlag Berlin Heidelberg: 1983; pp 227.

(17) Liu, T.; Diemann, E.; Mueller, A. *J. Chem. Educ.* **2006**, *84*, 526–532.

(18) Gouzerh, P.; Che, M. *Actual. Chim.* **2006**, *298*, 9–22.

(19) Berzelius, J. J. *Pogg. Ann.* **1826**, *6*, 369–380.

(20) Marignac, C. *C. R. Acad. Sci.* **1862**, *55*, 888.

(21) Baker, L. C. W.; Glick, D. C. *Chem. Rev.* **1998**, *98*, 3–49.

(22) Brock, W. H. In *The Norton History of Chemistry;* Porter, R., Ed.; Norton History of Science; WW Norton & Co Inc.; 1993.

(23) Nyholm, R. S. *J. Chem. Educ. ,* **1956**, *34 (4)*, 166–169.

(24) Pauling, L. *J. Am. Chem. Soc.* **1929**, *51*, 2868–2880.

(25) Pauling, L. Letter from Linus Pauling to W.L. Bragg. October 22, 1928. *http://scarc.library.oregonstate.edu/coll/pauling/bond/corr/corr30.1–lp–bragg–19281022–transcript.html* (accessed 12/11, 2015).

(26) Keggin, J. F. *Nature* **1933**, *132*, 351.

(27) Keggin, J. F. *Proc. R. Soc. A* **1934**, *144*, 75–100.

(28) Bradley, A. J.; Illingworth, J. W. *Proc. R. Soc. A* **1936**, *157*, 113–131.

(29) Illingworth, J. W.; Santos, J. A. *Nature* **1934**, *134*, 971.

(30) Illingworth, J. W.; Keggin, J. F. *J. Chem. Soc.* **1935**, 575–580.

(31) Jahr, K. F. *Naturwissenschaften* **1941**, *29*, 505–514.

(32) O'Daniel, H. *Z. Kristallogr. , Kristallgeom. , Kristallphys. , Kristallchem.* **1942**, *104*, 225–227.

(33) Nekrasov, B. V. *Zh. Obshch. Khim.* **1941**, *11*, 373–375.

(34) Ivanov–Emin, B. N. *Zh. Obshch. Khim.* **1940**, *10*, 826–830.

(35) Signer, R.; Gross, H. *Helv. Chim. Acta* **1934**, *17*, 1076–1080.

(36) Anderson, J. S. *Nature* **1937**, *140*, 850.

(37) Lindqvist, I. *Ark. Kemi* **1950**, *2*, 325–341.

(38) Evans, H. T.,Jr *J. Am. Chem. Soc.* **1948**, *70*, 1291–1292.

(39) Wells, A. F. *Philos. Mag. (1798–1977)* **1940**, *30*, 103–134.

(40) Lindqvist, I. *Nova Acta Regiae Soc. Sci. Upsal.* **1950**, *15*, 22.

(41) Greenwood, N. N. *Recollections of a Scientist*; Xlibris; **2012**; Vol. 2.

(42) Dawson, B. *Acta Crystallogr.* **1953**, *6*, 113–126.

(43) Lindqvist, I. *Acta Chem. Scand.* **1948**, *2 (1)*, 88–89.

(44) Hansson, A.; Lindqvist, I. *Acta Chem. Scand.* **1949**, *3*, 1430–1436.

(45) Lindqvist, I. *Acta Chem. Scand.* **1950**, *4*, 1066–1074.

(46) Lindqvist, I. *Acta Chem. Scand.* **1950**, *4*, 551–552.

(47) Lindqvist, I. *Acta Crystallogr.* **1950**, *3*, 159–160.

(48) Lindqvist, I. *Acta Crystallogr.* **1952**, *5*, 667–670.

(49) Lindqvist, I. *Ark. Kemi* **1953**, *5*, 247–250.

(50) Pope, M. T. *Eur. J. Inorg. Chem.* **2013**, 1561.

(51) Müller, A.; Beckmann, E.; Bogge, H.; Schmidtmann, M.; Dress, *Angew. Chem. Int. Ed.* **2002**, *41*, 1162–1167.

(52) Ma, X.; Yang, W.; Chen, L.; Zhao, J. *CrystEngComm* **2015**, *17*, 8175–8197.

(53) Bassill, B. S.; Kortz, U. *Z. Anorg. Allg. Chem.* **2010**, *636*, 2222–2231.

(54) Zheng, S.; Yang, G. *Chem. Soc. Rev.* **2012**, *41*, 7623–7646.
(55) Chubarova, E. V.; Dickman, M. H.; Keita, B.; Nadjo, L.; Miserque, F.; Mifsud, M.; Arends, I. W. C. E.; Kortz, U. *Angew. Chem. Int. Ed.* **2008**, *47*, 9542–9546.
(56) Poblet, J. M.; López, X. In *Computational Inorganic and Bioinorganic Chemistry*; Edward, I. S., Robert, A. and King, R. B., Eds.; Wiley & Sons Ltd; 2009; pp 453–466.
(57) López, X.; Carbó, J. J.; Bo, C.; Poblet, J. M. *Chem. Soc. Rev.* **2012**, *41*, 7537–7571.
(58) Vila–Nadal, L.; Mitchell, S. G.; Long, D.; Rodriguez–Fortea, A.; Lopez, X.; Poblet, J. M.; Cronin, L. *Dalton Trans.* **2012**, *41*, 2264–2271.
(59) Mcnaught, A. D.; Wilkinson, A., Eds.; *Compendium of Chemical Terminology– Recommendations, 2nd edn.;* IUPAC Nomenclature Books Series; Blackwell Science: 2000; Vol. 17.
(60) Baker, L. C. W.; Figgis, J. S. *J. Amer. Chem. Soc.* **1970**, *92*, 3794–3797.
(61) Tsigdinos, G. A.; Hallada, C. J. *Inorg. Chem.* **1968**, *7*, 437–441.
(62) Pope, M. T.; Scully, T. F. *Inorg. Chem.* **1975**, *14*, 953–954.
(63) Greenwood, N. N.; Earnshaw, A. *Chemistry of the Elements;* Elsevier; 1997.
(64) Johansson, G. *Acta Chem. Scand.* **1960**, *14*, 771–773.
(65) Bradley, S. M.; Kydd, R. A.; Yamdagni, R. *J. Chem. Soc.* , *Dalton Trans.* **1990**, 413–417.
(66) Baskar, V.; Shanmugam, M.; Helliwell, M.; Teat, S. J.; Winpenny, R. E. P. *J. Am. Chem. Soc.* **2007**, *129*, 3042–3043.
(67) Guo, Y.; Pan, Q.; Wei, Y.; Li, Z.; Li, X. *J. Mol. Struct. (Theochem)* **2004**, *676*, 55–64.
(68) López, X.; Poblet, J. M. *Inorg. Chem.* **2004**, *43*, 6863–6865.
(69) López, X.; Maestre, J. M.; Bo, C.; Poblet, J. *J. Am. Chem. Soc.* **2001**, *123*, 9571–9576.
(70) Zhang, F.; Guan, W.; Zhang, Y.; Xu, M.; Li, J.; Su, Z. *Inorg. Chem.* **2010**, *49*, 5472–5481.
(71) Andre, O. C.; Rustad, J. R.; Casey, W. H. *Dalton Trans.* **2014**, *43*, 14533–14536.
(72) Zhang, F.; Guan, W.; Yan, L.; Zhang, Y.; Xu, M.; Hayfron–Benjamin, E.; Su, Z. *Inorg. Chem.* **2011**, *50*, 4967–4977.
(73) Contant, R.; Thouvenot, R. *Inorg. Chim. Acta* **1993**, *212*, 41–50.
(74) Johnson, G. K.; Schlemper, E. O. *J. Am. Chem. Soc.* **1978**, *100*, 3645–3646.
(75) Monakhov, K. Y.; Bensch, W.; Kögerler, P. *Chem. Soc. Rev.* **2015**, *44*, 8443–8483.
(76) Kiebach, R.; Näther, C.; Bensch, W. *Solid State Sci.* **2006**, *8*, 964–970.
(77) Antonova, E.; Näther, C.; Kögerler, P.; Bensch, W. *Dalton Trans.* **2012**, *41*, 6957–6962.
(78) Jeannin, Y. P. T *Chem. Rev.* **1998**, *98*, 51–76.
(79) Jeannin, Y.; Fournier, M. *Pure Appl. Chem.* **1987**, *59*, 1529–1548.
(80) Klevtsova, R. F.; Yurchenko, E. N.; Glinskaya, L. A.; Detusheva, L. G.; Kuznetsova, L. I. *Zh. Strukt. Khim.* **1981**, *22*, 49–61.
(81) Deng, Q.; Zhang, Y.; Huang, Y.; Hu, S.. *Jiegou Huaxue* **1993**, *12*, 430–436.
(82) Nishikawa, K.; Kobayashi, A.; Sasaki, Y. *Bull. Chem. Soc. Jpn.* **1975**, *48*, 3152–3155.
(83) Hashimoto, M.; Selling, A.; Hakansson, M.; Pettersson, L. *Acta Chem. Scand.* **1999**, *53*, 305–313.
(84) O'Donnell, S. E.; Pope, M. T. *Dalton Trans.* **1976**, 2290–2297.
(85) Pettersson, L.; Andersson, I.; Grate, J. H.; Selling, A. *Inorg. Chem.* **1994**, *33*, 982–993.
(86) Selling, A.; Andersson, I.; Grate, J. H.; Pettersson, L. *Eur. J. Inorg. Chem.* **2000**, 1509–1521.
(87) Leparulo–Loftus, M. A.; Pope, M. T. *Inorg. Chem.* **1987**, *26*, 2112–2120.
(88) Pope, M. T.; O'Donnell, S. E.; Prados, R. A. *Adv. Chem. Ser.* **1976**, *150*, 85–94.
(89) Guan, W.; Yan, L.; Su, Z.; Liu, S.; Zhang, M.; Wang, X. *Inorg. Chem.* **2005**, *44*, 100–107.
(90) Chermette, H.; Lefebvre, F. *C. R. Chim.* **2012**, *15*, 143–151.
(91) Laurencin, D.; Proust, A.; Gerard, H. *Inorg. Chem.* **2008**, *47*, 7888–7893.
(92) Hasenknopf, B.; Micoine, K.; Lacote, E.; Thorimbert, S.; Malacria, M.; Thouvenot, R. *Eur. J. Inorg. Chem.* **2008**, 5001–5013.
(93) Du, D.; Yan, L.; Su, Z.; Li, S.; Lan, Y.; Wang, E. *Coord. Chem. Rev.* **2013**, *257*, 702–717.
(94) Chen, W.; Tan, H.; Wang, E. *J. Coord. Chem.* **2012**, *65*, 1–18.
(95) Crassous, J. *Chem. Commun.* **2012**, *48*, 9684–9692.
(96) Yan, L.; Lopez, X.; Carbo, J. J.; Sniatynsky, R.; Duncan, D. C.; Poblet, J. M. *J. Am. Chem. Soc.* **2008**, *130*, 8223–8233.
(97) Garvey, J. F.; Pope, M. T. *Inorg. Chem.* **1978**, *17*, 1115–1118.
(98) Pope, M. T. *Inorg. Chem.* **1976**, *15*, 2008–2010.
(99) Privalov, V. I.; Lapkin, V. V.; Tarasov, V. P.; Busalaev, Y. A. *Appl. Magn. Reson.* **1991**, *1*, 445–456.
(100) Privalov, V. I.; Lapkin, V. V.; Tarasov, V. P.; Buslaev, Y. A. *Mendeleev Commun.* **1991**, 59–61.
(101) Pley, M.; Wickleder, M. S. *Angew. Chem. Int. Ed.* **2004**, *43*, 4168–4170.
(102) Izarova, N. V.; Vankova, N.; Heine, T.; Biboum, R. N.; Keita, B.; Nadjo, L.; Kortz, U. *Angew. Chem. Int. Ed.* **2010**, *49*, 1886–1889.
(103) Torapava, N.; Elding, L. I.; Maendar, H.; Roosalu, K.; Persson, I. *Dalton Trans.* **2013**, *42*, 7755–7760.

(104) Sonne, P.; Müller–Buschbaum, H. *Z. Anorg. Allg. Chem.* **1993**, *619*, 1004–1006.
(105) Tatarchuk, V. V.; Sergievskaya, A. P.; Kuratieva, N. V.; Korol'kov, I. V.; Sheludyakova, L. A.; Gromilov, S. A. *J. Struct. Chem.* **2014**, *55*, 142–146.
(106) Izarova, N. V.; Vankova, N.; Banerjee, A.; Jameson, G. B.; Heine, T.; Schinle, F.; Hampe, O.; Kortz, U. *Angew. Chem. Int. Ed.* **2010**, *49*, 7807–7811.
(107) Scullion, R. A.; Surman, A. J.; Xu, F.; Mathieson, J. S.; Long, D.; Haso, F.; Liu, T.; Cronin, L. *Angew. Chem. Int. Ed.* **2014**, *53*, 10032–10037.
(108) Barsukova–Stuckart, M.; Izarova, N. V.; Barrett, R. A.; Wang, Z.; van Tol, J.; Kroto, H. W.; Dalal, N. S.; Jimenez–Lozano, P.; Carbo, J. J.; Poblet, J. M.; von Gernler, M. S.; Drewello, T.; de Oliveira, P.; Keita, B.; Kortz, U. *Inorg. Chem.* **2012**, *51*, 13214–13228.
(109) Izarova, N. V.; Kondinski, A.; Vankova, N.; Heine, T.; Jaeger, P.; Schinle, F.; Hampe, O.; Kortz, U. *Chem. Eur. J.* **2014**, *20*, 8556–8560.
(110) Barsukova, M.; Izarova, N. V.; Biboum, R. N.; Keita, B.; Nadjo, L.; Ramachandran, V.; Dalal, N. S.; Antonova, N. S.; Carbo, J. J.; Poblet, J. M.; Kortz, U. *Chem. —Eur. J.* **2010**, *16*, 9076–9085.
(111) Yang, P.; Xiang, Y.; Lin, Z.; Bassil, B. S.; Cao, J.; Fan, L.; Fan, Y.; Li, M.; Jimenez–Lozano, P.; Carbo, J. J.; Poblet, J. M.; Kortz, U. *Angew. Chem. Int. Ed.* **2014**, *53*, 11974–11978.
(112) Lin, Z.; Wang, B.; Cao, J.; Chen, B.; Gao, Y.; Chi, Y.; Xu, C.; Huang, X.; Han, R.; Su, S.; Hu, C. *Inorg. Chem.* **2012**, *51*, 4435–4437.
(113) Lin, Z.; Wang, B.; Cao, J.; Chen, B.; Xu, C.; Huang, X.; Fan, Y.; Hu, C. *Eur. J. Inorg. Chem.* **2013**, *2013*, 3458–3463.
(114) Izarova, N. V.; Dickman, M. H.; Biboum, R. N.; Keita, B.; Nadjo, L.; Ramachandran, V.; Dalal, N. S.; Kortz, U. *Inorg. Chem.* **2009**, *48*, 7504–7506.
(115) Xu, F.; Scullion, R. A.; Yan, J.; Miras, H. N.; Busche, C.; Scandurra, A.; Pignataro, B.; Long, D.; Cronin, L. *J. Am. Chem. Soc.* **2011**, *133*, 4684–4686.
(116) Delferro, M.; Graiff, C.; Elviri, L.; Predieri, G. *Dalton Trans.* **2010**, *39*, 4479–4481.
(117) Izarova, N. V.; Biboum, R. N.; Keita, B.; Mifsud, M.; Arends, I. W. C. E.; Jameson, G. B.; Kortz, U. *Dalton Trans.* **2009**, 9385–9387.
(118) Barsukova–Stuckart, M.; Izarova, N. V.; Jameson, G. B.; Ramachandran, V.; Wang, Z.; van Tol, J.; Dalal, N. S.; Biboum, R. N.; Keita, B.; Nadjo, L.; Kortz, U. *Angew. Chem. Int. Ed.* **2011**, *50*, 2639–2642.
(119) Izarova, N. V.; Lin, Z.; Yang, P.; Kondinski, A.; Vankova, N.; Heine, T.; Kortz, U. *Dalt. Trans.;* **2016***;* (Ahead of print).
(120) Xu, F.; Miras, H. N.; Scullion, R. A.; Long, D.; Thiel, J.; Cronin, L. *Proc. Natl. Acad. Sci. U. S. A.* **2012**, *109*, 11609–11612.
(121) Xiang, Y.; Izarova, N. V.; Schinle, F.; Hampe, O.; Keita, B.; Kortz, U. *Chem. Commun.* **2012**, *48*, 9849–9851.
(122) Kondinski, A.; Vankova, N.; Schinle, F.; Jaeger, P.; Hampe, O.; Kortz, U.; Heine, T. *Eur. J. Inorg. Chem.* **2014**, *2014*, 3771–3778.
(123) Vasilchenko, D.; Berdugin, S.; Tkachev, S.; Baidina, I.; Romanenko, G.; Gerasko, O.; Korenev, S. *Inorg. Chem.* **2015**, *54*, 4644–4651.
(124) Bridgeman, A. J.; Cavigliasso, G. *Chem. Phys.* **2002**, *279*, 143–159.
(125) Bridgeman, A. J. *Chem. Phys.* **2003**, *287*, 55–69.
(126) Bridgeman, A. J. *Chem. Eur. J.* **2004**, *10*, 2935–2941.
(127) Ravelli, D.; Dondi, D.; Fagnoni, M.; Albini, A.; Bagno, *J. Comput. Chem.* **2011**, *32*, 2983–2987.
(128) Tucher, J.; Wu, Y.; Nye, L. C.; Ivanovic–Burmazovic, I.; Khusniyarov, M. M.; Streb, C. *Dalton Trans.* **2012**, *41*, 9938–9943.
(129) Son, J.; Ohlin, C. A.; Casey, W. H. *Dalton Trans.* **2012**, *41*, 12674–12677.
(130) Wang, J.; Yang, G.; Yan, L.; Guan, W.; Wen, S.; Su, Z. *Dalton Trans.* **2012**, *41*, 10097–10104.
(131) Sang, Y.; Yan, L.; Wang, J.; Su, Z. *J. Phys. Chem. A* **2012**, *116*, 4152–4158.
(132) Sang, Y.; Yan, L.; Ma, N.; Wang, J.; Su, Z. *J. Phys. Chem. A* **2013**, *117*, 2492–2498.
(133) Bagno, A.; Bini, R. *Angew. Chem. Int. Ed.* **2010**, *49*, 1083–1086.
(134) Vankova, N.; Heine, T.; Kortz, U. *Eur. J. Inorg. Chem.* **2009**, 5102–5108.
(135) Banerjee, A.; Raad, F. S.; Vankova, N.; Bassil, B. S.; Heine, T.; Kortz, U. *Inorg. Chem.* **2011**, *50*, 11667–11675.
(136) Kozhevnikov, I. In *Catalysts for Fine Chemical Synthesis, Catalysis by Polyoxometalates;* Roberts, S. M., Ed.; Catalysts for Fine Chemical Synthesis, Volumes 1–5, Set; Wiley-VCH: Weinheim, Germany, 2002; Vol. 2.
(137) Kozhevnikov, I. V. In *Heterogeneous catalysis by heteropoly compounds.* Borrás–Almenar, J. J., Coronado, E., Müller, A. and Pope, M., Eds.; Catalysis, Reaction Kinetics, and Inorganic Reaction Mechanisms; Springer, Netherlands, 2003; Vol. 98, pp 351–380.
(138) Kozhevnikov, I. V. *J. Mol. Catal. A: Chem.* **2007**, *262*, 86–92.
(139) Kozhevnikov, I. In *Sustainable heterogeneous acid catalysis by heteropoly acids.* Crabtree, R. H., Ed.; Green Catalysis – Heterogeneous Catalysis; John Wiley & Sons, Chichester, England, 2009; Vol. 2, pp 153–174.

(140) Kozhevnikov, I. V. *J. Mol. Catal. A: Chem.* **2009**, *305*, 104–111.
(141) Wang, S.; Yang, G. *Chem. Rev. (Washington, DC, U. S.)* **2015**, *115*, 4893–4962.
(142) Carraro, M.; Sartorel, A.; Toma, F. M.; Puntoriero, F.; Scandola, F.; Campagna, S.; Prato, M.; Bonchio, M. *Top. Curr. Chem.* **2011**, *303*, 121–150.
(143) Puntoriero, F.; Sartorel, A.; Orlandi, M.; La Ganga, G.; Serroni, S.; Bonchio, M.; Scandola, F.; Campagna, S. *Coord. Chem. Rev.* **2011**, *255*, 2594–2601.
(144) Dolbecq, A.; Dumas, E.; Mayer, C. R.; Mialane, P. *Chem. Rev. (Washington, DC, U. S.)* **2010**, *110*, 6009–6048.
(145) Puntoriero, F.; La Ganga, G.; Sartorel, A.; Carraro, M.; Scorrano, G.; Bonchio, M.; Campagna, S. *Chem. Commun.* **2010**, *46*, 4725–4727.
(146) Toma, F. M., Sartorel, A., Iurlo, M., Carraro, M., Parisse, P., Maccato, C., Rapino, S,. Gonzalez, B. R., Amenitsch, H., Da Ros, T., Casalis, L., Goldoni, A., Marcaccio, M., Scorrano, G., Scoles, G., Paolucci, F., Prato, M., Bonchio, M., *Nat. Chem.* **2010**, *2*, 826–831.
(147) Symes, M. D.; Cronin, L. *Nat. Chem.* **2013**, *5*, 403–409.
(148) Izarova, N. V.; Kögerler, P. In *Trends in Polyoxometalates Research*; Ruhlmann, L., Schaming, D., Eds.; Nova Science Publishers Incorporated, 2015; pp 121–149.
(149) Tsukerblat, B.; Tarantul, A. *World Sci. Ser. Nanosci. Nanotechnol.* **2012**, *3*, 109–179.
(150) Clemente–Juan, J. M.; Coronado, E.; Gaita–Arino, A. *Chem. Soc. Rev.* **2012**, *41*, 7464–7478.
(151) Hungerford, G.; Hussain, F.; Patzke, G. R.; Green, M. *Phys. Chem. Chem. Phys.* **2010**, *12*, 7266–7275.
(152) Lis, S. *Acta Phys. Pol. A* **1996**, *90*, 275–283.
(153) Papaconstantinou, E.; Hiskias, A.; Troupis, A. *Front. Biosci.* **2003**, *8*, 813–825.
(154) Papaconstantinou, E.; Hiskia, A. In *Polyoxometalate Molecular Science*; Borrás–Almenar, J. J., Coronado, E. and Müller, A., Pope, M., Eds.; Springer Netherlands, 2003, *98*, pp 381–416.
(155) Bonchio, M.; Carraro, M.; Scorrano, G.; Bagno, A. *Adv. Synth. Catal.* **2004**, *346*, 648–654.
(156) Dolbecq, A.; Mialane, P.; Keita, B.; Nadjo, L. *J. Mater. Chem.* **2012**, *22*, 24509–24521.
(157) Janell, D.; Tocilj, A.; Kölln, I.; Schlünzen, F.; Glühmann, M.; Hansen, H. A. S.; Harms, J.; Bashan, A.; Agmon, I.; Bartels, H.; Kessler, M.; Weinstein, S.; Franceshi, F.; Yonath, A. In *Polyoxometalate Chemistry From Topology via Self–Assembly to Applications;* Pope, M. T., Müller, A., Eds.; Kluwer Academic Publishers; **2001**; pp 391–415.
(158) Kowalewski, B.; Poppe, J.; Demmer, U.; Warkentin, E.; Dierks, T.; Ermler, U.; Schneider, K. *J. Am. Chem. Soc.* **2012**, *134*, 9768–9774.
(159) De Clercq, E. *Med. Res. Rev.* **2002**, *22*, 531–565.
(160) De Clercq, E. *Biochim. Biophys. Acta, Mol. Basis Dis.* **2002**, *1587*, 258–275.
(161) De Clercq, E. *Curr. Med. Chem.* **2001**, *8*, 1543–1572.
(162) De Clercq, E. *Rev. Med. Virol.* **2000**, *10*, 255–277.
(163) Zhang, G.; Keita, B.; Craescu, C. T.; Miron, S.; de Oliveira, P.; Nadjo, L. *Biomacromolecules* **2008**, *9*, 812–817.
(164) Herrmann, S.; Ritchie, C.; Streb, C. *Dalton Trans.* **2015**, *44*, 7092–7104.
(165) Mitchell, S. G.; de la Fuente, J. M. *J. Mater. Chem.* **2012**, *22*, 18091–18100.
(166) Bamoharram, F. F.; Ahmadpour, A.; Heravi, M. M.; Ayati, A.; Rashidi, H.; Tanhaei, B. *Synth. React. Inorg. , Met. –Org. , Nano–Met. Chem.* **2012**, *42*, 209–230.
(167) Haso, F.; Yang, P.; Gao, Y.; Yin, P.; Li, H.; Li, T.; Kortz, U.; Liu, T. *Chem. Eur. J.* **2015**, *21*, 9048–9052.
(168) Sholl, D. S.; Steckel, J. A., Eds.; *Density Functional Theory: A Practical Introduction*, 2009.
(169) Klamt, A.; Schueuermann, G. *J. Chem. Soc. , Perkin Trans. 2* **1993**, 799–805.
(170) Politzer, P.; Truhlar, D. G.; **1981**, 472.
(171) ADF 2014, SCM, Theoretical Chemistry, Vrije Univesity, Amsterdam, The Netherlands http://www.scm.com/.
(172) Te Velde, G.; Bickelhaupt, F. M.; Baerends, E. J.; Fonseca Guerra, C.; Van Gisbergen, S. J. A.; Snijders, J. G.; Ziegler, T. *J. Comput. Chem.* **2001**, *22*, 931–967.
(173) Levine, I. N. *Quantum Chemistry;* Prentice Hall: Instock, 2013.
(174) Jungwirth, P. *Angew. Chem. Int. Ed.* **2010**, *49*, 485.
(175) Hohenberg, P.; Kohn, W. *Phys. Rev. , B Condens. Matter* **1964**, *136*, 864–871.
(176) Kohn, W.; Sham, L. J. *AEC Access. Nos.* **1965**, 21.
(177) Kohn, W.; Sham, L. J. *Phys. Rev.* **1965**, *137*, 1697–1705.
(178) Perdew, J. P.; Schmidt, K. *AIP Conf. Proc.* **2001**, *577*, 1–20.
(179) Vosko, S.; Wilk, L.; Nusair, M. *Can. J. Phys.* **1980**, *58*, 1200–1211.
(180) Bridgeman, A. J. *Chem. Eur. J.* **2006**, *12*, 2094–2102.
(181) Becke, A. D. *Phys. Rev. A: Gen. Phys.* **1988**, *38*, 3098–3100.
(182) Perdew, J. *Phys. Rev. B* **1986**, *33*, 8822–8824.
(183) Perdew, J. P.; Chevary, J. A.; Vosko, S. H.; Jackson, K. A.; Pederson, M. R.; Singh, D. J.; Fiolhais, C. *Phys. Rev. B: Condens. Matter* **1992**, *46*, 6671–6687.

(184) Perdew, J. P.; Chevary, J. A.; Vosko, S. H.; Jackson, K. A.; Pederson, M. R.; Singh, D. J.; Fiolhais, C. *Phys. Rev. B: Condens. Matter* **1993**, *48*, 4978.
(185) Perdew, J. P.; Burke, K.; Ernzerhof, M. *Phys. Rev. Lett.* **1996**, *77*, 3865–3868.
(186) Perdew, J. P.; Burke, K.; Ernzerhof, M. *Phys. Rev. Lett.* **1997**, *78*, 1396.
(187) Zhang, Y.; Yang, W. *Phys. Rev. Lett.* **1998**, *80*, 890.
(188) Lee, C.; Yang, W.; Parr, R. G. *Phys. Rev. B: Condens. Matter* **1988**, *37*, 785–789.
(189) Johnson, B. G.; Gill, P. M. W.; Pople, J. A. *J. Chem. Phys.* **1993**, *98*, 5612–5626.
(190) Stephens, P. J.; Devlin, F. J.; Chabalowski, C. F.; Frisch, M. J. *J. Phys. Chem.* **1994**, *98*, 11623–11627.
(191) Cohen, A. J.; Handy, N. C. *Mol. Phys.* **2001**, *99*, 607–615.
(192) Xu, X.; Goddard, W. A., *Proc. Natl. Acad. Sci. U. S. A.* **2004**, *101*, 2673–2677.
(193) Kang, J. K.; Musgrave, C. B. *J. Chem. Phys.* **2001**, *115*, 11040–11051.
(194) López, X.; De Graaf, C.; Maestre, J. M.; Benard, M.; Rohmer, M.; Bo, C.; Poblet, J. M. *J. Chem. Theory Comput.* **2005**, *1*, 856–861.
(195) Vlcek, A.; Zalis, S. *Coord. Chem. Rev.* **2007**, *251*, 258–287.
(196) Runge, E.; Gross, E. K. U. *Phys. Rev. B* **1984**, *52 (12)*, 997–1000.
(197) Klamt, A. *J. Phys. Chem.* **1995**, *99*, 2224–2235.
(198) Klamt, A.; Jonas, V. *J. Chem. Phys.* **1996**, *105*, 9972–9981.
(199) Sjoberg, P.; Politzer, P. *J. Phys. Chem.* **1990**, *94*, 3959–3961.
(200) Jacobs University Bremen Computational Laboratory for Analysis, Modeling, and Visualization (CLAMV). *www.clamv.jacobs–university.de* (accessed 12/15, 2015).
(201) Van Lenthe, E.; Baerends, E. J. *J. Comput. Chem.* **2003**, *24*, 1142–1156.
(202) van Lenthe, E.; Baerends, E. J.; Snijders, J. G. *J. Chem. Phys.* **1993**, *99*, 4597–4610.
(203) van Lenthe, E.; Baerends, E. J.; Snijders, J. G. *J. Chem. Phys.* **1994**, *101*, 9783–9792.
(204) van Lenthe, E.; Ehlers, A.; Baerends, E. *J. Chem. Phys.* **1999**, *110*, 8943–8953.
(205) Pye, C. C.; Ziegler, T. *Theor. Chem. Acc.* **1999**, *101*, 396–408.
(206) Ernzerhof, M.; Scuseria, G. E. *J. Chem. Phys.* **1999**, *110*, 5029–5036.
(207) Adamo, C.; Barone, V. *J. Chem. Phys.* **1999**, *110*, 6158–6170.
(208) Zhao, Y.; Truhlar, D. G. *Theor. Chem. Acc.* **2008**, *120*, 215–241.
(209) Proust, A.; Thouvenot, R.; Gouzerh, P. *Chem. Commun. (Cambridge, U. K.)* **2008**, 1837–1852.
(210) Errington, R. J. In Polyoxometalate Molecular Science; Pope, M. T., Müller, A., Eds.; Springer Netherlands: **2001**; pp 7–22.
(211) Errington, R. J. In Polyoxometalate Molecular Science.; Borrás–Almenar, J. J., Coronado, E. and Müller, A., Pope, M., Eds.; Springer Netherlands; **2003**; Vol. 98, pp 55–78.
(212) Cronin, L.; Mueller, A. *Chem. Soc. Rev.* **2012**, *41*, 7333–7334.
(213) Miras, H. N.; Cronin, L. In *Inorganic Chemicals and Reactions*; Cannizzaro, S. Ed.; **2012**; pp 3–32.
(214) Jackson, M. N., Jr.; Kamunde–Devonish, M. K.; Hammann, B. A.; Wills, L. A.; Fullmer, L. B.; Hayes, S. E.; Cheong, P. H.; Casey, W. H.; Nyman, M.; Johnson, D. W. A *Dalton Trans.* **2015**, *44*, 16982–17006.
(215) Mingos, D. M. P., Ed.; *Bonding and Charge Distribution in Polyoxometalates: A Bond Valence Approach.;* Springer–Verlag Berlin Heidelberg: **1999**; Vol. 93, pp 340.
(216) Ratajczak, H.; Barnes, A. J.; Bielański, A.; Lutz, H. D.; Müller, A.; Pope, M. T. In *Polyoxometalate Chemistry From Topology via Self–Assembly to Applications*; Pope, M. T., Müller, A., Eds.; Springer Netherlands, 2001; pp 101–116.
(217) Balogh, E.; Casey, W. H. *Prog. Nucl. Magn. Reson. Spectrosc.* **2008**, *53*, 193–207.
(218) Fedotov, M. A.; Maksimovskaya, R. I. *J. Struct. Chem.* **2006**, *47*, 952–978.
(219) Chen, Y.; Gong, J.; Qu, L. *Coord. Chem. Rev.* **2004**, *248*, 245–260.
(220) Keita, B.; Nadjo, L. In *Encyclopedia of Electrochemistry*; Bard, A. J., Stratmann, M., Rubinstein, I., Fujihira, M. and Rusling, J. F., Eds.; Wiley–VCH Verlag GmbH & Co. KGaA: 2007; Vol. 850, pp 607–700.
(221) Hiraoka, K. *J. Mass Spectrom. Soc. Jpn.* **2010**, *58*, 139–154.
(222) Molin, L.; Traldi, P. *J. Chromatogr. Libr.* **2007**, *72*, 1–9.
(223) Deery, M.; Howarth, O.; Jennings, K. *Dalton Trans.* , **1997**, 4783–4788.
(224) Wu, C.; Ma, T.; Yan, L.; Zhang, T.; Su, Z. *Phys. Chem. Chem. Phys.* **2015**, *17*, 11521–11526.
(225) McDaniel, D. H. *Inorg. Chem.* **1972**, *11*, 2678–2682.
(226) Gatteschi, D.; Pardi, L.; Barra, A. L.; Müller, A. *Mol. Eng.* **1993**, *3*, 157–169.
(227) Tripathi, A.; Hughbanks, T.; Clearfield, A. *J. Am. Chem. Soc.* **2003**, *125*, 10528–10529.
(228) Pitzschke, D.; Wang, J.; Hoffmann, R.; Pöttgen, R.; Bensch, W. *Angew. Chem. Int. Ed.* **2006**, *45*, 1305–1308.
(229) Huan, G.; Greaney, M. A.; Jacobson, A. J. *J. Chem. Soc. , Chem. Commun.* **1991**, 260–261.

(230) Zheng, S.; Zhang, J.; Yang, G. *Z. Anorg. Allg. Chem.* **2005**, *631*, 170–173.
(231) Hu, X.; Xu, J.; Cui, X.; Song, J.; Wang, T. *Inorg. Chem. Commun.* **2004**, *7*, 264–267.
(232) Zhang, L.; Zhao, X.; Xu, J.; Wang, T. *J. Chem. Soc. , Dalton Trans.* **2002**, 3275–3276.
(233) Müller, A.; Döring, J. *Z. anorg. allg. Chem.* **1991**, *595*, 251–274.
(234) Winter, R. S.; Yan, J.; Busche, C.; Mathieson, J. S.; Prescimone, A.; Brechin, E. K.; Long, D.; Cronin, L. *Chem. Eur. J.* **2013**, *19*, 2976–2981.
(235) Jolly, W. L. Modern Inorganic Chemistry. **1983**, 786.
(236) Sokolov, M. N.; Korenev, V. S.; Izarova, N. V.; Peresypkina, E. V.; Vicent, C.; Fedin, V. P. *Inorg. Chem.* **2009**, *48*, 1805–1807.
(237) Liu, C. *Mol. Phys.* **2011**, *109*, 1851–1857.
(238) Wei, X.; Bachman, R. E.; Pope, M. T. *J. Am. Chem. Soc.* **1998**, *120*, 10248–10253.
(239) Jolly, W. L. Modern Inorganic Chemistry. **1983**, 786.
(240) Izarova, N. V.; Banerjee, A.; Kortz, U. *Inorg. Chem.* **2011**, *50*, 10379–10386.
(241) Bennett, M. A.; Bhargava, S. K.; Cheng, E. C.; Lam, W. H.; Lee, T. K.; Priver, S. H.; Wagler, J.; Willis, A. C.; Yam, V. W. *J. Am. Chem. Soc.* **2010**, *132*, 7094–7103.
(242) Shin, Y. G. K.; Miskowski, V. M.; Nocera, D. G. *Inorg. Chem.* **1990**, *29*, 2308–2313.

Eidesstattliche Erklärung zur Abgabe einer digitalen Dissertation

(Statutory Declaration on Publication of a Digital Dissertation)

Verfasser/in (Author)	Aleksandar Kondinski
Titel der Dissertation (Title of dissertation)	On the Isomer Problem of Mixed−Addenda and Heterogroup −Substituted Polyoxometalates
Datum der mündlichen Prüfung (Date of defense)	22.01.2016
Hauptgutacher/in (Main referee)	Prof. Dr. Thomas Heine
Area	Life Sciences & Chemistry

- Ich versichere an Eides statt, dass ich die vorgelegte Dissertation selbstständig und ohne unzulässige fremde Hilfe angefertigt und verfasst habe, dass alle Hilfsmittel und sonstigen Hilfen angegeben und dass alle Stellen, die ich wörtlich oder dem Sinne nach aus anderen Veröffentlichung entnommen habe, kenntlich gemacht worden sind.
  Ich versichere, dass die Dissertation in der vorgelegten oder einer ähnlichen Fassung noch nicht zu einem früheren Zeitpunkt an einer anderen in- oder ausländischen Universität eingereicht wurde.
- In Kenntnis der Strafbarkeit auch einer uneidlich falschen Versicherung versichere ich hiermit an Eides Statt, dass sowohl die abgegebene digitale Dissertation als auch die gedruckten Exemplare mit dem vom Promotionsauschuß zur Veröffentlichung freigegebenen Exemplar übereinstimmen. Für die digitale Version sichere ich die Vollständigkeit und Lesbarkeit zu und erkläre, dass alle abgegebenen Dateien frei sind von schädlichen Inhalten, insbesondere Computer-Viren, Würmern, Trojanern, Dialern und Ausspähmechanismen.
- Ich erkläre mich damit einverstanden, dass die Jacobs University Bremen gGmbH (Jacobs University) die digitale Version und die dazugehörigen Daten (inkl. der Abstracts) auf ihren Servern speichert, vervielfältigt, archiviert und in Datennetzen zur öffentlichen Nutzung bereitstellt.
  Die Jacobs University ist ebenfalls berechtigt, die digitale Dissertation und die dazugehörigen Daten zum gleichen Zweck an Die Deutsche Bibliothek und ggf. an die DFG-Sondersammelgebietsbibliothek weiterzugeben. Die genannten Institutionen dürfen, wenn dies technisch erforderlich ist, eine Migration in ein anderes Datenformat vornehmen.
- Ich versichere, dass ich Urheber der Dissertation bin und der Veröffentlichung keine Rechte Dritter entgegenstehen. Die für die vorgenannten Arten der Verwertung erforderlichen Urheber-Verwertungsrechte übertrage ich hiermit der Jacobs University.
  Das Veröffentlichungsrecht der Jacobs University kann insoweit auch nicht durch eine spätere Verlagspublikation eingeschränkt werden.
- Mir ist bekannt, dass die Jacobs University keine Haftung oder Gewähr übernimmt, wenn die Dissertation von dritter Seite unrechtmäßig heruntergeladen, verändert oder an anderer Stelle ohne Einwilligung aufgelegt wird.
- Ich willige darin ein, dass auch die gegebenenfalls zur Dissertation gehörenden persönlichen Daten (Lebenslauf) maschinell gespeichert und zusammen mit der Dissertation bereitgestellt (veröffentlicht) werden.
- Mir ist bekannt, dass eine nachträgliche Änderung der abgegebenen Dissertation nicht möglich ist.
- Die englische Übersetzung dieser Erklärung habe ich erhalten.

Aachen, 05.02.2016

Ort, Datum (Place, Date)

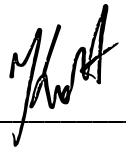

Unterschrift (Signature)

Eidesstattliche Erklärung zur Abgabe einer digitalen Dissertation
(Statutory Declaration on Publication of a Digital Dissertation)

JACOBS UNIVERSITY

Appendix: Translation of the Statutory Declaration

- I hereby declare that I have written this PhD thesis independently, unless where clearly stated otherwise. I have used only the sources, the data and the support that I have clearly mentioned. This PhD thesis has not been submitted for conferral of degree elsewhere.
- I am aware that it is a criminal offence to make even an unsworn false affirmation, and I hereby affirm in lieu of an oath that both the submitted digital dissertation and the printed copies are the same as the copy approved by the examining committee for publication. I assure that the digital version is complete and legible and that all the files submitted are free of harmful content, in particular computer viruses, worms, trojans, dialers and spyware.
- I hereby consent to the Jacobs University Bremen gGmbH (Jacobs University) saving the digital version and the associated data (incl. abstracts) on its servers, archiving and making copies thereof and making it available on data networks for public use. The Jacobs University is also entitled to make the digital dissertation and the associated data available to the German Library (Deutsche Bibliothek) and, if appropriate, to the DFG-Sondersammelgebietsbibliothek (German Research Association special collection library) for the same purpose. The above-named institutions may, if required for technical reasons, migrate the data into another format.
- I affirm that I am the author of the dissertation and that no third party rights exist which preclude publication. I hereby assign the necessary copyrights for the above-mentioned types of use to the Jacobs University. The Jacobs University's right of publication thus cannot be restricted by subsequent publication by a publishing house.
- I am aware that the Jacobs University assumes no liability or responsibility if the dissertation is downloaded illegally by a third party, or if it is changed or published without permission in another place.
- I consent to the fact that any personal data which belongs to the dissertation (CV) will be saved electronically and will be made available (published) together with the dissertation.
- I am aware that it is not possible to make subsequent changes once the dissertation has been submitted.
- I have received an English translation of this declaration.